AD-A247 258

AFOSR-TR- 9 2 0 1 6 6

THE CONVECTION SPEED OF THE DYNAMIC STALL VORTEX

by

R.B. Green, R.A.McD. Galbraith and A.J. Niven,
Department of Aerospace Engineering,
University of Glasgow,
Glasgow,
Scotland.
G12 8QQ

DTIC
ELECTE
MAR 0 4 1992
S D
D

prepared for

92-05480

1st January 1992

92 3 02 165

Best
Available
Copy

REPORT DOCUMENTATION PAGE

Public reporting burden for this collection of information is estimated to average 1 hour per response, including the time for reviewing instructions, searching existing data sources, gathering and maintaining the data needed, and completing and reviewing the collection of information. Send comments regarding this burden estimate or any other aspect of this collection of information, including suggestions for reducing this burden, to Washington Headquarters Services, Directorate for information Operations and Reports, 1215 Jefferson Davis Highway, Suite 1204, Arlington, VA 22202-4302, and to the Office of Management and Budget, Paperwork Reduction Project (0704-0188), Washington, DC 20503.

1. AGENCY USE ONLY (Leave blank)	2. REPORT DATE	3. REPORT TYPE AND DATES COVERED
	1st JANUARY 1992	FINAL 1st NOV 1989 TO 31st OCT 1991

4. TITLE AND SUBTITLE

The Convection Speed of the Dynamic Stall Vortex

5. FUNDING NUMBERS

AFOSR-89-0397

6. AUTHOR(S)

R.B. Green, R.A.McD. Galbraith and A.J. Niven

7. PERFORMING ORGANIZATION NAME(S) AND ADDRESS(ES)

Department of Aerospace Engineering,
University of Glasgow,
Glasgow,
Scotland.
G12 8QQ

8. PERFORMING ORGANIZATION REPORT NUMBER

G.U. Aero Report No 9202

9. SPONSORING/MONITORING AGENCY NAME(S) AND ADDRESS(ES)

Air Force Office of Scientific Research,
Directorate of Aerospace Sciences,
Bolling AFB,
DC 20332-6448

10. SPONSORING/MONITORING AGENCY REPORT NUMBER

AFOSR -
89-0397

11. SUPPLEMENTARY NOTES

12a. DISTRIBUTION/AVAILABILITY STATEMENT

APPROVED FOR PUBLIC RELEASE
DISTRIBUTION IS UNLIMITED

12b. DISTRIBUTION CODE

13. ABSTRACT (Maximum 200 words)

This report describes measurements of the convection speed of the dynamic stall vortex. A survey reveals a disharmony between the various researchers as to the dependency of the convection speed upon the aerofoil motion. A preliminary analysis of pressure data from aerofoil models tested at the University of Glasgow at Reynolds and Mach numbers of 1.5 million and 0.11 respectively showed that the convection speed was independent of aerofoil motion and model type to a first order. The former conclusion is in disagreement with the work of Lorber & Carta (1987) in particular. Their data was analysed independently at the University of Glasgow, and the results reinforced the anomaly. Testing a high aspect ratio NACA 0015 at the University of Glasgow showed that wind tunnel constraint was not a significant factor. An enhanced analysis technique produced results which, in spite of their poor accuracy, suggest that at low pitch rates the convection speed falls with increasing reduced pitch rate to a constant value for the NACA 0015 and 0018 models. The effect of a leading edge trip was to significantly alter the details of the dynamic stall and to change the vortex convection speed. Although the convection speed/ aerofoil motion dependency anomaly has not been not fully solved, it is suggested that leading edge effects influence the convection speed, and the aerofoil leading edge geometry, Reynolds and Mach numbers are highlighted.

14. SUBJECT TERMS

Dynamic stall, unsteady flow, separated flow, vortex propagation, super-manoeuvrability, aerodynamic testing

15. NUMBER OF PAGES

· 122 ·

16. PRICE CODE

17. SECURITY CLASSIFICATION OF REPORT	18. SECURITY CLASSIFICATION OF THIS PAGE	19. SECURITY CLASSIFICATION OF ABSTRACT	20. LIMITATION OF ABSTRACT
UNCLASSIFIED	UNCLASSIFIED	UNCLASSIFIED	UNLIMITED

NSN 7540-01-280-5500

THE CONVECTION SPEED OF THE DYNAMIC STALL VORTEX

by

R.B. Green. R.A.McD. Galbraith and A.J. Niven,
Department of Aerospace Engineering,
University of Glasgow,
Glasgow,
Scotland.
G12 8QQ

prepared for

Accesion For		
NTIS CRA&I		☑
DTIC TAB		☐
U.announced		☐
Justification		
By		
Distribution/		
Availability Codes		
Dist	Avail and/or Special	
A-1		

Declaration:
The views and conclusions contained in this document are those of the authors and should not be interpreted as necessarily representing the official policies or endorsements, either expressed or implied, of the Air Force Office of Scientific Research or the U.S. Government

1st January 1992

THE CONVECTION SPEED OF THE DYNAMIC STALL VORTEX.

by

R.B. Green, R.A. McD. Galbraith and A.J. Niven,
Department of Aerospace Engineering,
University of Glasgow,
Glasgow,
Scotland.

Summary.

This report describes the phenomenon of dynamic stall and considers in detail the role of the so-called stall vortex. A survey of the available data reveals an anomaly concerning the dependency of the convection speed upon aerofoil motion. The University of Glasgow Unsteady Aerodynamics test facility is then described, and measurements of the stall vortex convection speed from a variety of aerofoil models and pitching motions are presented. The results of the preliminary analysis, relating to conditions at Reynolds and Mach numbers of 1.5 million and 0.11 respectively, strongly suggest that the convection speed is independent of the aerofoil motion and model type to a first order, which disagrees with the results of other notable studies. This disharmony is re-inforced by an independent analysis of an anomalous data set at the University of Glasgow. Differences in constraint effects were suspected to be the cause of the anomaly, and the report then continues to describe a test programme for a model of half the chord length of the models so far tested at the University of Glasgow. The results of these tests show that wind tunnel constraint, within the limits tested, does not significantly affect the vortex convection speed. An enhanced technique allowed pressure data to be analysed at a much lower pitch rate than for the preliminary analysis. In spite of the relatively poor accuracy of the susequent measurements, the results suggest that the convection speed is reduced pitch rate dependent at low pitch rates for the thicker aerofoil sections, although in an opposite manner to other results in the literature survey. A further test programme investigated the effects of a leading edge boundary layer trip. The nature of the dynamic stall and the stall vortex convection speed were seen to completely change throughout the entire pitch rate range. Thus, although the basic convection speed/ pitching motion anomaly has not been fully solved, it is suggested that the aerofoil model type, Reynolds and Mach numbers are of importance, in that the flow conditions at the leading edge may influence the stall vortex convection speed.

1

Contents.

2

contents (contd)...

contents (contd)...

Nomenclature.

AR   model aspect ratio

C_D drag coefficient

C_L lift coefficient

C_m moment coefficient

C_n normal force coefficient

C_p pressure coefficient

C_t thrust coefficient

c   aerofoil chord length (m)

h   wind tunnel height

k $\omega c/2U$ reduced frequency (sinusoidal motion)

M_∞ free stream Mach number

Re   Reynolds number

r $\omega c/2U$ reduced pitch rate

t   time (s) (non-dimensionalised as tU/c)

U   free stream speed (m/s)

u   stall vortex convection speed (m/s)

x   distance along aerofoil chord (m)

α incidence (degrees)

α mean angle of oscillation (degrees)

α amplitude of oscillation (degrees)

ω pitch rate (ramp-up, radians/s), oscillation frequency (sinusoidal motion, radians/s)

6

7

8

11

mid-chord.

Figure 74.   Stall vortex convection speed plotted as a function of reduced pitch rate for all the symmetrical sections tested at the University of Glasgow.

Figure 75.   Individual pressure transducer traces for the clean leading edge, high AR model. Ramp-up test at r=0.0215, Re=1.0x10^6. The initial vortex growth region is indicated at the mid-chord.

Figure 76.   Individual pressure transducer traces for the clean leading edge, high AR model. Ramp-up test at r=0.0074, Re=1.0x10^6. The initial vortex growth region is indicated aft of the mid-chord.

TABLES

Table 1.   Test conditions for measurements of stall vortex convection speed

Table 2.   Vortex convection speed as a function of hold angle during ramp-up tests at various reduced pitch rates for the NACA 0012 aerofoil (University of Glasgow data)

Table 3.   Comparison of contour plot/ ridge-line measurements with suction peak measurements

Table 4.   Comparison of convection speed from averaged and unaveraged data (NACA 0015, ramp-up)

Table 5.   Variation of aerodynamic coefficients with reduced pitch rate

13

1. INTRODUCTION.

The major limitation on the performance of an aerofoil is the phenomenon of stall; at a high enough fixed incidence, the effect of the increasingly strong adverse pressure gradient on the upper surface boundary layer causes it to separate, which is manifested by a drop in C_L and a rise in C_D. If the aerofoil is pitched rapidly, however, the symptoms of static stall can be suppressed and the catastrophic effects can be delayed to a much higher incidence. This is known as dynamic stall. Because of the delay in stall, very high lift coefficients can be generated, although very high drag and pitching moment coefficients can also result. In dynamic stall, the pitch range α, mean pitch angle α and reduced pitch rate r or reduced frequency k are of fundamental importance.

Dynamic stall is normally characterised by the initiation, shedding and convection over the upper surface of the aerofoil of a vortex-like disturbance (the so-called stall vortex) which induces a highly non-linear fluctuating pressure field. McCroskey et al (1981) described two fundamental types of dynamic stall:

1) Deep stall, occurring under extreme conditions of pitch rate, α and α. There are very large fluctuations in the aerodynamic coefficients and the qualitative features of the flow field are effectively independent of aerofoil shape, Re and motion type. Very strong vortex shedding occurs and there are large hysteresis loops on the aerodynamic loading history curves.

2) Light stall occurs under less severe conditions. Hysteresis still occurs on the aerodynamic loading history and the maximum values of the aerodynamic coefficients remain in the same range as their static equivalents. In this regime, the stall vortex is still formed, although it is quite weak.

Excellent descriptions of the overall effects of the stall vortex can be found in McCroskey et al (1981), McCroskey (1981), and Lorber & Carta (1987). Figures 1, 2 and 3 show typical plots of C_L, C_D and C_m versus α for the ramp-up pitching motion of a NACA 23012C aerofoil. Briefly, the events that are influenced by the stall vortex are as follows:

1) The beginning of the increased rate of increase of C_L and C_D and the fall in C_m (i.e. moment stall) relate to the formation of the stall vortex. Moment stall occurs as the stall vortex is released.

2) The maximum lift coefficient occurs when the vortex is at such a position over the

14

aerofoil to exert maximum suction.

3) Peaks in C_D and C_m occur as the vortex approaches the trailing edge.

The unsteady increments to C_L, C_D and C_m are related to the strength and speed of the stall vortex. Large changes in C_p also occur as the vortex passes over the aerofoil. Excellent flow visualisation pictures of the growth and convection of the stall vortex are presented by Walker et al (1985).

1.1 Applications of dynamic stall research and the present work.

Dynamic stall has always been of interest to helicopter researchers. The retreating blade is prone to the effects of dynamic stall as it is pitched up to compensate for its lower airspeed. Blade fatigue failure is to be avoided, so dynamic stall becomes a limiting factor (Ham & Garelick (1968)).

The present work, however, relates to a fundamental process in dynamic stall, that of the convection of the stall vortex, and finds its most direct application in the design of super-manoeuvrable aircraft. Super-manoeuvrability is a term used to describe flight patterns that involve drastic, dynamic changes in flight path, e.g. from a level cruise to nose vertical in a matter of seconds, perhaps as part of a missile avoidance procedure or a "point to shoot" manoeuvre. Lang & Francis (1985) present a detailed account of the requirements and likely flight envelope of

a super-manoeuvrable aircraft. As an example consider the case of a pitch-up to high α (after Lang & Francis (1985)). Figure 4 shows the aircraft attitudes and important features of the flow. Figure 4a shows the initiation of the manoeuvre, which may require large amplitude control surface deflections. These will generate powerful vortex structures which will affect neighbouring and

downstream lift and control surfaces. At higher α, as in Figure 4b, the high pitch rate will lead to dynamic stall of the lift and control surfaces; there is a temporary reorganisation of the flow field and high aerodynamic coefficients are generated. If these are to be exploited then the prediction and control of dynamic stall becomes necessary. Poor structural design and incorrectly tailored flight control system parameters, which would be the result of a poor appreciation of the dynamic stall effects, could lead to a catastrophic failure of the aircraft or an unsuccessful attempt at that manoeuvre.

Thus, potentially serious implications accompany any research into dynamic stall and this leads to the present problem. Since the motion of the stall vortex influences the dynamic response of the flight vehicle, the stall vortex convection velocity needs to be considered. While it is

15

generally accepted that this velocity is around one third of the free stream velocity, a degree of controversy exists over its dependency on the aerofoil motion. The convection velocity has been measured in a variety of ways by several researchers. Lorber & Carta (1987) performed a series of ramp-up tests on a Sikorsky SSC-A09 aerofoil; their data show that downstream of x/c=0.1 the vortex speed is uniform and that it increases linearly with reduced pitch rate from a value of about 0.13U at r=0.001 to 0.33U at r=0.02 (Figure 5). This conclusion that the convection speed is a function of the aerofoil motion is in agreement with the works of Carta (1974), St. Hilaire & Carta (1983), Robinson & Luttges (1983) and Aihara et al. (1984). No functional dependency was reported by Chandrasekhara & Carr (1989) and Jumper et al. (1986), however. In addition, a preliminary analysis of the stall duration by Galbraith et al. (1986) showed no functional dependency on aerofoil motion. The following section discusses the results and measurement techniques in greater detail.

1.2 Previous measurements of the stall vortex convection speed.

As the stall vortex passes over the aerofoil, the pressure on the aerofoil surface changes. This appears as a wave on the surface pressure time history, as in Figure 6. Carta (1974) calculated the velocity of the wave over a sinusoidally oscillating NACA 0012 aerofoil by contour plotting C_p in time and space. The contour plot derived from Figure 6 is shown in Figure 7; the locus of the

wave is indicated on the figure by the ridge line. Note the kink in the ridge line at x/c=0.25. In the vicinity of the leading edge, multiple waves were seen to emerge, and Carta attributed the presence of the kink to wave coalescence. The wave speed is given by the gradient of the ridge line. Figure 8 shows Carta's measurements of the initial and average wave velocities as a function of reduced frequency. The results indicate that the mean convection speed is increasing with increasing reduced frequency and that it depends on the mean incidence. Of particular concern, however, is the accuracy of measurement, which must ultimately depend on how well defined the ridge line is. The above method of analysis may therefore be prone to subjective errors.

The same contour plot/ ridge line technique was used by St. Hilaire & Carta (1983), again on a sinusoidally oscillating NACA 0012. They measured the wave velocity over three portions of the aerofoil (x/c = 0.004 to x/c = 0.028, x/c = 0.028 to x/c = 0.149 and x/c = 0.149 to the trailing edge). The vortex convection speed increased with reduced frequency over each part of the aerofoil, the variation being stronger further along the aerofoil. They also observed that the wave speed was lowest where the pressure gradient was highest, i.e. in the leading edge region.

The analysis technique adopted by Lorber & Carta (1987), although related to the contour plot/ ridge line method, was more direct and was not prone to subjective errors. Data was gathered

16

for ramp-up and sinusoidal motions of a Sikorsky SSC-A09 aerofoil. They observed that minima in the local pressure-time histories accompanied the passage of the stall vortex. The chordwise positions of these suction peaks were then plotted against time, and the resulting straight line showed that the convection speed (equal to the gradient) was constant along the chord. The vortex speed was found to increase linearly with reduced pitch rate, as shown in Figure 5. These data were a significant improvement on Carta's (1974) data by virtue of improved facilities and instrumentation and a greater number of pressure tappings on the model (18 chordwise locations as opposed to 10). Thus, Lorber & Carta's (1987) data tends to confirm the dependency of the convection speed on the aerofoil motion.

Other contributions are as follows:

1) Robinson & Luttges (1983) performed their experiments at substantially lower Reynolds numbers than Carta ($6 < Re \times 10^{-4} < 14$ compared to $Re > 10^6$). Convection speed was measured from flow visualisation results, and it was found to increase with increasing reduced frequency (from $u/U=0.17$ at $k=0.25$ to $u/U=0.28$ at $k=0.75$). Interestingly, there was no dependency on the Reynolds number.

2) Jumper et al (1986) measured the stall and separation angles relative to the static case for ramp-up motions of a NACA 0015 aerofoil. The Re range investigated was $1.58 < Re \times 10^{-5} < 2.81$. The convection speed was deduced from the delay angle and it was found to be independent of reduced frequency with a value of 0.4U.

3) Chandrasekhara & Carr (1989) performed flow visualisation tests on a sinusoidally oscillating NACA 0012 aerofoil in the range $2 < Re \times 10^{-5} < 9$. Their results showed that the convection speed was constant at 0.3U.

4) Finally, rather than using Carta's contour plot/ ridge line analysis technique for determining the wave speed, Galbraith et al (1986) used two distinct features associated with the passage of the stall vortex to determine a stall vortex time delay. These features were the divergence in C_p at 34% chord and the minimum C_p at the trailing edge. The time delay was found to remain constant as reduced pitch rate was varied. Galbraith et al. also used timing marks on McCroskey et al's (1982) data to measure a time delay, which was also found to be independent of reduced frequency. An appraisal of time delay measurements is given in section 5.

It may be concluded from the above that, where the dependency of convection speed on aerofoil motion is concerned, significant differences exist between the various works.

17

Other aerodynamic phenomena were reported to depend on reduced frequency, a description of which follows.

1.3 Stall events and aerodynamic coefficients.

The formation and release of the stall vortex influences the behaviour of the lift, drag and pitching moment coefficients (see earlier). Lorber & Carta (1987) reported on how the stall event angles (i.e. the incidences at which moment stall, lift and drag rise, minimum C_m and maximum C_L and C_D occur) increased with increasing reduced pitch rate. These results are shown in Figure 9. The difference between the incidences at C_m min and C_m stall varies approximately linearly with $\sqrt{r}$. According to Lorber & Carta, this shows that the convection speed is proportional to r (compare this with Jumper et al's observations). Lorber & Carta also reported that the dynamic increments in C_L, C_m and C_D had an approximately linear dependence upon r (Figure 10).

St. Hilaire & Carta (1983) defined the stall inception angle as the incidence at which the first precipitous collapse in C_p occurred. This angle was found to increase linearly with reduced frequency. In addition, they found the aerodynamic damping to be reduced frequency dependent. Increasing the reduced pitch rate reduces the lift-curve slope, as has been reported by several authors (e.g. Jumper et al (1986), Lorber & Carta (1987)).

1.4 The present work.

The purpose of this report is to outline a course of research that is intended to shed light on the convection speed problem. Those works involving Carta are of most direct relevance, since the test conditions most closely resemble those of the University of Glasgow database, although the results of other studies will be useful. Carta's data suggests that the model motion is important, whereas analysis of the University of Glasgow database suggests the opposite. A point which at this stage can be noted is, that if the vortex speed is reduced pitch rate dependent for ramp-up motion, then why should a similar dependence exist for a sinusoidal motion, where pitch rate is constantly changing?

It may be that the free stream Mach number has an important effect on the dynamic stall process. Lorber & Carta (1987) performed tests at $M_\infty = 0.2$, 0.3 and 0.4. As M_∞ increased, convection speed was still found to increase with r. The University of Glasgow data, however, is mostly for $M_\infty=0.12$. For $M_\infty=0.12$, $C_{p\ sonic}=-46.3$, whereas for $M_\infty=0.2$, $C_{p\ sonic}=-16.3$, although at $M_\infty = 0.2$ Lorber & Carta's data did not appear to show any locally supersonic flow.

18

Chandrasekhara & Carr (1989) carried out a series of flow visualisation tests in the range $2 < Re \times 10^{-5} < 9$ with M_∞ increasing from 0.15 to 0.45. They observed that the behaviour of the stall vortex (particularly its inception) changed above the range $M_\infty = 0.25$ to 0.3; the point of inception was seen to move downstream as M_∞ increased. Further more, the inception became reduced frequency dependent above this critical Mach number. They proposed that locally supersonic flow could play an important part in the process of vortex formation, and that the effects of compressibility could weaken the stall vortex. Certainly, stall was observed to occur at lower incidence as Mach number increased.

An additional influence on the data is the restricted wind tunnel flow. All of the experiments cited have fairly high blockage ratios. As dynamic stall occurs large changes in wind tunnel dynamic pressure will occur, which may to some extent drive the dynamic stall phenomena. Table 1 shows the test conditions for all the works cited. The original measurements of convection speed by Carta (1974) were from a model with AR=0.8 and a chord to tunnel height ratio (c/h) of 0.28. These compare to Lorber & Carta's (1987) model dimensions of AR=5.56 and c/h=0.18. The conditions for the University of Glasgow data are AR=2.91 and c/h=0.26. Thus, although Lorber & Carta's (1987) measurements were at high AR and low c/h, Carta's (1974) measurements at low AR and high c/h still produced a motion dependency. This matter complicates the assessment of the University of Glasgow data (moderate AR and c/h comparable to Carta (1974)) for wind tunnel effects. Ericsson & Reding (1971) commented that the effect of a change of AR was enough to change the stall type from trailing edge to leading edge. This comment was based on data available from tests on a NACA 0012 aerofoil, which is liable to experience changes in stall type. However, the effect of a change of stall type on the convection speed is not clear, since after the stall vortex has been released the aerofoil is fully stalled anyway.

1.5 Summary.

There appears to be a significant disharmony between the existing data as to the convection speed of the dynamic stall vortex. A comprehensive analysis of the University of Glasgow Dynamic Stall database to measure the stall vortex convection speed over a number of aerofoil models as a function of pitch rate and motion type will be carried out in an attempt to shed light on the problem.

19

2. THE UNIVERSITY OF GLASGOW DYNAMIC STALL
TEST FACILITY AND AEROFOIL MODELS.

The test aerofoils, of chord length 0.55m and span 1.61m were constructed of a fibre-glass skin filled with an epoxy resin foam and bonded to an aluminium spar. The profile shapes were accurate to 0.1mm. Data from the NACA 23012, 23012A, 23012B, 23012C, 0012, 0015 and 0018 aerofoils were analysed and the aerofoil shapes and coordinates are shown in figures 11 to 17 respectively. The NACA 23012 is essentially a trailing edge stall type aerofoil. The 'Λ' modification has a reflex trailing edge to enhance forward movement of the separation point, the 'B' modification is a thickened version of the NACA 23012 with a modified lower surface, and the 'C' modification is a high camber version of the basic profile designed to enhance trailing edge separation. Each model was mounted vertically in the University of Glasgow Handley-Page wind tunnel, which is a low-speed, closed-return type with a 1.61m by 2.13m octagonal working section as shown in figure 18. The aerofoil models were pivoted about the quarter chord point using a linear hydraulic actuator and crank mechanism.

The instantaneous aerofoil incidence was determined by a linear, angular potentiometer geared to the model's tubular support. The dynamic pressure in the wind tunnel working section was obtained from the difference between the static pressure in the working section, 1.2m upstream of the leading edge, and the static pressure in the settling chamber, as measured by an electronic manometer. Thirty ultra-miniature pressure transducers were installed below the surface of the centre-span of each model.

A series of experiments was performed on each aerofoil by rotating it about the quarter chord axis under four types of motion: steady, oscillatory (sinusoidal) and constant pitch-rate ramp motions in both positive and negative directions. The collected data were stored in unformatted form on a DEC MicroVAX mini-computer in a dedicated database.

2.1 Test procedure.

2.1.1 Ramp-up test.

During a ramp-up test, the model's angle of attack was changed at a constant pitch rate over a preset arc, in this case from -1° to 40°. Five sets of 256 data sweeps were recorded for each test condition.

20

2.1.2 Sinusoidal test.

For a sinusoidal test, the model was oscillated about its quarter chord point so that its angle of incidence varied sinusoidally with time. Ten sets of 128 data sweeps were recorded for each test condition.

3. PRELIMINARY RESULTS OF ANALYSIS OF THE UNIVERSITY OF GLASGOW DYNAMIC STALL DATABASE.

Collected data for the NACA 23012, 23012A, 23012B, 23012C, 0012, 0015 and 0018 aerofoils were analysed. This section discusses measurements of the stall vortex convection speed for all the above aerofoils. Some assessments of the aerodynamic coefficients are also presented. For the NACA 23012C aerofoil, additional measurements of the stall vortex velocity found using the pressure contour technique and the stall vortex duration time are discussed. The nominal test conditions were Re= 1.5×10^6 and $M_\infty = 0.11$. The complete test data for the above aerofoil models are described in Seto & Galbraith (1984) for the NACA 23012, Niven (1988) for the NACA 23012A, Herring & Galbraith (1988) for the NACA 23012B, Gracey & Galbraith (1988) for the NACA 23012C and Angell, Musgrove & Galbraith (1988a, b) for the NACA 0015 and NACA 0018 sections. The NACA 0012 has only recently been tested and the test data is not yet available in a standard report form.

3.1 Stall Vortex Convection Speed

3.1.1 Ramp-up Motion.

To measure the vortex convection speed from the pressure data, the suction peak technique adopted by Lorber & Carta (1987) was used; its advantage over the contour plot/ ridge line technique used by Carta (1974) is its systematic nature. Figure 19 shows the pressure data for the NACA 23012C aerofoil performing a ramp-up pitching motion from -1^0 to 40^0 at a reduced pitch rate of 0.032. Only the pressures on the upper surface are shown. Each trace shows the pressure recorded as a function of time at a particular chordwise location. The variation of incidence with time is shown at the bottom of the figure. The suction peaks caused by the passage of the stall vortex are indicated by the symbols. As the vortex passes over the trailing edge, an in-rush of air develops (a vortex shedding from the trailing edge), and the pressures measured by the last three transducers (at $x/c = 0.9, 0.97$ and 0.9875) are indicating this rather than the stall vortex motion itself. Thus, the suction peaks measured at these locations were not used in the analysis.

21

The timing of the relevant suction peaks was measured using an interactive graphics programme running on the MicroVAX. The software could be used to analyse any run of any motion type. After measuring the occurrence time of each of the suction peaks, the passage of the vortex was plotted in terms of chordwise position, x/c, against non-dimensional time, tU/c. The plot of vortex position against time for Figure 19 is shown in Figure 20. The important region is the last 70% of chord. The motion of the stall vortex in the range $0.27<x/c<0.83$ is approximately uniform and the least squares straight line fit through the relevant points gives a correlation coefficient of 0.994. The gradient of the straight line is a measure of the stall vortex convection speed and Figure 20 shows that at a reduced pitch rate of 0.032 it is 34.9% of the free stream speed.

The above analysis technique was applied to the ramp-up test cases for the NACA 23012C aerofoil in the reduced pitch rate range $0.008<r<0.034$. Excellent least square fits in the range $0.27<x/c<0.83$ were obtained in each case, and the correlation coefficient was always above 0.97. Figure 21 shows the stall vortex convection speed for this aerofoil plotted as a function of reduced pitch rate. Although the scatter is large, the tentative conclusion made from this Figure is that the stall vortex convection speed is independent of reduced pitch rate in the range $0.008<r<0.034$ under the present conditions. It is important to note here that measurements of the convection speed for $r<0.008$ were not taken because the induced suction peaks were too weak.

Pressure data held on the University of Glasgow Dynamic Stall database for the NACA 23012, NACA 23012A, NACA 23012B, NACA 0012, NACA 0015 and NACA 0018 aerofoils undergoing ramp-up motions were analysed as above. The data for the NACA 0021, NACA 0025 and NACA 0030 aerofoils could not be analysed in the same way since the vortex induced suction peaks were too poorly defined. The individual results for vortex speed as a function of reduced pitch rate for each aerofoil are shown in Figures 22 to 27. All the vortex speeds were measured over the last 70% of chord, and in each case the least squares fit correlation coefficient was good indicating a uniform convection speed. In general the convection speed is independent of reduced pitch rate for each case, over the measured range of reduced pitch rate. At low r, the suction peaks for the NACA 0015 and 0018 models become too poorly defined, hence the range of reduced pitch rate shown for these two models is restricted. Some results, notably Figure 26 for the NACA 0015 appear to show an oscillatory variation of the convection speed about the mean value. When the general level of scatter shown by the results of the other aerofoils is considered, this apparent variation becomes insignificant. In addition, the variation disappears when the unaveraged data are analysed (see later).

Figure 28 shows all the measured stall vortex convection speeds plotted together. The level of scatter is large, although the result of over one hundred tests are shown. If the scatter is taken

22

into account, it may be concluded that the mean convection speed is the same for each aerofoil, with the notable exception of the NACA 0012, which has a mean convection speed an appreciable amount lower than the rest of the models. This will be referred to later. The data strongly suggest that the stall vortex convection speed is independent of reduced pitch rate to a first order.

3.1.2 Oscillatory Motion and Effect of Motion Type.

The dynamic stall database contains a great deal of data relating to sinusoidal tests. To measure the stall vortex convection speed, Lorber & Carta's (1987) suction peak analysis technique was applied in the same way as for the ramp-up cases. Figure 29 shows the plot of vortex position against time for the NACA 23012C aerofoil oscillating at a reduced frequency of 0.176 with a mean angle of 20^0 and an amplitude of 10^0. It is important to note that in the region of interest (x/c>0.27) the vortex speed is uniform in spite of the non-uniform aerofoil motion. The least squares straight line fit is excellent and the vortex convection speed is 32.7% of free stream. Figure 30 shows the variation of convection speed with reduced frequency for the NACA 23012C oscillating with a mean angle of 20^0 and an amplitude of 10^0 and 8^0. The amount of scatter is similar to the results for the ramp-up motion and the conclusion made from this Figure is that the convection speed is independent of reduced frequency for sinusoidal oscillations.

It is felt that the convection speed is independent of motion type in general. A region of non-linear motion is indicated on Figure 28 for the ramp-up data (the degree of non-linearity increases with increasing reduced pitch rate). In this region, the aerofoil is decelerating to zero pitch rate while the vortex is still over the aerofoil surface, and in spite of this the convection speed is independent of reduced pitch rate throughout. In addition, Figure 30 shows that the convection speed is independent of oscillation amplitude for a sinusoidal test (instantaneous pitch rate is proportional to amplitude). Thus, the results shown in Figures 28 and 30 in fact indicate a range of motion types as well as pitch rates, and the convection speed is constant throughout.

3.1.3 Ramp-and-hold motion tests on the NACA 0012

Further testing at University of Glasgow involved ramp-and-hold motion tests, where the aerofoil was pitched up and held at a comparatively low incidence, particularly below the start of vortex convection. The purpose of these tests was to further assess the effect of motion type upon convection speed. The results are shown in table 2 for a variety of hold angles and pitch rates. Also shown on this table are the incidences at which the stall vortex is at x/c=0.17 for the standard test case at each pitch rate. Considering the normal level of scatter for the NACA 0012, the hold angle can be judged to have had no noticeable effect upon the vortex speed, i.e. the vortex convects at the same speed even though the aerofoil is no longer pitching. Note that the motion of the stall vortex

23

remained uniform throughout the ramp-and-hold period.

3.2 Summary of results of preliminary analysis.

Measurements of the stall vortex convection speed from pressure data held on the University of Glasgow dynamic stall database show that:

i) The convection speed is independent of reduced pitch rate for a ramp-up motion and reduced frequency for a sinusoidal motion to a first order.

ii) The convection speed is independent of model type to a first order.

iii) The convection speed is independent of motion type to a first order.

The above statements are made with the reservation that the NACA 0015 and NACA 0018 data analysis was confined to high r only, and that the scatter in the data is high. That the results for the NACA 0012 are consistently lower than for the other models may be significant, and further comment is offered in section 7.

3.3 Alternative Measurements of Convection Speed

Carta's (1974) contour plot/ ridge line analysis technique was applied to a few test cases from the database. Figure 31 shows the contour plot for the NACA 23012C aerofoil performing a ramp-up motion at a reduced pitch rate of 0.032. The upper surface of the aerofoil is on the left half of the plot and time is plotted on the vertical axis. The trailing edge is on the left and the leading edge is at the centre of the plot. The stall vortex wave starts at $tU/c=11.4$ just behind the leading edge, which then appears as a ridge on the contour plot pointing from right to left and in the direction of increasing non-dimensional time as indicated. The ridge line is curved near to the leading edge, indicating non-uniform motion, although over the rest of the aerofoil surface the ridge line locus is reasonably straight. The gradient of the ridge line indicates the wave speed, and in this case the measured wave speed is 30% of the free stream speed. Figure 32 shows the variation of convection speed with reduced pitch rate for the NACA 23012C aerofoil undergoing ramp-up motion found using the contour plot/ ridge line analysis technique. Also shown on this Figure are the results from the previously described suction peak location technique. In general, the comparison between the two techniques is good, although the less systematic nature of the contour plot technique generates more scatter.

The contour plot analysis technique was also used for sample ramp-up test cases for all the

24

other aerofoils and for a sinusoidally oscillating NACA 23012C test. Table 3 shows how the results from this technique agree with those of the suction peak analysis technique. On the whole the agreement is good, although during the analysis it was noticed that the likely error on measuring the ridge-line gradient was large when the vortex induced suction was weak, i.e. at low pitch rate or on a thick aerofoil.

3.4 Analysis of Unaveraged Data.

The results discussed so far have related to the analysis of averaged data only; ramp-up motions were averaged over five cycles and sinusoidal motions were averaged over ten cycles. Three sets of unaveraged data for the NACA 0015 results were analysed. Table 4 shows how the unaveraged data results compare with the averaged data. The first point to note is that the two sets of data are slightly different which is a consequence of the averaging process. However, the results of the averaged data lie within the range of scatter of the unaveraged data, which indicates that the analysis of the averaged data gives representative results. Additionally, the apparent oscillatory variation of convection speed with reduced pitch rate shown by the averaged data referred to earlier is not shown by the unaveraged data, and so is insignificant within the level of scatter shown.

3.5 Stall Duration Time

The subject of Galbraith et al's (1986) paper was the duration of dynamic stall as defined by the time delay between the rise in C_p at x/c=34% and the peak suction at the trailing edge (see the later section on the appraisal of this technique). C_p rise at x/c=34% was chosen because it is the first manifestation of dynamic stall for the particular aerofoil (this phenomenon coincides with C_n rise). Their measurements indicated that the stall duration was independent of the reduced pitch rate. (Note that the stall duration is equal to a vortex development time plus the time for the vortex to convect over the aerofoil, and it cannot therefore be compared directly to the present measurements of convection speed.)

These stall duration time measurements were repeated during the present analysis. The transducer at x/c=83% was used for the final timing mark rather than one close to the trailing edge since the pressure traces there appeared to show the development of an in-rush of fluid and the formation of a trailing edge vortex. Figure 3 shows the results of the present analysis for the NACA 23012C; the stall vortex duration is independent of reduced pitch rate. This result verifies Galbraith et als' (1986) original measurements.

3.6 Aerodynamic Coefficients

The development and convection of the stall vortex influence the timing and magnitude of the aerodynamic coefficients. For example the times of $C_n$rise and C_p divergence at x/c=34% are strongly correlated with each other, as are the times of $C_n$max and $C_p$min at x/c=48%. Likewise, C_m divergence correlates with C_n rise, and $C_m$min occurs when the stall vortex is close to the trailing edge.

As part of the analysis, the incidences at which $C_n$max and $C_m$min occurred were measured for each aerofoil for ramp-up motions. In addition, the incidence at $C_n$rise was measured. Only the results for the NACA 23012C aerofoil are presented here, since the results for the other aerofoils showed similar trends. Figure 34 shows the variation of α at $C_n$max with reduced pitch rate. The variation is linear up to r<0.029. Above this pitch rate, the aerofoil motion becomes non-linear during the vortex convection phase; the aerofoil is decelerating to zero pitch rate. Figure 35 shows the corresponding variation of $C_n$max with r, which approximately reflects the variation in stall vortex strength with reduced pitch rate. The corresponding incidences and coefficient values for minimum C_m are shown in Figures 36 and 37. Finally, the incidences at C_n rise and C_m divergence vs r are shown in Figures 38 and 39. All the variations with reduced pitch rate are linear, as shown by the excellent least square fits to the data.

4. COMPARISON OF THE RESULTS OF THE UNIVERSITY OF GLASGOW DATABASE WITH THE RESULTS OF LORBER & CARTA (1987).

The present section compares the data from the University of Glasgow tests with results presently available. Lorber & Carta's (1987) results are also assessed based on analysis of their data at University of Glasgow.

4.1 Stall vortex convection speed.

Figure 28 shows how the measurements of convection speed from the present analysis compare with the results of Lorber & Carta (1987). The University of Glasgow data strongly suggests that the convection speed is independent of reduced pitch rate. Lorber & Carta's (1987) results, however, indicated that the vortex velocity increased linearly from u/U=0.13 at r=0.001 to u/U=0.33 at r=0.02, which is in direct contrast to the present results. In spite of the large amount of scatter contained in the present results, no dependency similar to Lorber & Carta's result can be

26

reasonably found to fit the data. Similarly, the stall vortex speed for a sinusoidally oscillating aerofoil is independent of reduced frequency (Figure 30), whereas the results of Lorber & Carta's data appear to show a strong dependency on reduced pitch rate at stall, and the results of Carta (1974) show a strong dependency on reduced frequency.

4.2 Aerodynamic coefficients.

Table 5 shows how the dependency of the aerodynamic coefficients on reduced pitch rate from the present analysis compare with the results of Lorber & Carta (1987). Only the gradients of the straight line fits are presented, since the actual coefficient values depend on the aerofoil shape and individual stalling characteristics. Note that measurements of $C_n max$ are being compared with Lorber & Carta's results for C_L.

The incidence at $C_n max$ compares well with Lorber & Carta's result for C_L, although the comparison of the actual values of $C_n max$ with Lorber & Carta's C_L is poor. However, the wide variation between the $C_n max$ values shown by the different aerofoils in the present analysis suggests that the latter comparison may only be qualitative; $C_n max$ is influenced by the behaviour of the flow prior to stall, and not just the stall vortex, and therefore, it is hardly surprising that the variations are different from one another. A similar pattern can be seen when comparing the maximum absolute moment coefficient; the incidence shows a similar trend to Lorber & Carta's data, while the value of C_m itself compares relatively poorly.

As a final comparison, figure 40 shows the time delay between Cd rise and Cm min for the NACA 23012C and Lorber & Carta's data as a function of reduced pitch rate. The agreement between the two data sets is excellent and this is discussed in section 5.

4.3 Appraisal of Lorber & Carta's data

Lorber & Carta's (1987) data were made available to the University of Glasgow by the AFOSR for our own scrutiny. This provided an ideal opportunity to assess the data and eliminate differences such as analysis technique.

4.3.1. Lorber & Carta's experimental rig

As part of their test programme, Lorber & Carta (1987) performed ramp-up tests on a Sikorsky SSC-A09 aerofoil, the profile and surface coordinates of which are shown in figure 41. The Sikorsky SSC-A09 is a 9% thick, supercritical section with a sharp leading edge (0.7%

27

leading edge radius) and the model used had a chord length of 43.9cm. The model was constructed from a 14cm wide by 2.5cm thick steel spar which spanned the 2.44m working section of the UTRC Large Subsonic Wind Tunnel. It was supported at the ends by 10cm diameter circular shafts, and two quarter chord supports were attached to the spar to add further support and to prevent excessive oscillations during testing. Spar bending and twist deflections were measured using strain gauge bridges. Fibre glass panels were mounted along the spar to make up the surface profile. Each end of the model span was driven by a hydraulic actuator, the positions of which were set by rapidly responding servo valves. High frequency angular transducers were mounted at each end of the spar, and safety circuits were used to shut down the actuators if the angular difference between the two ends became too great. A digital waveform synthesiser supplied the external signal to the controller for the actuators.

The model was instrumented with surface mounted pressure transducers, pressure tappings and hot film anemometers. In all there were 72 surface mounted pressure transducers (Kulite model XQC-73U-093-15D) positioned in four arrays. The main array consisted of 36 (18 on each surface) mounted 20.3cm away from the wind tunnel centreline. Two secondary arrays of 10 upper and 6 lower surface mounted transducers were positioned 40.6cm and 70cm away from the tunnel centreline. These secondary arrays were used to assess the two dimensionality of the flow which was found to be satisfactory. Finally, four pressure transducers were mounted at an angle of 30 degrees to the flow direction which were for use in future swept wing experiments. The surface pressure tappings were connected via a scanivalve to a single pressure transducer, and they were used to measure the steady flow and to verify the operation of the pressure transducers. These tappings were situated on the opposite side of the wind tunnel centreline (15.2cm) to the surface mounted gauges. Finally the hot film gauges were located in a staggered array near to the primary pressure transducer array. The positions of the pressure transducers and hot film gauges are shown in figure 42.

Data acquisition was performed as follows. Analogue signals from the pressure transducers, hot films, pitch angle transducers, spar twist angle and bending strain were first conditioned by a set of pre-amplifiers. Additional signal conditioning (subtracting of offsets, amplification and low pass filtering) was performed by a pre-programmed 26 channel ATLAS. A Perkin-Elmer 3210 super mini-computer acted as the central processor. Simultaneous sample-and-hold analogue to digital converters (variable sampling frequency between 0.3KHz and 250KHz) digitised the signals and held the measured voltages in local memories of 1024 samples each. A separate digitising system driven by the Perkin-Elmer was used to measure parameters such as barometric pressure, dewpoint, wind tunnel temperature, total pressure and test section static pressure.

28

4.3.2 Test details

The data provided by the AFOSR were mostly from ramp-up tests, although one sinusoidal test case was included. The tests at a Mach number of 0.2 were of greatest importance, since they most closely resemble the test conditions at University of Glasgow. FORTRAN subroutines were written which read in the supplied data in a format which allowed all the standard analysis software at University of Glasgow to be used. In this way, any ambiguities in the analysis techniques could be eliminated and any important differences in the pressure data would be apparent.

Figures 43a and b show the standard plots (pseudo 3-D surface pressure plot and Cn, Ct, Cm as a function of incidence and time) from the primary pressure transducer array for ramp-up tests at r=0.001 and r=0.02 respectively. A vortex like disturbance moving along the aerofoil surface can be clearly seen on both of the test cases.

4.3.3 Results of analysis

Lorber & Carta's (1987) analysis technique was applied to their data in the same way as to the University of Glasgow data. Figure 44 shows the pressure data/ surface-time history for a 0-30 deg ramp-up at r=0.02. The trailing edge pressure trace is at the lower portion of the figure and the leading edge trace is at the top. The measured timing points are indicated by the symbols. The vortex locus is shown in figure 45, and it can be seen that it is linear over the majority of the aerofoil surface (i.e. the convection speed is constant). The convection speed is equal to the gradient, which was found from the least squares fit. The convection speed measurements for the 0-20 deg and 0-30 deg ramp-ups plotted as a function of reduced pitch rate are shown in figures 46a and 46b. As can be seen, the speeds increase with increasing reduced pitch rate. The agreement between the measurements for a 0-20 deg ramp and for the 0-30 ramp is good, which indicates a respectable level of repeatability and accuracy. Lorber & Carta's original measurements for the 0-30 deg ramp are also shown, together with their straight line fit; the overall level of agreement between the independent analyses by Lorber & Carta and at the University of Glasgow is excellent.

4.3.4 Discussion

The analysis of Lorber & Carta's data at University of Glasgow has shown that the discrepancy between the two data sets is not due to a fundamental difference in analysis technique. The problem is complicated, however, by the excellent agreement between the pitch rate trend shown by the time delay between C_D rise and C_m min (figure 40). (C_D rise is associated with stall

29

vortex growth, while C_m min occurs when the vortex is near to the trailing edge.) C_m min is primarily influenced by the strength of the stall vortex, while the timing of C_D rise can indicate the encroachment of trailing edge separation, so the above described quantities may not be entirely relevant to the convection speed.

An important difference is that Lorber & Carta obtained measurements at a lower pitch rate than would be expected from the University of Glasgow data. As the reduced pitch rate decreases, the strength of the stall vortex also decreases. It was found during the analysis of the University of Glasgow data that if the stall vortex was too weak, then the convection speed was difficult to measure since the suction peaks were also too weak. Until the testing of the NACA 0012 the lowest pitch rate at which the convection speed was measured was r=0.008 for the NACA 23012C. The suction peaks for Lorber & Carta's data, however, were strong enough even at r=0.001 for sufficiently accurate definition of the vortex convection.

The main difference between the two data sets at low pitch rate is the sampling frequency. At r=0.001, Lorber & Carta used a sampling frequency of 470Hz, while a 54Hz sampling rate was used at r=0.0016 for the NACA 0012 tested at University of Glasgow (compare figures 47 and 48 for the two tests respectively). The effect on the quality of the data is significant; Lorber & Carta's data is smooth, while the University of Glasgow data shows poorer resolution., which is a consequence of the smaller number of samples in the incidence range of interest. The main reason for the difference in sampling rates is that the DEC MINC II recorded up to 256 sweeps, while Lorber & Carta's system recorded up to 1024. In addition, the University of Glasgow data was sampled over -1° to 40° with a period of hold afterwards, while Lorber & Carta's data was sampled over an incidence range of 20° or 30° with no period of hold. Therefore, in an attempt to obtain data of similar resolution to Lorber & Carta's at low r, tests were performed on the NACA 0012 model with high sampling frequency over the relevant incidence range (the maximum sampling frequency was 550Hz). Figures 49a and 49b show the data at r=0.006 for a low and a high sampling frequency respectively. The passage of the vortex is clearer and the resolution of the suction peaks is much better. Using the higher sampling frequency, the convection speed down to r=0.006 could be measured for the NACA 0012 (compared to r=0.01 under normal circumstances for this aerofoil).

In a response to the preliminary analysis at the University of Glasgow, Lorber & Carta (private communication) suggested that the convection speed was constant at high r, while at low r it was pitch rate dependent. The University of Glasgow high sampling frequency result at r=0.006, however, shows no reasonable indication that this might be true.

30

As a final note, Lorber & Carta (1987) performed ramp-up tests with limited ramp arcs. Although they found that stopping the aerofoil motion while the vortex was still convecting did not affect the value of the convection speed, they noticed that the motion of the vortex was temporarily affected, which they attributed to the formation of a stopping vortex which convected downstream from the leading edge. (Compare this with the University of Glasgow result for the NACA 0012, where the vortex convects uniformly through the ramp-and-hold.) During the convection of this vortex, the stall vortex motion was interrupted, which then continued at the same speed as before after the two vortices merged. (The implication is that the stall vortex motion would be unaffected if the stopping vortex had not formed from the leading edge.) These tests suggest that the role of pitching motion even in Lorber & Carta's data is secondary once the vortex is convecting; i.e. the behaviour of the vortex is dictated before it has shed, through its size, strength and position of origin.

4.4 Summary of comparison of University of Glasgow data with Lorber & Carta's data and continuation of the research

A significant anomaly exists between the convection speed measurements of Lorber & Carta (1987) and those obtained at the University of Glasgow for its seven aerofoils. Independent analysis of Lorber & Carta's data and further experiments at University of Glasgow have reinforced the anomaly, rather than lead to any clues as to its cause. Various features, such as the variation of the aerodynamic coefficients with reduced pitch rate, are common between the two data sets, however.

In an effort to further validate the University of Glasgow data, it was decided to build and test a NACA 0015 model with a blockage half that of the exisiting models. This model would therefore be of slightly superior dimensions than Lorber & Carta's SSC-A09. The motivation behind this test programme was to assess the University of Glasgow data for constraint effects, which at this stage might be seen as a major cause of the anomaly (see table 1). The testing and results of this new model are described in section 6.

5. APPRAISAL OF MEASUREMENT OF TIME DELAYS FROM AERODYNAMIC COEFFICIENT DATA.

Galbraith et al's (1986) analysis of McCroskey et al's (1982) data used the time delay between C_D rise and the minimum C_D immediately after C_D max to infer a vortex development time. (Time delays measured in this fashion relate to the development of the stall vortex and part of its convection over the aerofoil surface, and therefore do not fully relate to the present stall vortex convection speed problem.) These measurements were repeated for the NACA 23012C data for the

31

purpose of the present analysis. The analysis showed, however, that the use of aerodynamic coefficients alone to find time delays may be inadvisable. The reasons for this are as follows:

i) The time delays for $C_D$rise to $C_D$min from McCroskey et al's (1982) data and the University of Glasgow data for sinusoidal motion are independent of reduced frequency. However, a comparable time delay measured from the University of Glasgow *ramp-up* data shows a dependency on reduced pitch rate.

ii) The time delay between $C_D$rise and $C_m$min was measured from Lorber & Carta's (1987) ramp-up data and the University of Glasgow data. The same dependency on reduced pitch rate was shown by each (i.e. high time delay at low r reducing to a more or less constant value at high r). This apparently contradicts the result for the convection speed. However, the phasing of leading edge suction, trailing edge separation and vortex development are all important in determining the airload time history, so the cause of $C_D$rise may change as the pitch rate changes and as the aerofoil shape is altered. This is particularly important if it is considered that Lorber & Carta's test aerofoil was a sharp leading edge type of only 9% maximum thickness, whereas all the University of Glasgow aerofoil models were thicker with rounder leading edges. It was considered, therefore, that use of such time delays in the absence of pressure data of adequate quality to scrutenise will contribute little to the convection speed problem.

6. INVESTIGATION OF CONSTRAINT EFFECTS: TESTING OF A HIGH ASPECT RATIO NACA 0015 MODEL

As described at the end of chapter 4, a NACA 0015 model of half the chord length of the existing models at University of Glasgow was to be built and tested. This chapter describes the testing and data analysis of this model, which will be referred to as the high AR model. The previous models tested will be referred to as standard models.

6.1 Description of test rig and data acquisition system

Owing to its shortened chord length, the blockage and aspect ratio of the high AR model, when installed in the Handley Page wind tunnel, were slightly superior to Lorber & Carta's (1987) test configuration. However, because of the higher tunnel speed to reach the required Re (the maximum in this case 1.1×10^6), the DEC MINC data acquisition system could not be used, since its highest sampling rate was only 550Hz. At this sampling rate, the vortex convection phase

would be completed in about 10 samples, which would lead to poor resolution of data and a subsequent loss of accuracy (this problem is somewhat reminiscent of the differences in the quality of data at low r between Lorber & Carta's (1987) and the NACA 0012 data). Thus it was decided to use the Thorn EMI BE-256 420 series transient data recording system for the ramp-up tests, details of which follow.

The aerofoil model was instrumented with 30 Kulite XCS-093-psi G ultra miniature pressure transducers, which were surface mounted along the centre span of the model. The transducers were mounted at the same chordwise locations as on the normal chord length model, which are shown in figure 50. The transducers were of the vented gauge type, with one side of the diaphragm open to the outside of the tunnel. Each transducer was fitted with its own temperature compensation module. Output signals from the pressure transducers were amplified and passed through a Butterworth filter and then a comparator before being sent to the BE-256 for analogue to digital conversion. The A-D convertor as configured offered 32 channels with a maximum sampling rate of 50KHz and 12 bit resolution, and internal buffers of 8K samples per channel. The data acquisition unit was programmed via an IBM PS/2 model 80/041 and the code was written in Microsoft 'C', which allowed interactive setting of the sampling rate and the number of sampling cycles. When programmed the BE-256 system was to record 1024 data sweeps per cycle (as opposed to 256 per cycle for the MINC system), and the input sampling rate was calculated so that the 1024 samples were taken over a predetermined sampling arc at the test pitch rate. To trigger data sampling, the voltage signal from the angular potentiometer was fed through a specially designed circuit board, so that when the voltage reached a value corresponding to a preset incidence a pulse was sent to the BE-256. The preferred number of sampling cycles per test case was six. After the test run, the data were transferred to an optical disc and reduced and averaged.

The model itself was constructed in a similar fashion to the previous models, but with a chord length of 27.5cm. The model was made of fibre glass mounted on a steel spar, and filled with an epoxy resin foam. A 3-axis profiler was used to machine the aerofoil to shape, and the final result was an accuracy of better than 0.1mm.

6.2 The test programme for the high AR model

The main bulk of the tests performed on the standard models were at Re=1.5x10^6. The maximum speed of the wind tunnel permitted a maximum Re for the high AR model of 1.1x10^6, however. In addition, the maximum reduced pitch rate would be lower. Two test Re were chosen; Re=8.0x10^5 and Re= 1.0x10^6. The lower Re was chosen to compromise high reduced pitch rate with low Re, bearing in mind that an excessively low Re might change the separation characteristics of the test aerofoil too greatly, and that for the standard NACA 0015 the vortex

33

convection wave began to be too poorly defined below r=0.018. The maximum test r at the lower Re was 0.029.

For a later set of tests, a sand strip was fixed to the leading edge of the model to attempt to simulate a higher Re. Landon (1977) used a leading edge sand strip to fix transition on a NACA 0012, which was used as the basis for the present case. The sand strip consisted of sand of average grain size 0.15mm coarsely distributed completely round the leading edge to 2% chord on both surfaces. Spray on glue was used to stick the sand grains onto the aerofoil surface.

The final actual test conditions will be listed in a University of Glasgow standard report.

6.3 Test results and comparison with the standard chord NACA 0015.

6.3.1 Effects of Re on the standard sized NACA 0015

Since the high AR tests were at lower Re than the standard model, a comparison between ramp-up tests at Re=1.5×10^6 and Re=1.0×10^6 for the standard NACA 0015 will be made. Figures 51a, b and c present comparisons of Cn at the two Re plotted as a function of α for r=0.005, 0.017 and 0.034. Figure 51a shows that for r=0.005, the effect of the fall in Re is to suppress the formation of the stall vortex (as shown by the absence of a rise in Cn). In addition, the reduction in the gradient of the curve at high α implies greater boundary layer thickening, which is to be expected. At r=0.017 (figure 51b) the stall vortex is very much in evidence at the lower Re. Cn rise occurs earlier, and the maximum Cn is fractionally lower than the higher Re case. Cn rise indicates the formation and imminent convection of the stall vortex, and that it happens earlier at the lower Re is not unexpected, since the fall in Re alters the laminar-turbulent transition and the thickness of the boundary layer. As a result of the earlier stall, Cn max is also reached earlier. The above trends are reflected in the final figure of this sequence, figure 51c, for r=0.034.

In summary the effects of a fall in Re seem to be an increased susceptibility to stall and a weakening of the stall vortex. These effects will have to be considered when the high AR and standard models are compared with each other.

6.3.2 Comparison of Cn-α plots between the high AR model and the standard model

6.3.2.1 Static data

Figure 52 shows a comparison of the static data at Re=1.1×10^6 for the two models. Prior to

34

stall there are no appreciable differences in behaviour. The standard model stalls earlier than the high AR model, although the maximum Cn are identical. In addition, with decreasing the incidence, the standard model displays less hysteresis before re-attachment. The differences indicated can only be the result of differences in constraint. The increased hysteresis for the high AR model indicates a greater effect of the wake upon the re-attachment process and possibly upon laminar-turbulent transition. This is due to the smaller wall constraint, the result being that the wake can adopt a more natural shape. The gradual nature of the stall of both models indicates that the high AR model still stalls with a trailing edge type mechanism.

The overall results of the static behaviour are encouraging in that the attached flow behaviour has not changed significantly. The greater hysteresis from the high AR data is not particularly worrying since the dynamic stall and vortex convection processes relate to the initial formation of the wake and its short term behaviour.

6.3.2.2 Dynamic data

Figures 53a-e show Cn-α plots comparing ramp-up data from the standard model and the high AR model. Figure 53a shows a comparison for r=0.005, with the high AR model at Re=0.8x10^6 and the standard model at Re=1.0x10^6. The two cases show no Cn rise (which is consistent with figure 51a for the standard model), and the high AR case has a lift curve slope lower than the standard model. The high AR model appears to stall later (as indicated by the moment when Cn falls). A comparison of a higher pitch rate case is shown in figure 53b, with the same two Re as for figure 53a. The gradient of the curve for the lower Re case is again lower than that of the higher Re, and Cn rise occurs earlier, although Cn max occurs later and its magnitude is larger. Figure 53c shows a comparison of the same high AR model run as figure 53b with a standard model test at Re=1.5x10^6. Again the lift curve slope is reduced and Cn rise occurs earlier for the low Re case, although this time Cn max occurs earlier. The same two pitch rates are shown in figure 53d, although in this case the high AR model test was at Re=1.0x10^6, and similar trends to figure 53c are seen in this figure. The final figure in this sequence, 53e, shows a comparison at r=0.03, with the high AR model at Re=0.8x10^6 and the standard model at Re=1.0x10^6. Differences in the curves prior to Cn rise are negligible, and as may be expected, Cn rise and Cn max occur earlier for the lower Re case.

The differences in Cn max and Cn rise are summarised in figures 54a, b and c , 55a, b and c and 56a, b and c. Figures 54a-c show the variation of Cn max with r for the standard model at Re=1.5x10^6, and for the high AR model at Re=0.8x10^6 and Re=1.0x10^6 respectively. The gradients of the three straight line fits are all in excellent agreement with each other, and the actual

35

value of Cn max varies with Re as may be expected, i.e. a decrease in Re results in a lower Cn max. Figures 55a-c show the variation of incidence at Cn max with r. Comparing figures 55a and

55b shows that there is virtually no difference between α at Cn max for the standard model at Re=1.5×10^6 and the high AR model at Re=1.0×10^6. This disagrees somewhat with the Reynolds number comparisons for the standard model, although only two cases were available for discussion, which obviates the need for further testing on the standard model at Re=1.0×10^6. Cn max occurs significantly earlier for the high AR model at Re=0.8×10^6, however. The gradients of the straight line fits are in reasonable agreement, indicating that the pitch rate trends are not affected by the combination of the fall in Re and the reduction in wind tunnel constraint. Finally, figures 56a-c show the variations of incidence at Cn rise with reduced pitch rate for the same cases as

above. The straight line fits show a decrease in α at Cn rise with decreasing Re, indicating a greater susceptibility to stall. These data reflect the changes with Re observed with the standard model.

6.3.3 Comparison of Cn-α data between the high AR and standard models at Re=1.0×10^6

The final comparison case in this section is that between the high AR model and the standard model at the same Re and r, shown in figure 57. The two cases are almost identical, except that the high AR model case lags the standard model test by about a degree, which could trivialise the differences in incidence cited in the above sections. This result relates to one test case only, which highlights the need for more testing on the standard model at Re=1.0×10^6. The point still remains, however, that the two models show the same overall behaviour at the same pitch rate and Re.

6.3.4 Summary

To summarise, a comparison of the Cn-α plots show little differences between the high AR and standard model data that cannot be attributed to Reynolds number effects. Further testing needs to be done on the standard model at Re=1.0×10^6 to make a more comprehensive data comparison, however.

6.4 Vortex convection speed measurements from the high AR model data

The stall vortex convection speed was to be measured using the same technique as for the standard model, i.e. using an interactive graphics screen and cross hair to pick off the suction peaks caused by the passage of the stall vortex. This method is reliable as long as the suction peaks are well defined. During the original analysis of the standard model ramp-up data, it was found that

36

the accuracy became too poor below r=0.018 at Re=1.5x10^6. Although results were obtained below this r, there was little confidence in them. In an attempt to analyse the low r data more accurately, a statistical method was developed, which was applied to the high AR model data. This led to a re-appraisal of the low r data from the standard sized NACA 0015 and 0018 models.

6.4.1 Statistical determination of the stall vortex convection speed from ramp-up data

6.4.1.1 Method

For this method of analysis, the assumption is made that, for a given test condition, the stall vortex convects over the surface of the aerofoil at a uniform speed. The basis of the method is then to correlate the pressure measurements at each of the transducer positions. In practice, a timing point is chosen on one pressure transducer trace (the reference trace) and the corresponding timing points on the remaining traces are calculated by back and forward projecting in time according to the convection speed and distance from the reference trace. The Cp values from each trace are then multiplied by each other, and the result represents the correlation coefficient for the particular timing point on the reference trace and convection speed. Correlation coefficient is found as a function of convection speed. The 'correct' convection speed has the maximum correlation coefficient. As a final check, the timing points on the transducer traces corresponding to the chosen convection speed are inspected visually. Although subjective, this check helps to discriminate between those measurements that are plainly wrong and those that are more reasonable.

6.4.1.2 Results

Figures 58a and 58b show two results of the correlation technique. A strong correlation is shown in figure 58a. The maximum correlation coefficient appears as a spike, the sharpness of which depends upon the timing point on the reference trace. A correlation function such as this occurs when the suction peaks are sharp and well defined. Figure 58b shows the correlation coefficient for a weaker case. Although a maximum is reached, the peak is broad, which is the result of poorly defined suction peaks. The broadness of the peak gives some idea of the accuracy of the convection speed. The pressure traces with the calculated timing points corresponding to the convection speeds indicated in figures 58a and 58b are shown in figures 59a and 59b. The timing points and suction peaks correspond excellently for figure 59a, when the maximum correlation was a sharp spike. Figure 59b gives a poorer fit, however, and a degree of uncertainty exists, although here the definition of the suction peaks is very poor indeed.

The statistical correlation technique was applied to all the high AR test cases and to the standard chord NACA 0015 and NACA 0018 model data, and the results are shown in figure 60.

37

The re-appraisal of the data for the standard models has led to an interesting result. In spite of the much poorer measurement accuracy, at low r the tendency is for the convection speed to fall with increasing reduced pitch rate. The evidence for the trend is strong, as the three aerofoil models exhibit it. When the reduced pitch rate is high enough, the convection speed tends to a constant value. For the standard NACA 0015, this value of convection speed is about 0.36, while for the high AR NACA 0015, it is about 0.44 for Re=0.8×10^6. The threshhold reduced pitch rate for the apparent change in convection speed is the same for the two models. For the high AR model at Re=1.0×10^6, not enough results were available above the threshold reduced pitch rate. Results from the NACA 0018 data show that the threshhold r is higher than for the NACA 0015 models. It must be stressed that the accuracy of the convection speed results at the low r are much poorer than the results at the high r (i.e. during the constant convection speed region). For this reason, trends are stressed in preference to an actual functional variation.

That the convection speed results for the high AR and standard models are similar is encouraging. The constant value of u/U at high r for the two models is different, however, which may be the result of lower Re or the reduced constraint. There is insufficient data at low Re for the standard model to be able to assert which is the controlling effect. It is known, however, that during a ramp-up test the dynamic pressure falls more greatly for the standard model than for the high AR model, which is simply an effect of the increased constraint, although the difference in the fall in dynamic pressure cannot account for the change in convection speed. Leaving aside the actual functional relationship between convection speed and reduced pitch rate for later discussion, application of the statistical correlation technique to the dynamic stall data has shown that wind tunnel constraint does not change the overall variation of convection speed with reduced pitch rate.

6.4.2 Effect of a leading edge modification on the stall vortex convection speed

6.4.2.1 Assessment of changes in boundary layer behaviour via static tests

The motivation behind the sand strip tests was to simulate a higher Re by forcing early transition. Figure 61 shows a comparison between the static test data for the 'clean' and sand strip leading edges at Re=1.0×10^6. The sand strip test has stalled much earlier, the lift curve slope is smaller before stall and the maximum C_l is smaller, which indicate increased boundary layer thickening caused by the sand strip. The gentle stall shows that the model still stalls from the trailing edge. Static tests with the clean leading edge show a large amount of hysteresis between increasing and decreasing incidence. This behaviour is absent with the leading edge modification. With a clean leading edge laminar-turbulent transition is free and is therefore sensitive to the presence of the wake. The effect of the sand strip, however, is to fix transition, hence the absence of hysteresis in this test.

38

It is clear that the leading edge sand strip has drastically altered the boundary layer behaviour over the whole of the aerofoil, by fixing leading edge transition similar to a very high Re. A great deal of boundary layer thickening has occurred, however. The same dynamic test programme as for the clean leading edge case was repeated.

6.4.2.2 Comparison of ramp-up data with clean leading edge high AR tests

6.4.2.2.1 Pressure data

Figures 62 and 63 show pseudo-3D representations of the pressure data from the high AR model at Re=1.0×10^6 and r= 0.0215 for the clean and sand strip leading edges respectively. The dynamic stall behaviour has altered drastically. Without the sand strip, there is a gradual build up of leading edge suction. A bulge in the pressure distribution at about the mid-chord appears just before leading edge suction collapse, and the stall vortex then convects along the aerofoil surface. The most significant feature is that the stall vortex appears to originate from a position well away from the leading edge. It is thought that the development of the bulge in the pressure distribution indicates stall vortex development. The test case with the sand strip shows the build up of leading edge suction, although the above described bulge in the pressure distribution does not appear, and the stall vortex convection wave appears directly from the leading edge suction collapse, in a fashion similar to Lorber & Carta's data (see section 2). In addition to the above, the stall occurs at a lower incidence than for the clean leading edge test.

Figures 64 and 65 show data at r=0.0074 for the same Re. The clean leading edge case shows only a weak stall vortex, only in evidence from the rise in Cn, which is very slight. The sand strip case, however, shows a strong convection wave which starts just after leading edge suction collapse.

6.4.2.2.2 Comparison of Cn-α plots between clean and sand strip leading edges

Shown in figure 66 is a comparison of the Cn-α plots corresponding to the test cases shown in figures 62 and 63. The lift curve slopes are more or less the same as each other, which may be expected since a high pitch rate suppresses boundary layer thickening and trailing edge separation. Cn rise occurs significantly earlier for the sand strip case, however, and the maximum Cn occurs earlier and is considerably smaller than for the clean leading edge case. Figure 67 shows the same two models at r=0.0074. The lift curve slope for the sand strip case is lower at high incidence than for the clean L.E. case and a minor maximum in Cn occurs just before the rise to the true Cn max. Figure 65 shows that leading edge suction drops just before the stall vortex causes apprecaible suction, hence the slight drop in Cn. Trailing edge separation is well established prior to vortex

convection. The clean L.E. case shows only a weak Cn rise. Cn max is again lower for the sand strip case, although the difference between the two cases is not so great at this lower r.

The variations in α at Cn rise and Cn max and the magnitude of Cn max as a function of reduced pitch rate are shown in figures 68a,b, 69a,b and 70 a,b at Re=0.8x10^6 and Re=1.0x10^6 respectively. Also shown on each of these plots are the straight line fits from the clean leading edge cases. Cn rise occurs earlier for the sand strip case tests, although the rates of change of incidence with r are similar. A similar pattern is shown in figures 69a and b for the incidence at Cn max. The most significant differences in pitch rate trends appear when comparing the variations of Cn max with reduced pitch rate, however. Although the stall vortex appears to be stronger from the pressure data, the Cn max for the sand strip tests are consistently lower than for the clean leading edge cases; unsteady motion suppresses separation, so for the clean leading edge tests a great deal of the lift overshoot above static Cn max is due to the delay in stall incidence. Note that although an increase in Re affects the maximum Cn significantly for the clean L.E. case, it hardly affects Cn max for the sand strip tests; the sand grain roughness outweighs the effects of the increase in Re in the present test range of Re. On a similar note, the incidences at Cn max are hardly different from one another for the two Re, although Cn rise does occur slightly earlier for the lower Re case.

6.4.2.3 Measurements of the stall vortex convection speed

The stall vortex wave was well defined for all the sand strip test cases, so the suction peak timing method was an adequate method of analysis, even at the lowest reduced pitch rate of 0.0075. Convection speed is shown plotted as a function of reduced pitch rate in figure 71. Also shown on this figure are the clean L.E. results. It can be seen that the sand strip has completely changed the nature of the relationship between convection speed and reduced pitch rate; u/U is constant right across the range of r, and the mean value is 0.19. The amount of scatter is very small, which reflects the excellent definition of the stall vortex in these tests.

7. FINAL DISCUSSION OF RESULTS

A preliminary analysis of the pressure data from seven aerofoil models at the University of Glasgow showed that the stall vortex convection speed was independent of reduced pitch rate to a first order, with the conclusion that there is a significant anomaly between the G.U. data set and other works, most notably that of Lorber & Carta (1987). Independent analysis of their data and ramp-and-hold tests and special low pitch rate tests at the University of Glasgow merely reinorcfed the result. Testing the high AR model uncovered a great deal about the stall vortex convection

40

speed. A re-appraisal of the data from the standard sized NACA 0015 and 0018 models revealed, at low pitch rates, a strong dependency of convection speed on pitch rate in a sense opposite to Lorber & Carta's (1987) result. The same dependency is shown by the high AR model. At higher pitch rate, the convection speed becomes constant, although the constant value is different for the standard and high AR NACA 0015 models, which may be caused by the difference in constraint or the difference in Re. The important result is that the change in constraint has not affected the functional variation between convection speed and reduced pitch rate. A severe leading edge modification on the high AR NACA 0015 completely eliminated the functional variation and reduced the mean convection speed to 0.19. In addition, the development of the vortex as seen from the surface pressures was drastically altered by the L.E. modification.

Testing of the NACA 0012 model in the preliminary analysis revealed convection speeds which were consistently lower than the rest of the then existing data. Little was made of this at the time because of the level of scatter in some of the other test data. The results of the re-appraisal of the standard NACA 0015 and 0018 models and the high AR model tests hint at a greater significance to the results from the NACA 0012, since a more important model dependency than was previously thought to exist has come to light. In fact the NACA 0012 results do not show the functional dependency of the NACA 0015 and 0018 models at all, and the pressure data for the NACA 0012 appears quite different from the other two models.

Figure 72 shows the pseudo 3-D surface plot of the pressure data from the NACA 0012 at r=0.035, which may be compared with figure 73 for the standard NACA 0015. The main difference in the pressure data is the absence of the pressure 'bulge' (described in section 6.4.2.2.1) in the NACA 0012 data. For the NACA 0015 models, the bulge appears closer to the trailing edge at low r, and moves further closer to the mid-chord at higher r. Thus the development of the dynamic stall for the NACA 0015 and 0018 sections is seen to vary with pitch rate in a way other than simply the strength of the stall vortex. The convection speed data for the symmetrical NACA sections tested at University of Glasgow are shown in figure 74, and the data imply that the convection speed is strongly influenced by the leading edge flow conditions; the NACA 0012 has a much sharper leading edge than the 0015 and 0018 models, and the leading edge modification applied to the high AR 0015 completely changes the boundary layer characteristics in that region. From figure 74, how would the data appear for a NACA 0009 section?

Thus at this stage it appears likely that the apparent convection speed anomaly between the University of Glasgow data and Lorber & Carta's (1987) data is a strong model dependency caused by differences in leading edge behaviour. Exactly what these differences are is unclear at present. Since it seems that leading edge behaviour is an important parameter, Reynolds and Mach number effects are implied. A high enough Re effectively fixes the leading edge boundary layer

41

behaviour, while an increase in M introduces compressibility effects. With this in mind, an appraisal of the data in table 1 is as follows:

i) Carta's (1974) experiments were at Re=1.0x10^{6} and at M=0.35, and St. Hilaire & Carta's (1983) work was at Re=2.8x10^{6} and at M=0.3. Both these sets of tests were from a NACA 0012 aerofoil. The high M for the former and the high Re for the latter could explain the functional dependency of convection speed upon reduced pitch rate. Velocity measurement was by pressure trace.

ii) Chandrasekhara & Carr (1983) also performed experiments upon a NACA 0012, although at Re=2-9x10^{5}. Although the highest M was 0.45, they found no functional dependency. Flow visualisation was used as the main experimental tool.

iii) Robinson & Luttges (1983) reported a dependency of the convection speed upon reduced pitch rate for the NACA 0012 at Re=6-14x10^{4} and M<0.024. Their highest Re is almost the same as Chandrasekhara & Carr's lowest Re. Flow visualisation was again used. Compared to Chandrasekhara & Carr, Robinson & Luttges experiments were at a much higher reduced frequency. There is the possibility that lower Re behaviour is different from behaviour at Reynolds numbers of one million.

iv) Jumper et al (1986) did not actually measure convection speed, although they assumed a constant value to model the stall delay. Their tests were performed on a NACA 0015 at low M and Re, over the pitch rate range on the University of Glasgow data where the convection speed falls and then attains a constant value. The results of their simple modelling fitted experimental data quite well, although further examination of their results reveals a possible margin of error for the convection speed of about 30%.

If the discussion is limited to the tests involving convection speed measured directly from pressure data, the leading edge flow argument explains the anomaly. It makes sense to restrict the discussion to these cases, since the test conditions and measurement techniques for the remaining works are too diverse. What now remains is the need to explain why a change in leading edge behaviour should affect the convection speed.

It is tempting to suggest that the changes in leading edge behaviour manifest themselves as changes in vortex size and strength. A change in the position of origin of the stall vortex can be seen on the clean leading edge, high AR NACA 0015 model as the pitch rate changes. Figures 62 and 64 show that the Cp 'bulge', described previously, moves towards the leading edge as r increases (it is believed that the bulge indicates vortex growth). The individual Cp traces for these

two figures, shown in figures 75 and 76 respectively, indicate the differences in growth more clearly. The first sign of divergence in the Cp traces has been described as the first onset of vortex growth (Gracey et al. (1989)). At high r, the transducer at x/c=0.37 first shows the characteristics of vortex development, while at low r the first signs of growth appear just behind the mid-chord position. For the leading edge modification, the stall vortex always appears from the leading edge, whatever the pitch rate. If vortex growth is triggered by some perturbation, that the stall vortex originates from the leading edge for the sand strip case is not surprising, since the rough surface has introduced a great deal of disturbance to the flow at the leading edge. For the NACA 23012, 23012A, 23012C and 0012 models, the change of vortex origin position is not as great as for the NACA 0015, and these aerofoils all have a constant convection speed from low to high reduced pitch rate. The NACA 0012 in particular has the vortex origin very close to the L.E. for the high reduced pitch rates (see figure 72).

It is tempting to link the change in vortex origin position to the changes in convection speed; the NACA 0015 and 0018 models experience a shift forward in origin with a reduction in speed. The NACA 0012 and the leading edge modified, high AR NACA 0015 have the vortex origin farthest forward, and they have the lowest convection speed. Whether or not this postulation fits in with Lorber & Carta's (1987) data for the SSC-A09 cannot be ascertained, since their data shows that the stall vortex forms at the leading edge, and any change in formation position is hidden by the development of leading edge suction. The physical significance of a change in vortex formation position is that it will manifest itself in a change in the vortex size and strength. A vortex growing near to the leading edge will be fed highly concentrated vorticity in a restricted space, whereas one forming further aft will be fed vorticity that is more diffuse, although the space available for growth is less restricted.

8. CONCLUSIONS

A survey of existing dynamic stall data showed that a significant disharmony exists between the data sets as to the dependency of stall vortex convection speed upon aerofoil motion. A preliminary analysis of pressure data from seven aerofoils at the University of Glasgow showed that the stall vortex convection speed was independent of aerofoil motion and model type to a first order. Most notably, this is in direct contradiction to the results of Lorber & Carta (1987).

Independent analysis of Lorber & Carta's (1987) data at the University of Glasgow served to re-inforce the convection speed anomaly, and further testing at low reduced pitch rates on the NACA 0012 did not show any signs of a convection speed/ reduced pitch rate dependency at low pitch rate, as suggested by Lorber & Carta.

43

A NACA 0015 aerofoil of half the chord length of the existing models at the University of Glasgow was built and tested, with the aim of investigating wind tunnel constraint effects. A comparison of data from this model with data from the standard sized NACA 0015 data showed that constraint effects were not significant.

An improved pressure data analysis technique for finding the stall vortex convection speed allowed the convection speed to be found at low reduced pitch rates, where the method of Lorber & Carta (1987) produced unreliable results. Although the accuracy was poor, the results suggested that the convection speed of the stall vortex pressure wave was reduced pitch rate dependent at low pitch rates for the NACA 0015 (both high AR and standard size) and the NACA 0018. The convection speed was seen to fall as reduced pitch rate increased, and then to become constant, and the reduced pitch rate at which the convection speed became constant for the NACA 0018 was higher than for the NACA 0015 models.

Convection speed was found to be independent of reduced pitch rate over the entire range of r when a leading edge boundary layer trip was placed on the high AR model. In addition the convection speed was significantly lower than the mean value from any of the other models tested, and the nature of the dynamic stall was seen to have changed significantly when compared with the clean leading edge model.

It is suggested that the stall vortex convection speed is influenced by the flow at the leading edge of the aerofoil, which partly explains the anomalous results found in the literature. It is proposed that the leading edge geometry and Reynolds and Mach numbers are of importance in determining the stall vortex convection speed.

Any pressure data from future models tested at the University of Glasgow will be analysed for convection speed. In particular a thin aerofoil with a very sharp leading edge is due to be tested, and the effect of leading edge transition strips will also be investigated.

44

REFERENCES.

Aihara, Y., Koyama, H. and Murashige, A. (1984) 'Transient Aerodynamic Characteristics of a Two-Dimensional Airfoil during Stepwise Incidence Variation.' University of Tokyo.

Angell, R.K., Musgrove, P.J. and Galbraith, R.A. McD. (1988a) 'Collected Data for Tests on a NACA 0015 Aerofoil.' Department of Aerospace Engineering, University of Glasgow, Scotland, Internal Report No 8803.

Angell, R.K., Musgrove, P.J. and Galbraith, R.A. McD. (1988b) 'Collected Data for Tests on a NACA 0018 Aerofoil.' Department of Aerospace Engineering, University of Glasgow, Scotland, Internal Report Nos 8815, 8816 and 8817.

Carta, F.O. (1974) 'Analysis of Oscillatory Pressure Data including Dynamic Stall Effects.' NASA CR 2394.

Chandrasekhara, M. and Carr, L.W. (1989) 'Flow Visualisation Studies of the Mach Number Effects on the Dynamic Stall of an Aerofoil.' AIAA 89-0023, 27th Aerospace Sciences meeting, Reno, Nevada.

Galbraith, R.A.McD., Niven, A.J. and Seto, L.Y. (1986) 'On the Duration of Low Speed Dynamic Stall.' Proc. ICAS conference, London.

Gracey, M.W. and Galbraith, R.A.McD. (1988) 'Data for a NACA 23012C Aerofoil Pitched about its Quarter Chord Axis.' Department of Aerospace Engineering, University of Glasgow, Scotland, Internal Report No 8901.

Gracey, M.W., Niven, A.J. and Galbraith, R.A.McD. (1989) 'A Consideration of Low Speed Dynamic Stall Onset' Paper 11, 15th European Rotorcraft Forum, Amsterdam, Netherlands, September, 1989.

Ham, N.D. and Garelick, M.S. (1968) 'Dynamic Stall Considerations in Helicopter Rotors.' J.A.H.S., **13**, 49.

Herring, D.G.F. and Galbraith, R.A.McD. (1988) 'The Collected Data for Tests on a NACA 23012B Aerofoil.' Department of Aerospace Engineering, University of Glasgow, Scotland, Internal Report Nos 8808, 8809, 8810, 8811.

Jumper, E.J., Shreck, S.J. and Dimmick, R.L. (1986) 'Lift-curve Characteristics for an Aerofoil Pitching at Constant Rate.' AIAA-86-0117, 24th Aerospace Sciences meeting, Reno, Nevada.

Landon, R.H. (1977) 'A Description of the A.R.A. Two-Dimensional Pitch and Heave Rig and some Results from the NACA 0012 Wing' A.R.A. Memo No. 199

Lang, J.D. and Francis, M.S. (1985) 'Unsteady Aerodynamics and Dynamic Aircraft Manoeuvrability.' AGARD conference proceedings, Nº 386.

Lorber, P.F. and Carta, F.O. (1987) 'Unsteady Stall Penetration Experiments at High Reynolds Number.' AFOSR TR-87-1202, UTRC Report Nº R87-956939-3.

McCroskey, W.J. (1981) 'The Phenomenon of Dynamic Stall.' NASA TM-81264.

McCroskey, W.J., McAlister, K.W., Carr, L.W., Pucci, S.L., Lambert, O. and Indergrand, R.F. (1981) 'Dynamic Stall on Advanced Airfoil Sections.' J.A.H.S., **26**, Nº3, 40.

McCroskey, W.J., McAlister, K.W., Carr, L.W. and Pucci, S.L. (1982) 'An Experimental Study of Dynamic Stall on Advanced Airfoil Sections.' NASA TM-84245, vol. 1, 2, 3.

Niven, A.J. (1988) 'An Experimental Investigation into the Influence of Trailing Edge Separation on an Aerofoil's Dynamic Stall Performance.' Ph.D. Dissertation, University of Glasgow, Scotland.

Robinson, M.C. and Luttges, M.W. (1983) 'Unsteady Flow Separation and Attachment Induced by Pitching Aerofoils.' AIAA-83-0131.

Seto, L.Y. and Galbraith, R.A.McD. (1984) 'The Collected Data for Ramp Function Tests on a NACA 23012 Aerofoil.' Department of Aerospace Engineering, University of Glasgow, Scotland, Internal Report Nº 8413.

St. Hilaire, A.O. and Carta, F.O. (1983) 'Analysis of Unswept and Swept Wing Pressure Data from an Oscillating NACA 0012 Airfoil Experiment. Volume I - Technical Report.' NASA CR-3567.

Walker, J.M., Helin, H.E. and Strickland, J.H. (1985) 'An Experimental Investigation of an Aerofoil Undergoing Large Amplitude Pitching Motions.' AIAA J. **23**, Nº8, 1141.

TABLE 1

Test conditions for measurements of stall vortex convection speed.

Author	Aerofoil	Re.	M	AR	c/h	Ramp	Sine	Range of k or r. Variation of wave speed
Carta (1974) [*]	NACA 0012	1×10^6	0.35	9.5 / 0.8	0.28	-	$\hat{\alpha}=8°$ $\bar{\alpha}=30-180°$	0 - 0.4, increasing
St. Hilaire & Carta (1983)	NACA 0012	2.8×10^6	0.3	6.1	0.163	-	$\hat{\alpha}=8°$ $\bar{\alpha}$ up to 15°	0 - 0.12, increasing
Lorber & Carta (1987)	SSC-A09	2.4×10^6	0.2-0.4	5.56	0.18	up to 30°	$\hat{\alpha}=10°, 20°$ $\bar{\alpha}=10°$	sine: 0.025 - 0.1 ramp: 0.005-0.02 increasing
Chandrasekhara & Carr (1983)	NACA 0012	$2-9\times10^5$	0.15-0.45	3.33	0.214	-	$\hat{\alpha}=10°$ $\bar{\alpha}=10°$	0 - 0.1, constant
Galbraith et al (1986) *	NACA23012 23012A	1.5×10^6	0.12	2.93	0.26	-1° to 40°	$\hat{\alpha}=10°$ $\bar{\alpha}=15°$	sine: - 0.24 constant time ramp: 0.045 delay
Robinson & Lutges (1983)	NACA 0012	$6-14\times10^4$	<0.024	2.4	0.417	-	$\hat{\alpha}$ up to 5° $\bar{\alpha}=130-150°$	0.25 - 0.75, increasing
Jumper et al (1986)	NACA 0015	$1.58-2.81 \times10^5$	<0.038	2.94	0.204	up to 40°	-	0.01 - 0.03, constant

* Also analysed McCroskey et al's (1982) sinusoidal test data. Time delay measured from C_D rise to C_D min. Time delay found to be constant for NACA 0012, NLR-1 and NLR-2. M up to 0.3, Re up to 4.0×10^6. c/h=0.2, AR=3.5. See section 5 for discussion.

TABLE 2.

VORTEX CONVECTION SPEED AS A FUNCTION OF HOLD ANGLE DURING RAMP-UP TESTS AT VARIOUS REDUCED PITCH RATES FOR THE NACA 0012 AEROFOIL (GLASGOW UNIVERSITY DATA)

Table 2 shows the convection speeds as a function of hold angle and reduced pitch rate. Also shown on this table are the incidences at which the vortex is at $x/c=0.17$ for each pitch rate (40 deg hold angle only). Ramp-up motion from -1 deg.

TABLE 2.

Reduced Pitch Rate	Hold Angle (deg)	Convection Speed (u/U)	Incidence at which vortex is at $x/c=0.17$ (Hold angle of 40 deg only)
0.03907	40	0.28	29.8
0.04196	32	0.29	
0.04162	30	0.28	
0.03790	28	0.29	
0.04009	26	0.29	
0.03791	24	0.32	
0.03750	22	0.31	
0.03700	40	0.26	29.5
0.03689	32	0.28	
0.03892	30	0.29	
0.03889	28	0.28	
0.03664	26	0.31	
0.03678	24	0.31	
0.03634	22	0.41	
0.03356	40	0.29	28.8
0.03527	30	0.30	
0.03276	28	0.28	
0.03458	26	0.29	
0.03325	24	0.30	
0.03315	22	0.35	
0.02645	40	0.27	27.2
0.02676	30	0.26	
0.02919	28	0.27	
0.02663	26	0.27	
0.02809	24	0.30	
0.02930	22	0.35	
0.02179	40	0.32	27.0
0.02161	28	0.29	
0.02285	25	0.31	
0.02193	24	0.32	
0.02188	22	0.40	

table 2. (contd.....)

Reduced Pitch Rate	Hold Angle (deg)	Convection Speed (u/V)	Incidence at which vortex is at x/c=0.17 (Hold angle of 40 deg only)
0.01686	40	0.28	25.1
0.01727	26	0.30	
0.01685	25	0.29	
0.01745	24	0.36	
0.01629	23	0.30	
0.01626	22	0.32	
0.01265	40	0.31	24.0
0.01348	25	0.26	
0.01407	24	0.31	
0.01324	23	0.28	
0.01398	22	0.37	
0.01384	21	0.27	

<u>Table 3</u>

Comparison of contour plot/ridge-line measurements with suction peak measurements.

aerofoil section	motion type	r	vortex velocity	
			contour	suction peak
NACA 23012C	ramp-up	0.032	0.30	0.35
NACA 23012C	sinusoidal	0.176	0.30	0.33
NACA 23012	ramp-up	0.034	0.33	0.38
NACA 23012A	ramp-up	0.032	0.30	0.35
NACA 23012B	ramp-up	0.032	0.32	0.37
NACA 0015	ramp-up	0.032	0.33	0.38
NACA 0018	ramp-up	0.033	0.36	0.37

<u>TABLE 4</u>

Comparison of convection speeds from averaged and
unaveraged data (NACA 0015, ramp-up)

reduced pitch rate	stall vortex convection speed (u/U)		
	results from unaveraged data	average of unaveraged	result from averaged data
0.036	0.37, 0.35, 0.33, 0.35, 0.29	0.34	0.36
0.035	0.35, 0.30, 0.34, 0.39, 0.34	0.34	0.35
0.034	0.38, 0.31, 0.34, 0.39, 0.39	0.36	0.32

TABLE 5

Variation of aerodynamic coefficients with reduced pitch rate

Aerofoil	Gradients of straight line fits (dependence upon r)				
	α at max C_n	max C_n	α at max C_m	max C_m	α at C_n rise
NACA 23012	526	39	549	-8	296
NACA 23012A	496	67	612	-14	
NACA 23012B	457	55	441	-17	
NACA 23012C	502	61	527	-19	
NACA 0012	451	26	480	-11	
NACA 0015	507	83	612	-20	391
NACA 0018	538	74	511	-22	
Lorber & Carta	500 (C_L)	40 (C_L)	550	-18	192
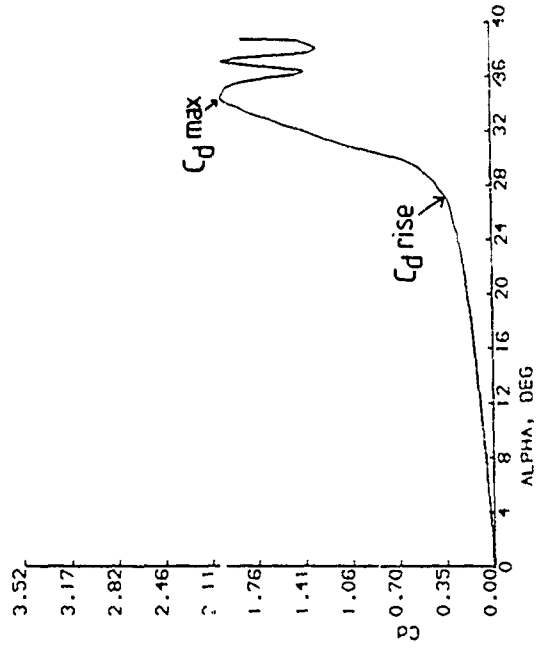
Figure 2. Drag coefficient vs pitch angle. NACA 23012C.
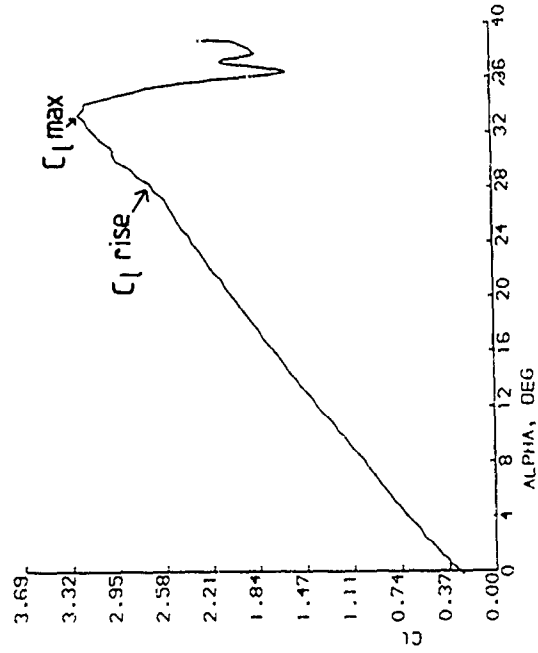
Figure 1. Lift coefficient vs pitch angle. NACA 23012C.

Figure 4. Likely aircraft attitudes and flow features shown by a super manoeuvrable aircraft. After Lang & Francis (1985).

ALPHA, DEG

Figure 3. Moment coefficient vs pitch angle. NACA 3012C.
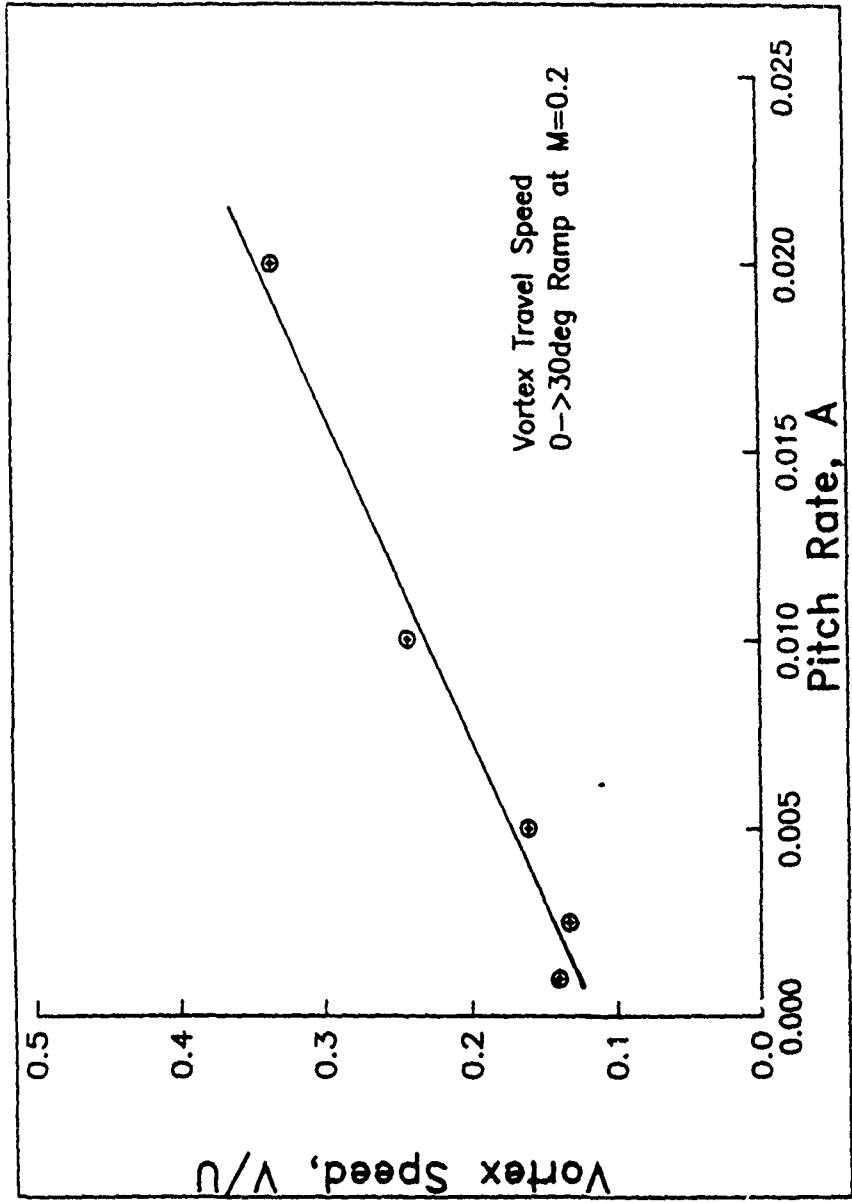
Figure 5. Lorber & Carta's (1987) measurements of stall vortex convection velocity as a function of reduced pitch rate.

PRESSURE DIFFERENCE

$\alpha_M = 11$ DEG

$\alpha_M = 14$ DEG

$\alpha_M = 16$ DEG
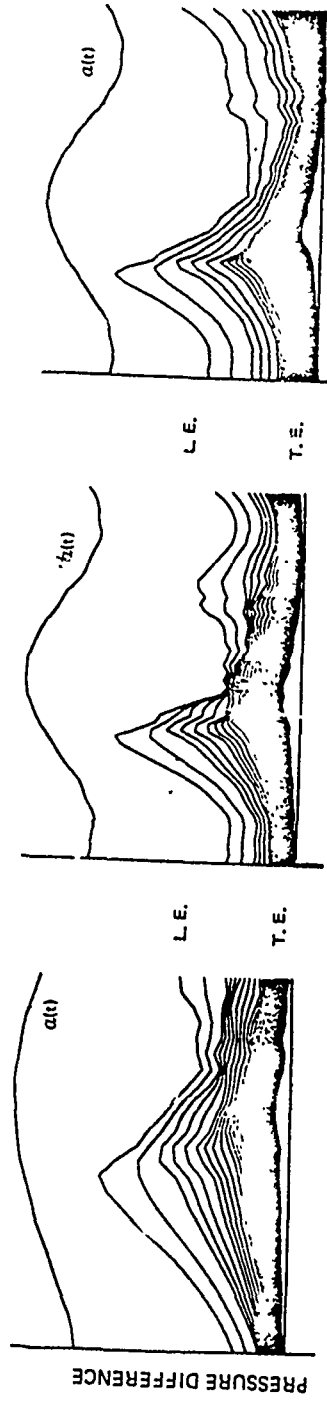
Figure 6. Pressure time histories along the aerofoil surface showing the wave associated with the stall vortex. (Carta's (1974) result).

CHORD

TIME, t, sec
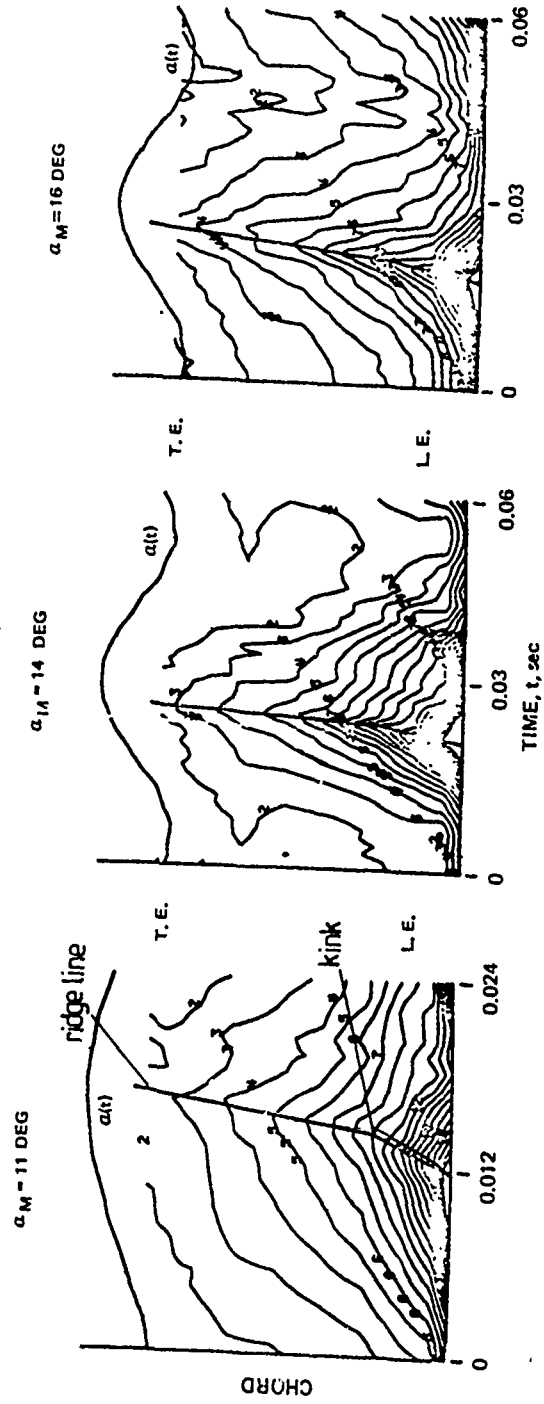
Figure 7. Pressure contour plot from figure 6 with superimposed ridge line.

SYMBOL	$\bar{\alpha}_M$
○	11
□	12
△	14
◇	16
◻	18
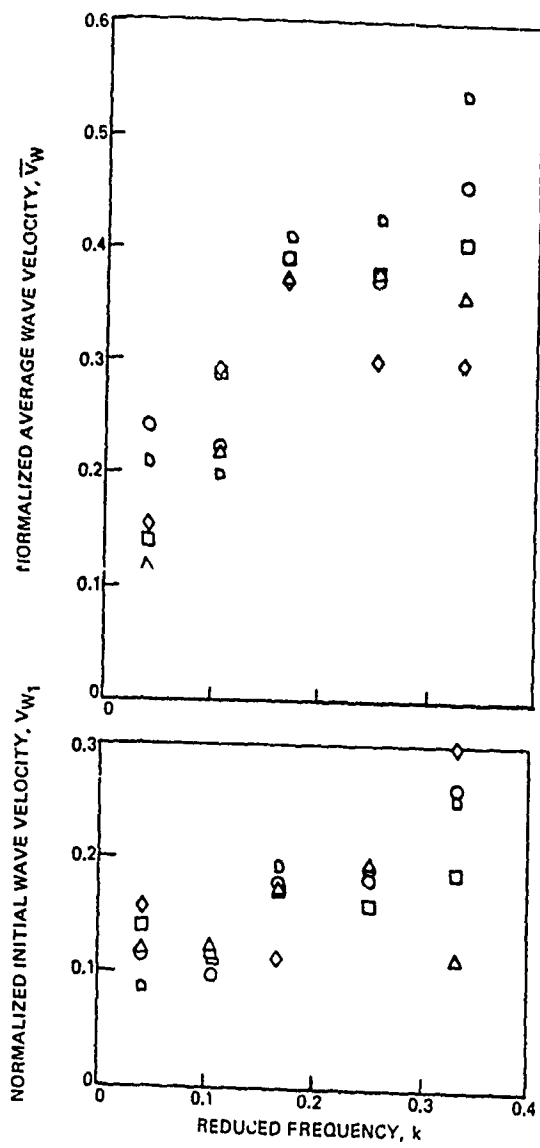
Figure 8. Carta's (1974) measurements of wave velocity as a function of reduced frequency.
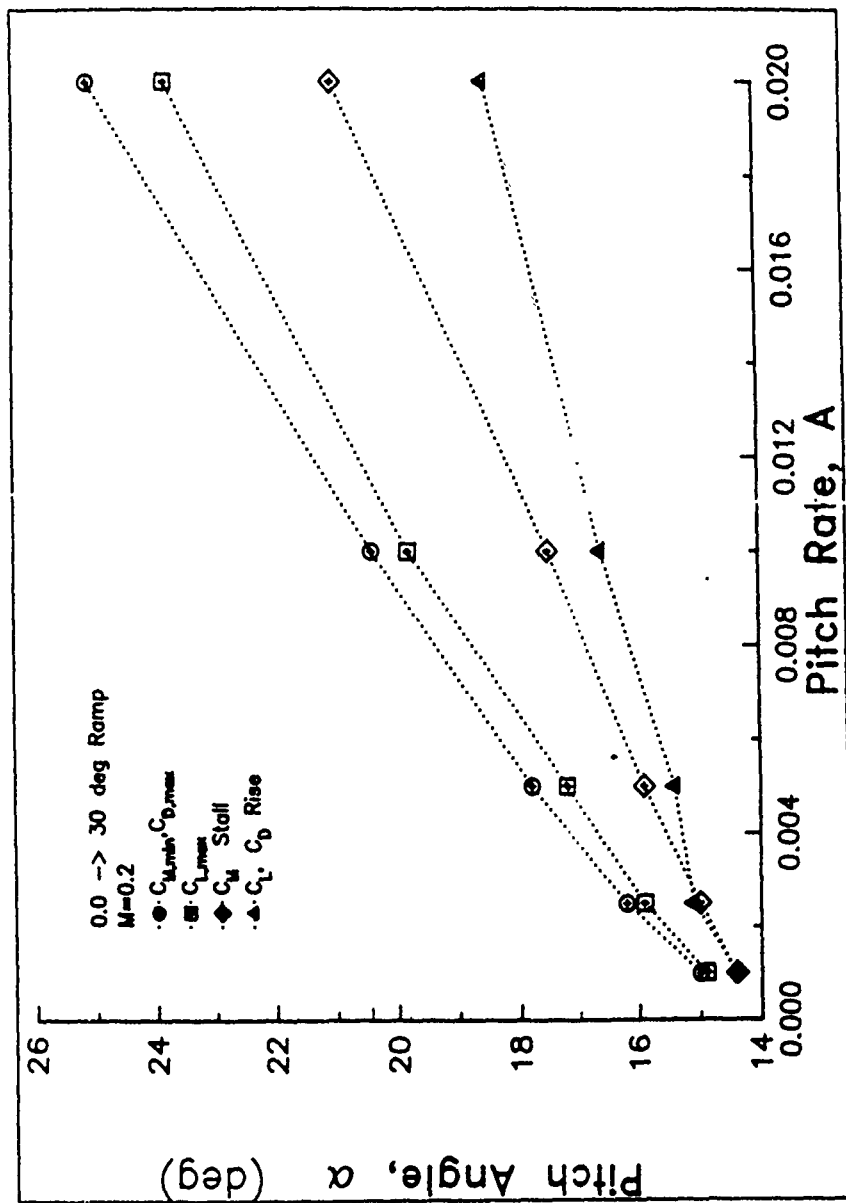
Figure 9.   Stall event angles as a function of reduced pitch
rate. (Lorber & Carta's (1987) result).
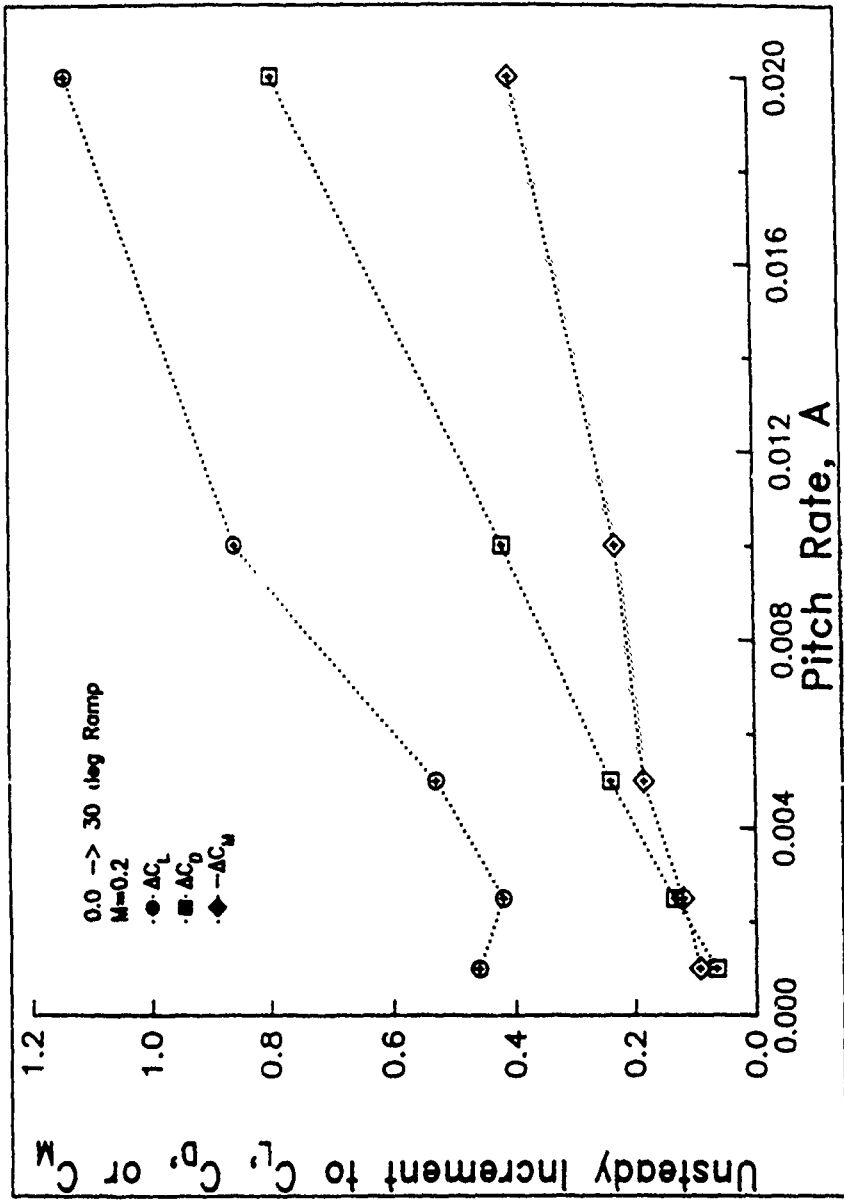
Figure 10. Dynamic increments to aerodynamic coefficients as a function of reduced pitch rate. (Lorber & Carta's (1987) result).
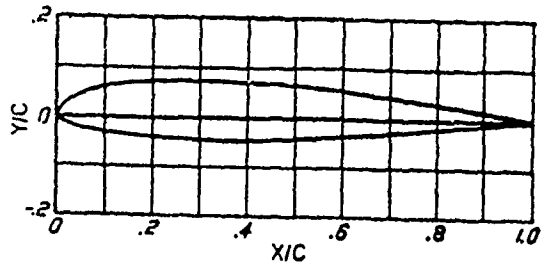
NACA 23012

(Stations and ordinates given in
per cent of airfoil chord)

Upper surface		Lower surface	
Station	Ordinate	Station	Ordinate
0	. . . . . .	0	0
1.25	2.67	1.25	− 1.23
2.5	3.61	2.5	− 1.71
5.0	4.91	5.0	− 2.26
7.5	5.80	7.5	− 2.61
10	6.43	10	− 2.92
15	7.19	15	− 3.50
20	7.50	20	− 3.97
25	7.60	25	− 4.28
30	7.55	30	− 4.46
40	7.14	40	− 4.48
50	6.41	50	− 4.17
60	5.47	60	− 3.67
70	4.36	70	− 3.00
80	3.08	80	− 2.16
90	1.68	90	− 1.23
95	0.92	95	− 0.70
100	(0.13)	100	(− 0.13)
100	. . . . . .	100	0

L.E. radius: 1.58
Slope of radius through L.E.: 0.305

Figure 11. NACA 23012 aerofoil shape and surface
coordinates.
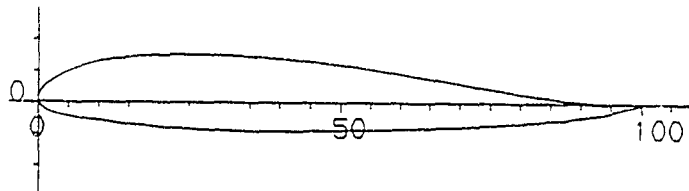
NACA 23012(A)

(Stations and ordinates given in
per cent of aerofoil chord)

Upper Surface		Lower Surface	
Station	Ordinate	Station	Ordinate
−0.044	0.802	0.000	0.000
0.000	0.000	0.436	−0.681
0.337	1.694	1.229	−1.226
1.166	2.657	2.354	−1.658
2.454	3.651	3.791	−2.008
4.207	4.626	5.529	−2.308
6.413	5.523	7.564	−2.588
9.048	6.286	9.910	−2.874
12.069	6.876	12.588	−3.180
15.421	7.276	15.631	−3.508
19.042	7.503	19.077	−3.838
22.902	7.603	22.925	−4.123
27.060	7.597	27.083	−4.333
31.507	7.479	31.530	−4.471
36.224	7.241	36.247	−4.540
41.195	6.872	41.216	−4.547
46.399	6.365	46.418	−4.498
51.815	5.725	51.831	−4.401
57.424	4.964	57.436	−4.261
63.202	4.103	63.209	−4.077
69.125	3.169	69.128	−3.843
75.169	2.202	75.169	−3.544
81.310	1.257	81.306	−3.147
87.521	0.422	87.515	−2.587
93.773	−0.125	93.768	−1.701
100.000	0.051	100.000	−0.050

Figure 12. NACA 23012A aerofoil shape and surface
coordinates.
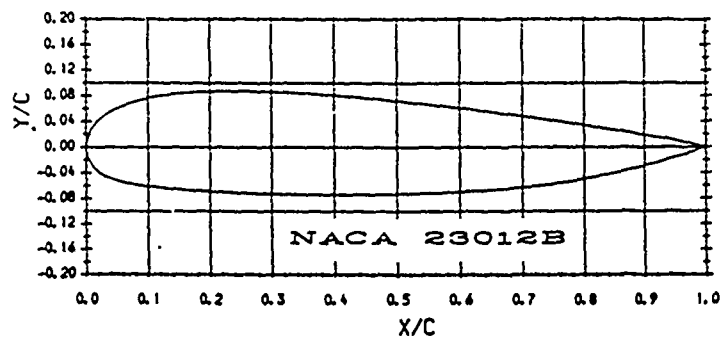
Upper Surface		Lower Surface	
Station	Ordinate	Station	Ordinate
0.000	0.000	0.000	0.000
0.110	0.943	0.035	-0.597
0.833	2.795	0.299	-1.697
1.800	4.043	1.221	-3.132
4.138	5.637	2.341	-4.089
5.371	6.220	3.728	-4.784
9.164	7.461	5.403	-5.333
12.135	8.052	7.455	-5.755
13.822	8.282	9.941	-6.111
17.151	8.568	12.811	-6.400
23.186	8.731	16.044	-6.651
25.174	8.724	19.622	-6.874
29.942	8.618	23.495	-7.059
32.324	8.524	27.634	-7.215
37.880	8.213	31.998	-7.324
40.656	8.016	36.540	-7.385
46.998	7.481	41.210	-7.406
50.168	7.175	45.989	-7.360
53.732	6.803	50.807	-7.264
60.859	5.986	55.625	-7.119
64.421	5.544	60.395	-6.925
68.378	5.030	65.076	-6.661
76.290	3.935	69.620	-6.309
80.245	3.356	73.987	-5.847
84.198	2.755	78.129	-5.287
92.103	1.488	85.588	-3.915
96.055	0.819	91.700	-2.459
99.500	0.135	96.256	-1.185
100.000	0.000	100.000	0.000

Figure 13. NACA 23012B aerofoil shape and surface
coordinates.
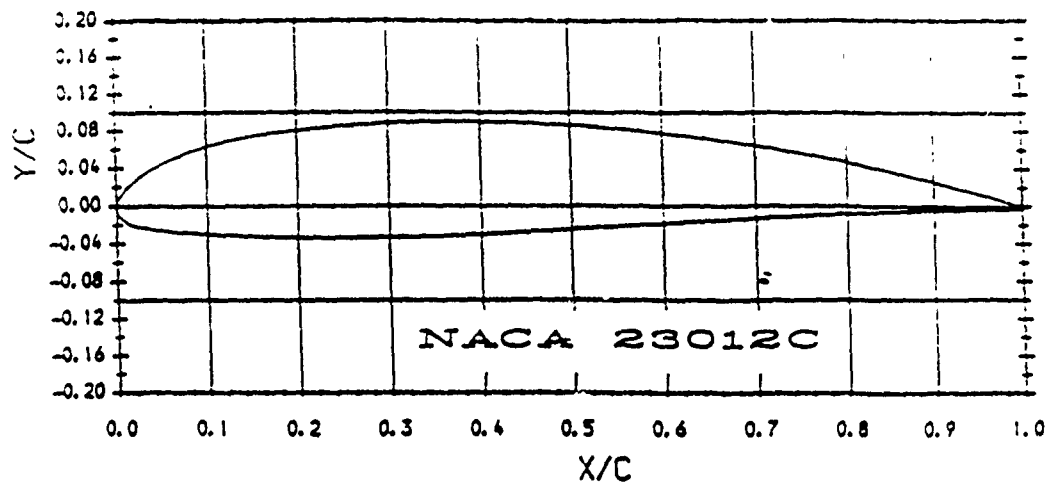
Upper surface		Lower surface	
Station	Ordinate	Station	Ordinate
0.000	0.000	0.000	0.000
0.341	0.917	0.657	-1.453
1.124	1.932	1.472	-1.948
2.366	3.009	2.614	-2.310
4.071	4.097	4.064	-2.568
6.232	5.136	5.811	-2.757
8.826	6.072	7.854	-2.905
11.813	6.862	10.206	-3.038
15.139	7.489	12.892	-3.167
18.741	7.965	15.942	-3.291
22.585	8.339	19.393	-3.386
24.873	8.529	23.243	-3.401
29.023	8.783	29.525	-3.345
33.467	8.942	33.969	-3.245
38.184	8.985	38.681	-3.062
43.156	8.914	43.641	-2.830
48.362	8.702	48.829	-2.515
53.782	8.335	54.223	-2.187
59.395	7.803	59.803	-1.857
65.178	7.105	65.546	-1.533
71.108	6.243	71.429	-1.224
77.162	5.222	77.429	-0.931
83.316	4.046	83.523	-0.657
89.547	2.684	89.686	-0.419
95.829	1.136	95.892	-0.340
100.000	0.000	100.000	-0.288

(Stations and ordinates given in %chord)

Figure 14. NACA 23012C aerofoil shape and surface coordinates.

Upper surface		Lower surface	
x/c	y/c	x/c	y/c
0.0	0.0	0.0	0.0
1.25	1.894	1.25	-1.894
2.5	2.615	2.5	-2.615
5.0	3.555	5.0	-3.555
7.5	4.20	7.5	-4.20
10.0	4.683	10.0	-4.683
15.0	5.345	15.0	-5.345
20.0	5.737	20.0	-5.737
25.0	5.941	25.0	-5.941
30.0	6.002	30.0	-6.002
40.0	5.803	40.0	-5.803
50.0	5.294	50.0	-5.294
60.0	4.563	60.0	-4.563
70.0	3.664	70.0	-3.664
80.0	2.623	80.0	-2.623
90.0	1.448	90.0	-1.448
95.0	0.807	95.0	-0.807
100.0	0.126	100.0	-0.126

All coordinates in % of chord

Figure 15.   NACA 0012 aerofoil shape and surface
coordinates
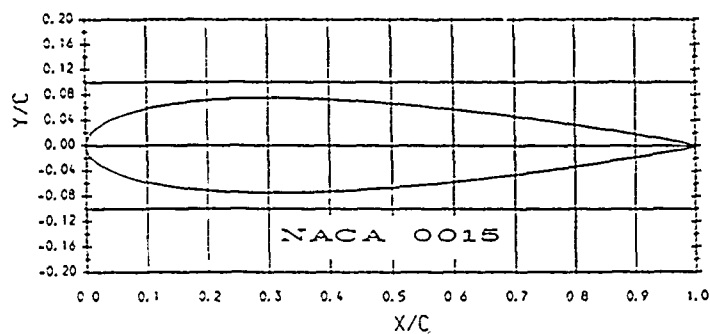
Upper surface		Lower surface	
Station	Ordinate	Station	Ordinate
0.000	0.000	0.000	-0.000
1.250	2 367	1.250	-2.367
2.500	3.268	2.500	-3.268
5.000	4.443	5.000	-4.443
7.500	5.250	7.500	-5.250
10.000	5.853	10.000	-5.853
15.000	6.681	15.000	-6.681
20.000	7.172	20.000	-7.172
25.000	7.427	25.000	-7.427
30.000	7.502	30 000	-7.502
40.000	7.254	40.000	-7.254
50.000	6.618	50.000	-6.618
60.000	5.704	60.000	-5.704
70.000	4.580	70.000	-4.580
80.000	3.279	80.000	-3.279
90.000	1.810	90.000	-1.810
95.000	1.008	95.000	-1.008
100.000	0.158	100.000	-0.158

(Stations and ordinates given in %chord)

Figure 16.   NACA 0015 aerofoil shape and surface coordinates.
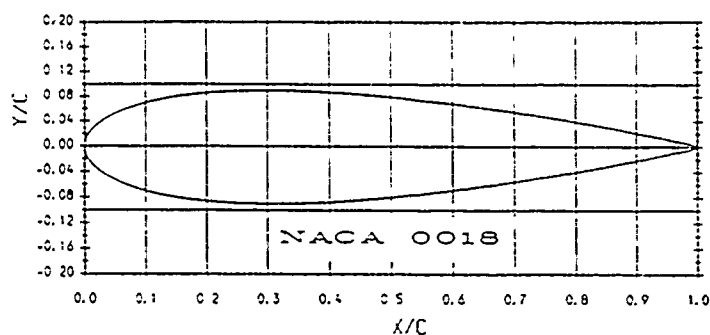
(Stations and ordinates given in %chord)

Station	Ordinate	Station	Ordinate
0.000	0.000	0.000	0.000
1 250	2.840	1.250	-2.840
2.500	3.922	2.500	-3.922
5.000	5.332	5.000	-5.332
7.500	6.300	7.500	-6.300
10.000	7.024	10.000	-7.024
15.000	8.018	15.000	-8.018
20.000	8 606	20.000	-8.606
25.000	8.912	25.000	-8.912
30.000	9.003	30.000	-9.003
40.000	8.704	40.000	-8.704
50.000	7.941	50.000	-0.941
60.000	6.845	60.000	-6 845
70.000	5.496	70.000	-5 496
80.000	3.935	80.000	-3.935
90 000	2.172	90.000	-2 172
95.000	1.210	95.000	-1 210
100 000	0.189	100.000	-0 189

Figure 17.   NACA 0018 aerofoil shape and surface
coordinates.
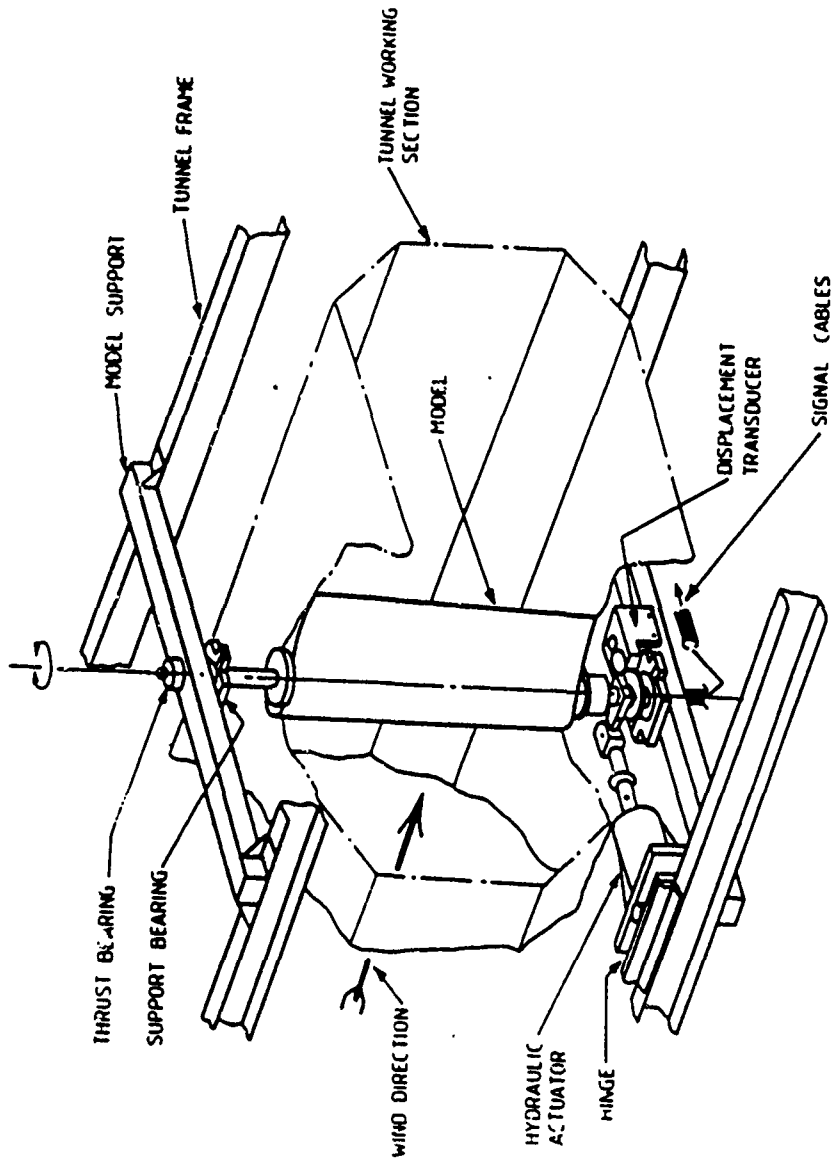
Figure 18. The University of Glasgow Handley-Page wind tunnel and the dynamic stall facility.

HISTORY OF TIMING POINTS   NACA 2301ZC

DATE OF TEST: 12/12/88
RUN REFERENCE NUMBER: 2781
REYNOLDS NUMBER: *1468732.
DYNAMIC PRESSURE: 1007.27 N/sq. m
NUMBER OF CYCLES: 5
MOTION TYPE RAMP UP 3

MACH NUMBER: 0.118
AIR TEMPERATURE: 20.0
SAMPLING FREQUENCY: 350.03 Hz
REDUCED PITCH RATE: 0.03178

AVERAGED DATA OF 5 CYCLES

STRAIGHT LINE FIT:

Y = 0.3491 X - 3.82078
CORR = 0.353916

Stall vortex position versus time for figure 19.

x/C vs tU/c plot

Figure 20. Stall vortex position versus time for figure 19.

x/C = 0.0025
x/C = 0.0100
x/C = 0.0250
x/C = 0.0500
x/C = 0.0750
x/C = 0.1000
x/C = 0.1500
x/C = 0.2000
x/C = 0.2700
x/C = 0.3400
x/C = 0.4100
x/C = 0.4800
x/C = 0.5500
x/C = 0.6200
x/C = 0.6900
x/C = 0.7600
x/C = 0.8300
x/C = 0.9000
x/C = 0.9700
x/C = 0.9875

Non-dimensional time, tuV/c

PRESSURE COEFFICIENT SCALE

ANGLE OF INCIDENCE

Figure 19. Pressure traces on the upper surface of the NACA 23012C aerofoil under-going ramp-up motion. The inverted triangles in... the ... von

STALL VORTEX CONVECTION SPEED

NOMINAL REYNOLDS NUMBER = 1500000.
NOMINAL MACH NUMBER = 0.113
MOTION TYPE: RAMP-UP

△ NACA 23012
MEAN VELOCITY = 0.34687
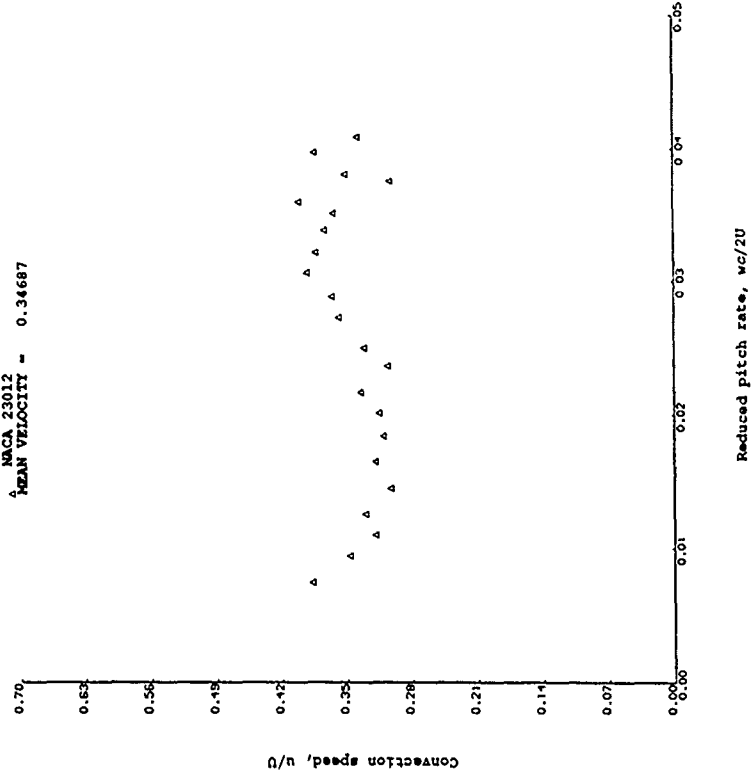
Figure 22. Stall vortex convection speed vs reduced pitch rate for the NACA 23012.

STALL VORTEX CONVECTION SPEED

NOMINAL REYNOLDS NUMBER = 1500000.
NOMINAL MACH NUMBER = 0.114
MOTION TYPE: RAMP-UP

× NACA 23012C
MEAN VELOCITY = 0.34157
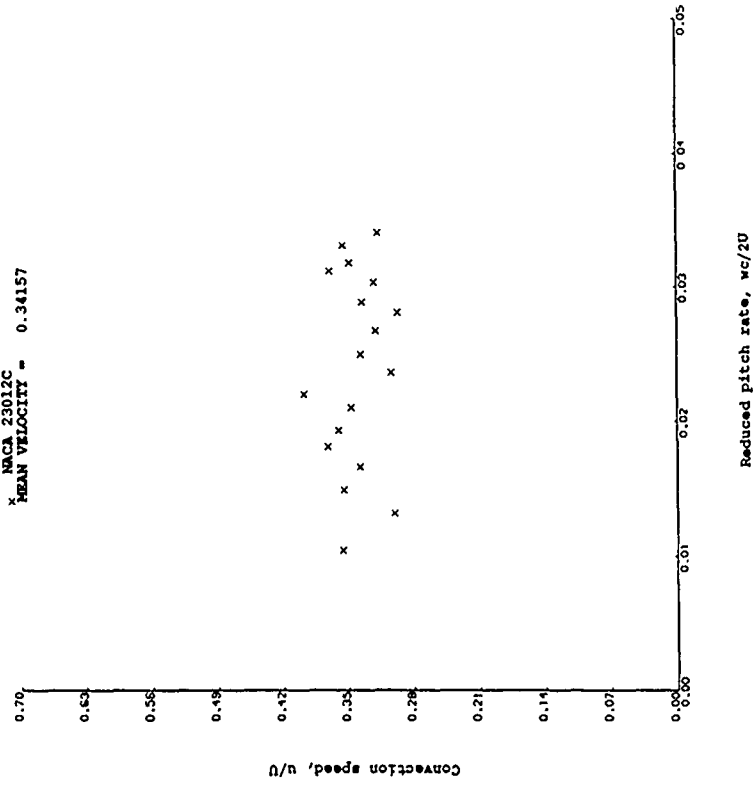
Figure 21. Stall vortex convection speed vs reduced pitch rate for the NACA 23012C.

STALL VORTEX CONVECTION SPEED

NOMINAL REYNOLDS NUMBER = 1500000.
NOMINAL MACH NUMBER = 0.115
MOTION TYPE: RAMP-UP

NACA 23012B
MEAN VELOCITY = 0.37282

Figure 24. Stall vortex convection speed vs reduced pitch rate for the NACA 23012B.

STALL VORTEX CONVECTION SPEED

NOMINAL REYNOLDS NUMBER = 1500000.
NOMINAL MACH NUMBER = 0.115
MOTION TYPE: RAMP-UP

NACA 23012A
MEAN VELOCITY = 0.36413

Figure 23. Stall vortex convection speed vs reduced pitch rate for the NACA 23012A.

STALL VORTEX CONVECTION SPEED

REYNOLDS NUMBER = 1500000.
MACH NUMBER = 0.115
MOTION TYPE: RAMP-UP

Figure 26.   Stall vortex convection speed vs reduced
             pitch rate for the NACA 0015.

STALL VORTEX CONVECTION SPEED

NOMINAL REYNOLDS NUMBER = 1500000.
NOMINAL MACH NUMBER = 0.120
MOTION TYPE: RAMP-UP
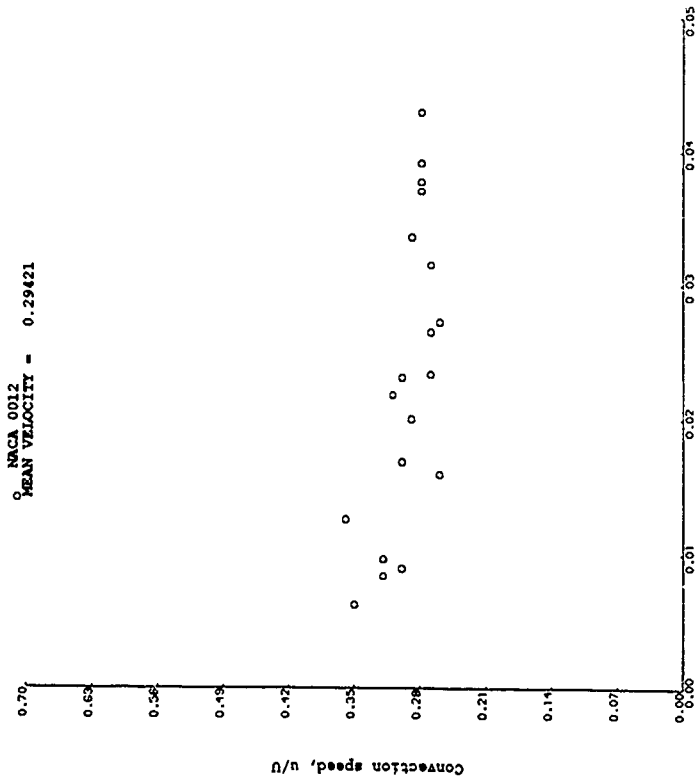
Figure 25.   Stall vortex convection speed vs reduced
             pitch rate for the NACA 0012.

STALL VORTEX CONVECTION SPEED

NOMINAL REYNOLDS NUMBER = 1500000.
NOMINAL MACH NUMBER = 0.120
MOTION TYPE: RAMP-UP

Legend:
- ▲ NACA 23012
- ▼ NACA 23012/
- + NACA 23012
- × NACA 23012(
- □ NACA 0015
- ◆ NACA 0018
- ○ NACA 0012

Non-linear motion

Result of Lorber & Carta
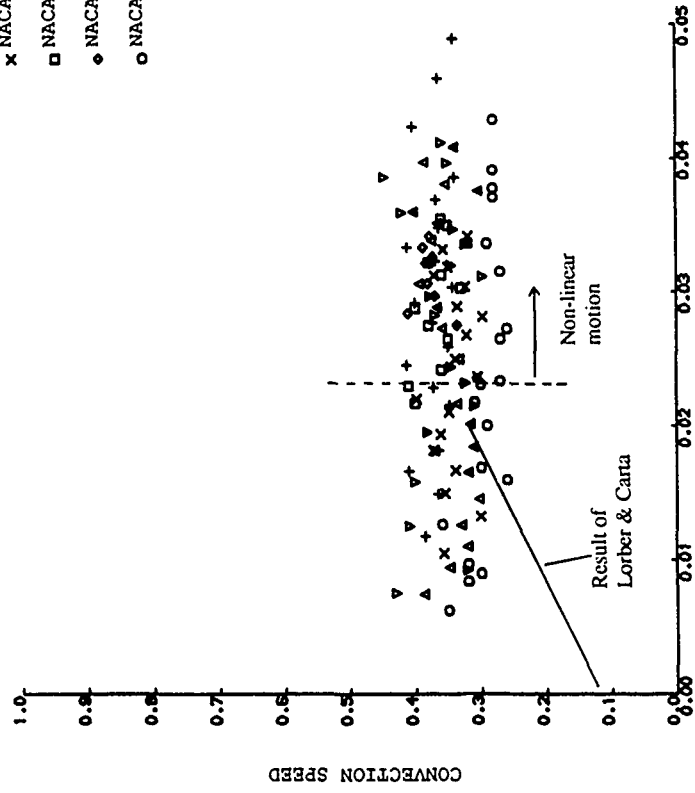
CONVECTION SPEED

REDUCED PITCH RATE

Figure 28.   The collected stall vortex convection speed data for ramp-up motion. Lorber & (res sh by t lid

---

STALL VORTEX CONVECTION SPEED

REYNOLDS NUMBER = 1500000.
MACH NUMBER = 0.115
MOTION TYPE: RAMP-UP

○ NACA 0018
MEAN VELOCITY = 0.37671

Convection speed, u/U

Reduced pitch rate, wc/2U

Figure 27.   Stall vortex convection speed vs reduced rat the AC

STALL VORTEX CONVECTION SPEED

NOMINAL REYNOLDS NUMBER = 1500000.
NOMINAL MACH NUMBER = 0.115
MOTION TYPE: SINUSOIDAL

▲ AMPLITUDE = 10.0 DEG
MEAN VELOCITY = 0.33
+ AMPLITUDE = 8.0 DEG
MEAN VELOCITY = 0.31

REDUCED FREQUENCY
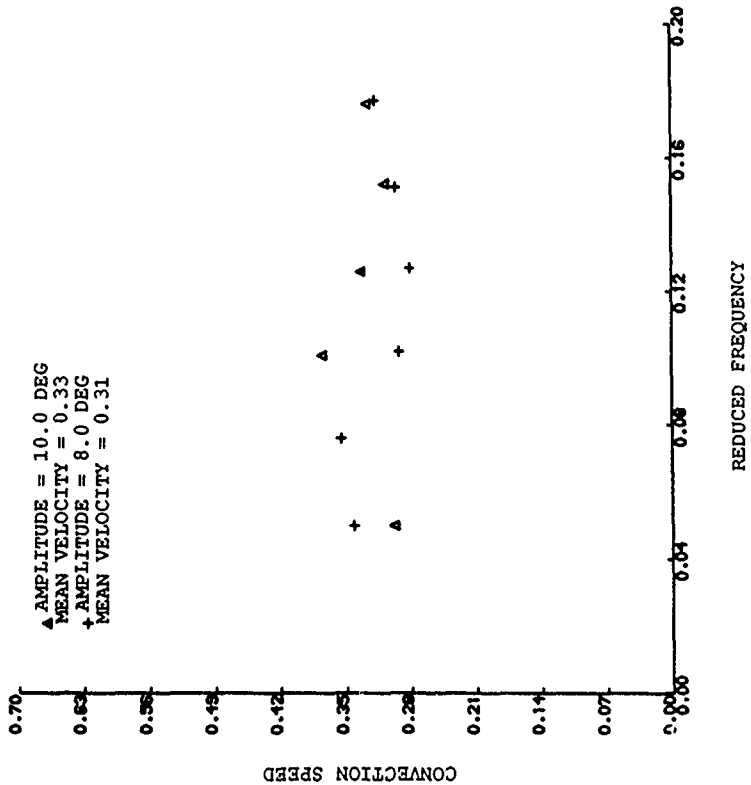
CONVECTION SPEED

Figure 30. Stall vortex convection speed vs reduced
frequency for the NACA 23012C.

HISTORY OF TIMING POINTS - NACA 23012C

RUN REFERENCE NUMBER: 15761   DATE OF TEST: 12/12/80
REYNOLDS NUMBER =1472519.   MACH NUMBER = 0.115
DYNAMIC PRESSURE : 1013.59 N/sq. m   AIR TEMPERATURE = 29.9
NUMBER OF CYCLES : 10   SAMPLING FREQUENCY = 541.13 Hz.
MOTION TYPE:SINUSOIDAL   AVERAGED DATA OF 10 CYCLES
MEAN ANGLE : 20.00
AMPLITUDE : 10.00

STRAIGHT LINE FIT:

T = 0.32680X - 0.76192
CORR = 0.981025

tU/c

x/c
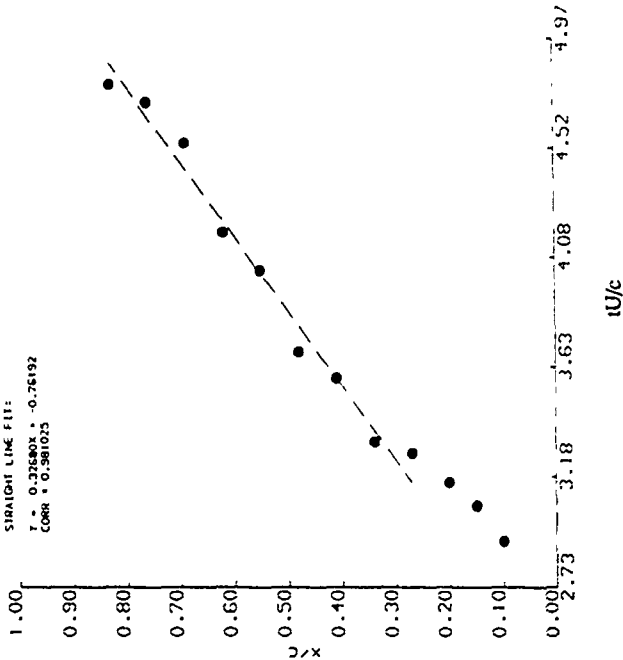
Figure 29. Stall vortex position vs time for the NACA
23012C aerofoil under-going sinusoidal
oscillations. Reduced frequency=0.176.

Surface Cp Contour Plot

Plotted on 19-JUL-90 at 14:08:13

Dynamic Stall Test Data

Model:	NACA 23012C
Run Reference Number:	04027811
Reynolds Number :	1.47E6
Dynamic Pressure =	1007.27
Motion Type:	RAMP UP
Sampling Frequency :	= 550.1 Hz
Pitch Rate	= 273.1 Deg/S
Reduced Pitch Rate =	0.032
Start Angle =	-1.0 Deg.
Ramp Arc =	11.0 Deg.

CONTOUR KEY

1	1.0
2	0.5
3	0.0
4	-0.5
5	-1.0
6	-1.5
7	-2.0
8	-2.5
9	-3.0
10	-3.5
11	-4.0
12	-4.5
13	-5.0
14	-5.5
15	-6.0
16	-6.5
17	-7.0

Upper - SURFACE - Lower

Figure 31.   Pressure contour plot for the NACA 23012C.
Conditions as for figure 19.

Time delay (x-axis: Reduced pitch rate, x10⁻¹): 5.76, 5.19, 4.61, 4.03, 3.46, 2.88, 2.31, 1.73, 1.15, 0.58, 0.00 — 0.00 0.10 0.20 0.30 0.40 0.50

Figure 33. Stall vortex time delay as a function of reduced pitch rate for the NACA 23012C.

STALL VORTEX CONVECTION SPEED

NOMINAL REYNOLDS NUMBER = 1500000
NOMINAL MACH NUMBER = 0.115
MOTION TYPE RAMP-UP

△ NACA 23012C - PEAKS
PEAK VELOCITY = 0.34137
+ NACA 23012C - CONTOURS
MEAN VELOCITY = 0.327448

Convection speed (x10⁻¹): 7.00, 6.30, 5.60, 4.90, 4.20, 3.50, 2.80, 2.10, 1.40, 0.70, 0.00 — Reduced pitch rate (x10⁻¹): 0.00 0.10 0.20 0.30 0.40 0.50
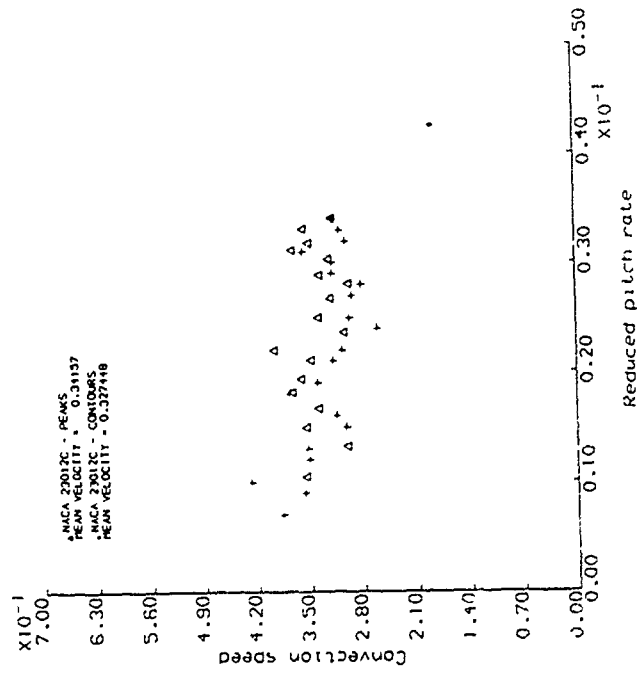
Figure 32. Stall vortex convection speed vs reduced pitch rate for the NACA 23012C as measured from the pressure contours. Also shown are the results of the suction peak technique.

MAXIMUM Cn FOR NACA 23012C

REYNOLDS NUMBER = 1500000
MACH NUMBER = 0.114
MOTION TYPE RAMP-UP

STRAIGHT LINE FIT
T = 61.7626X + 1.6941
CORR = 0.979121

Maximum Cn

4.00
3.60
3.20
2.80
2.40
2.00
1.60
1.20
0.80
0.40
0.00

0.00   0.73   1.46   2.20   2.93   3.66
                                  X10-2
Reduced pitch rate
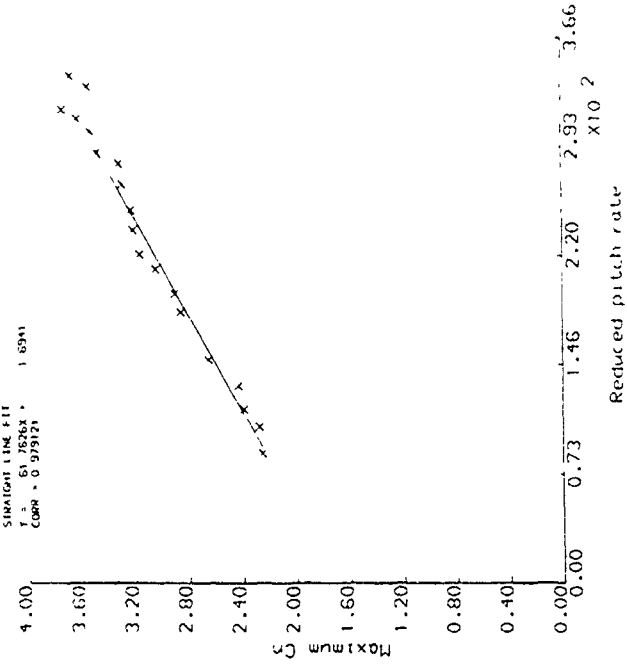
Figure 35.   Maximum Cn vs reduced pitch rate for the
              NACA 23012C.

ALPHA AT MAX Cn FOR NACA 23012C

REYNOLDS NUMBER = 1500000
MACH NUMBER = 0.113
MOTION TYPE RAMP-UP

STRAIGHT LINE FIT
T = 505.1236X + 18.6517
CORR = 0.984133

ALPHA AT CN MAX

40
36
32
28
24
20
16
12
8
4

0.00   0.73   1.46   2.20   2.93   3.66
                                  X10-2
Reduced pitch rate

Figure 34.   Alpha at maximum Cn vs reduced pitch rate for
              the NACA 23012C.

MAXIMUM CM FOR NACA 23012C

REYNOLDS NUMBER = 1500000.
MACH NUMBER = 0.115
MOTION TYPE RAMP-UP

STRAIGHT LINE FIT:
Y = -18.9028X +   -0.2314
CORR = 0.964752

Maximum Cm vs reduced pitch rate for the
NACA 23012C.

Figure 37.

ALPHA AT MAX CM FOR NACA 23012C

REYNOLDS NUMBER = 1500000.
MACH NUMBER = 0.115
MOTION TYPE RAMP-UP

STRAIGHT LINE FIT:
Y = 537.0078X +   19.0122
CORR = 0.961884
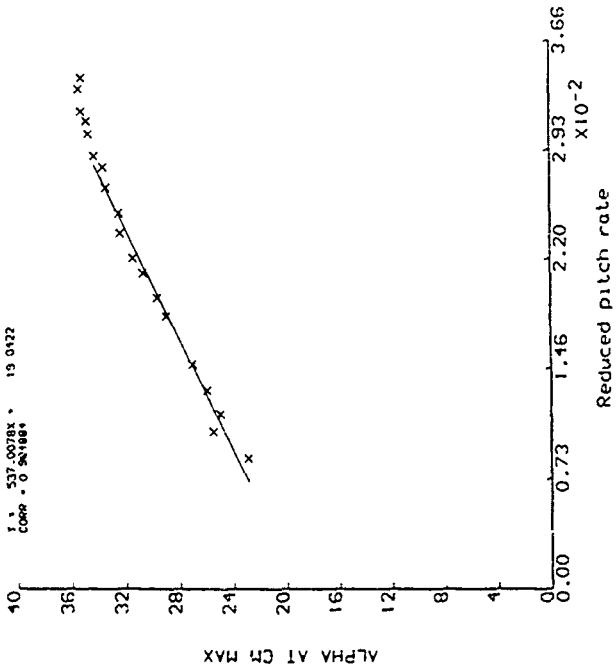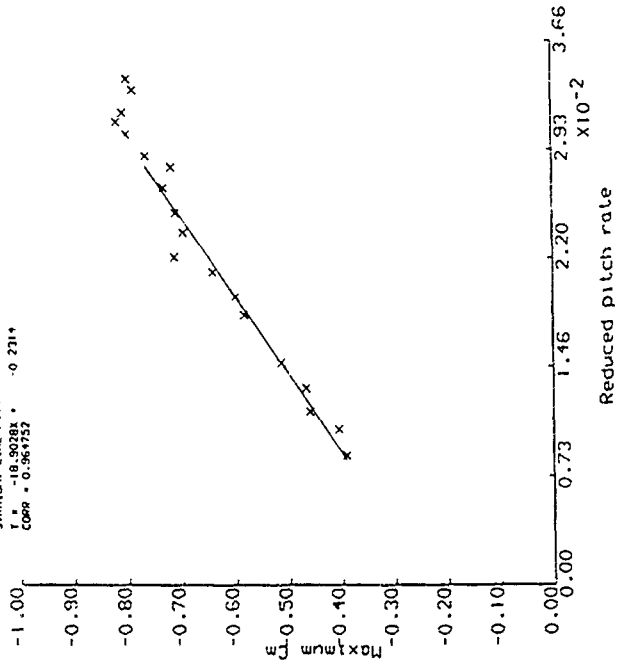
Alpha at maximum Cm vs reduced pitch rate for
the NACA 23012C.

Figure 36.

ALPHA AT CN RISE FOR NACA 23012C

REYNOLDS NUMBER : 1500000.
PITCH NUMBER : 0.15
MOTION TYPE : RAMP-UP

STRAIGHT LINE FIT:
Y = 285.84682X + 18.7251
CORR = 0.919920
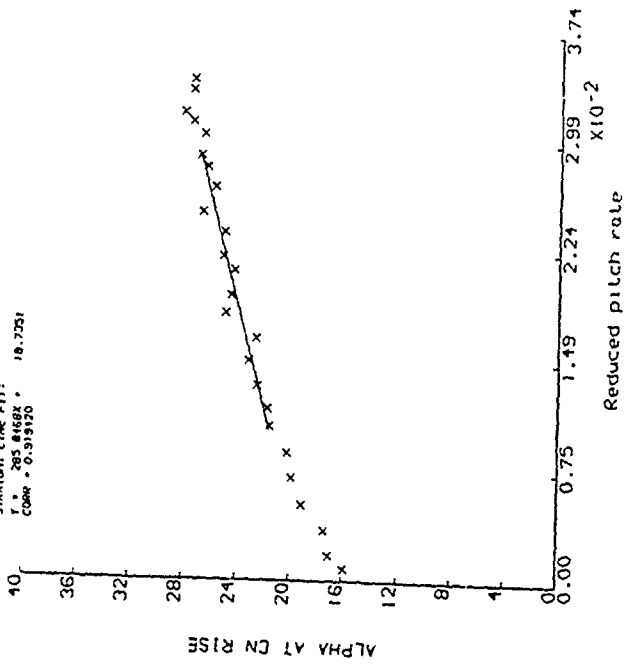
Figure 38. Alpha at Cn divergence vs reduced pitch rate for the NACA 23012C.

ALPHA AT CM BREAK FOR NACA 23012C

REYNOLDS NUMBER : 1500000.
PITCH NUMBER : 0.15
MOTION TYPE : RAMP-UP
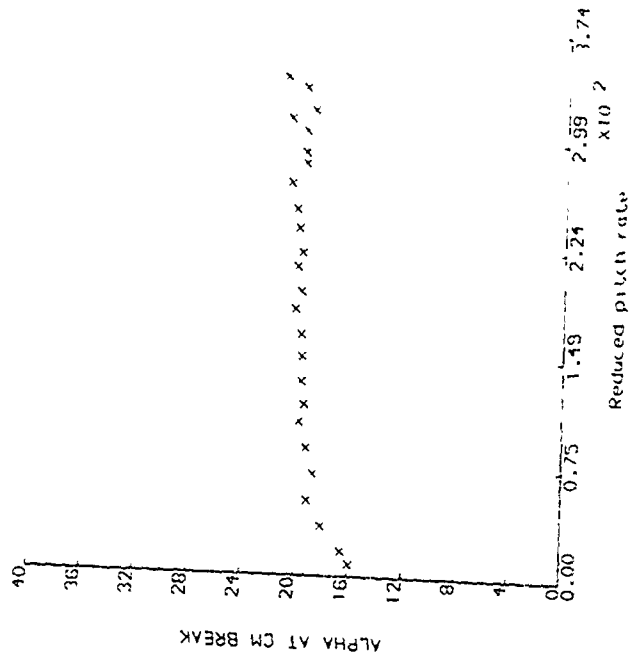
Figure 39. Alpha at Cm divergence vs reduced pitch rate for the NACA 23012C.

DYNAMIC STALL TIME DELAY
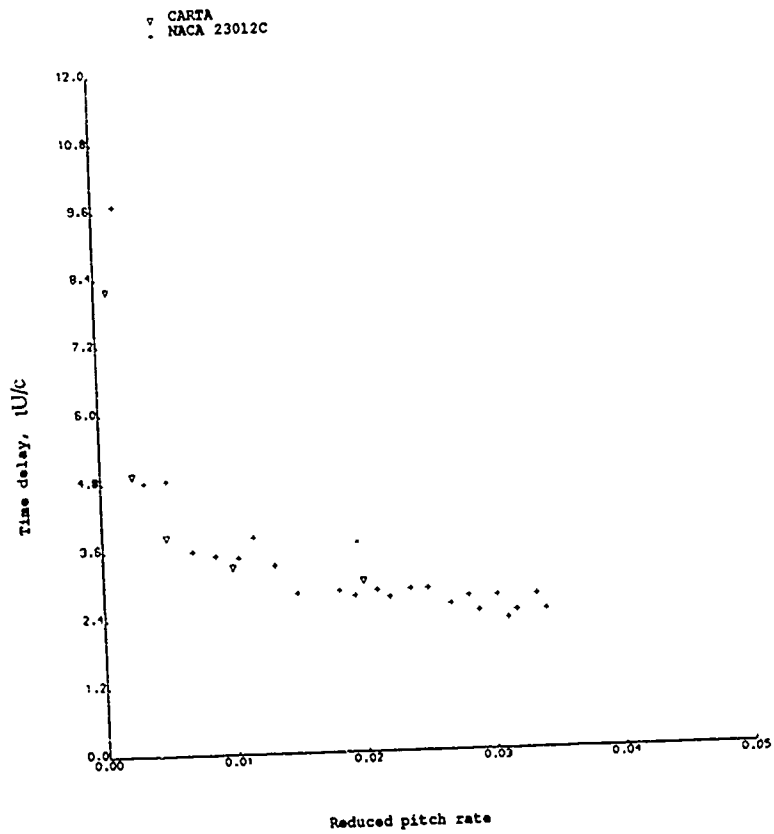
▽ CARTA
. NACA 23012C

Figure 40.   Time delay between C_D rise and $C_m$min.
Results from Lorber & Carta's data analysed at
University of Glasgow re compared with the
University of Glasgow data (NACA 23012C).
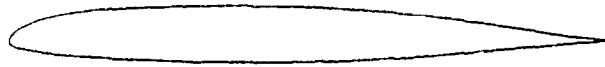
X/C	Y/C
0.9902	0.0021
0.9495	0.0045
0.8801	0.0144
0.7880	0.0277
0.6816	0.0408
0.5702	0.0494
0.4638	0.0540
0.3718	0.0555
0.3023	0.0553
0.2616	0.0546
0.2468	0.0543
0.2262	0.0537
0.1921	0.0524
0.1490	0.0498
0.1028	0.0452
0.0597	0.0367
0.0256	0.0243
0.0050	0.0104
0.0050	-.0067
0.0256	-.0130
0.0597	-.0185
0.1028	-.0237
0.1490	-.0265
0.1921	-.0291
0.2262	-.0307
0.2468	-.0310
0.2616	-.0321
0.3023	-.0331
0.3718	-.0344
0.4638	-.0343
0.5702	-.0312
0.6816	-.0253
0.7880	-.0169
0.8801	-.0092
0.9495	-.003
0.9902	-.000

SSC-A09

Figure 41. The Sikorsky SSC-A09 aerofoil profile and the coordinates of the main pressure transducer array.
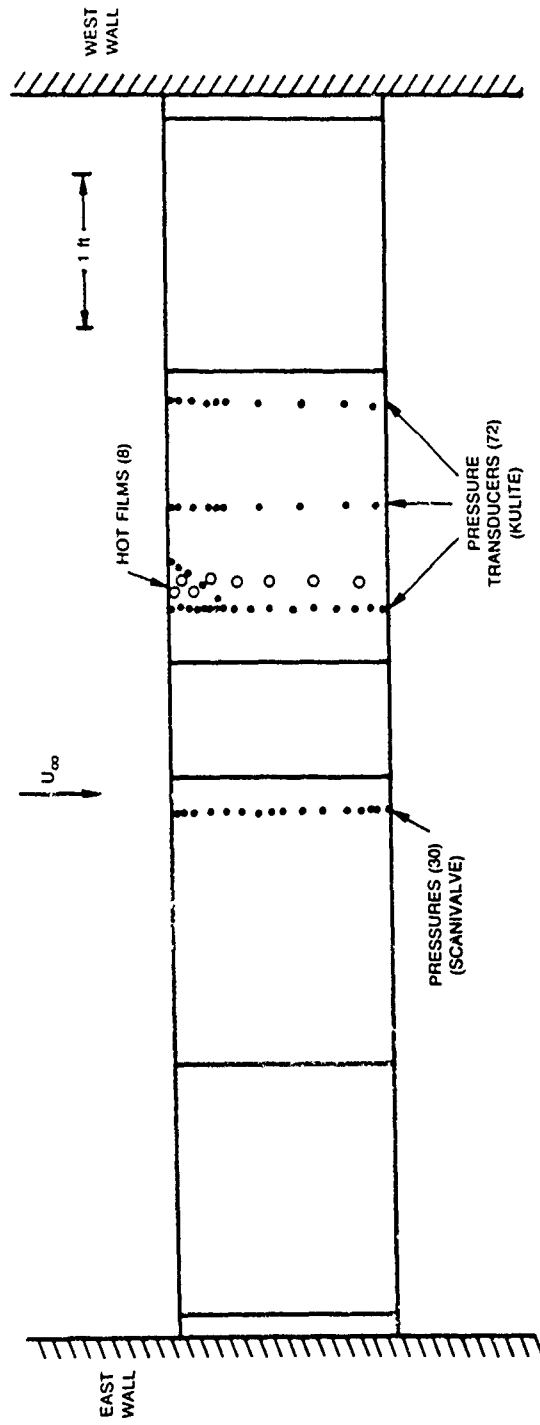
Figure 42. Pressure transducer, pressure tappings and hot film positions along the span of Lorber & Carta's model.

DYNAMIC CHARACTERISTICS FOR THE SSCA09 (Lorber & Carta)

RUN REFERENCE NUMBER -	9	DATE OF TEST 18/6/86
REYNOLDS NUMBER -	2	MACH NUMBER - 0 208
DYNAMIC PRESSURE - 3037 02 km⁻¹	AIR TEMPERATURE - 23 2°C
NUMBER OF CYCLES - 20	SAMPLING FREQUENCY - 200 00 Hz
MOTION TYPE: RAMP UP	REDUCED PITCH RATE - 0 00100
START ANGLE - 0 00°	LINEAR PITCH RATE - 17 5Hz
RAMP ARC - 30 000°	
AVERAGED DATA OF 20 CYCLES	
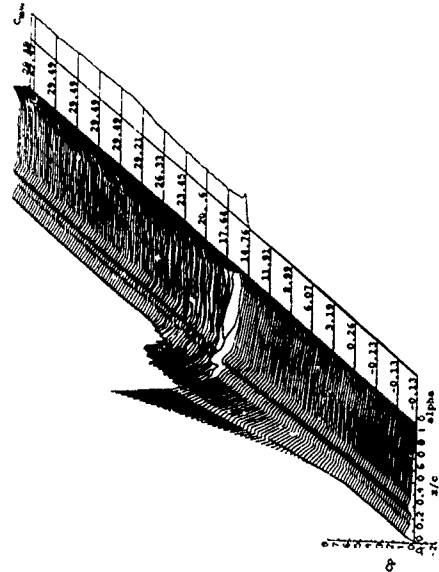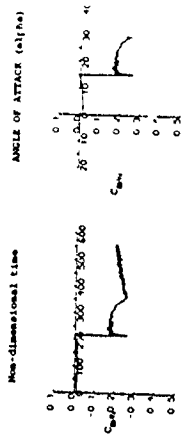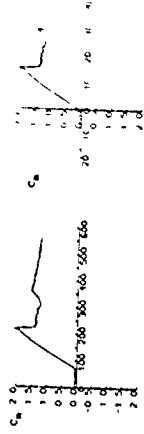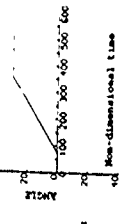
Figure 43a.   Standard plot for Lorber & Carta's data
r=0 001, 0-30 deg ramp-up The stall vortex
originates from just behind the leading edge.
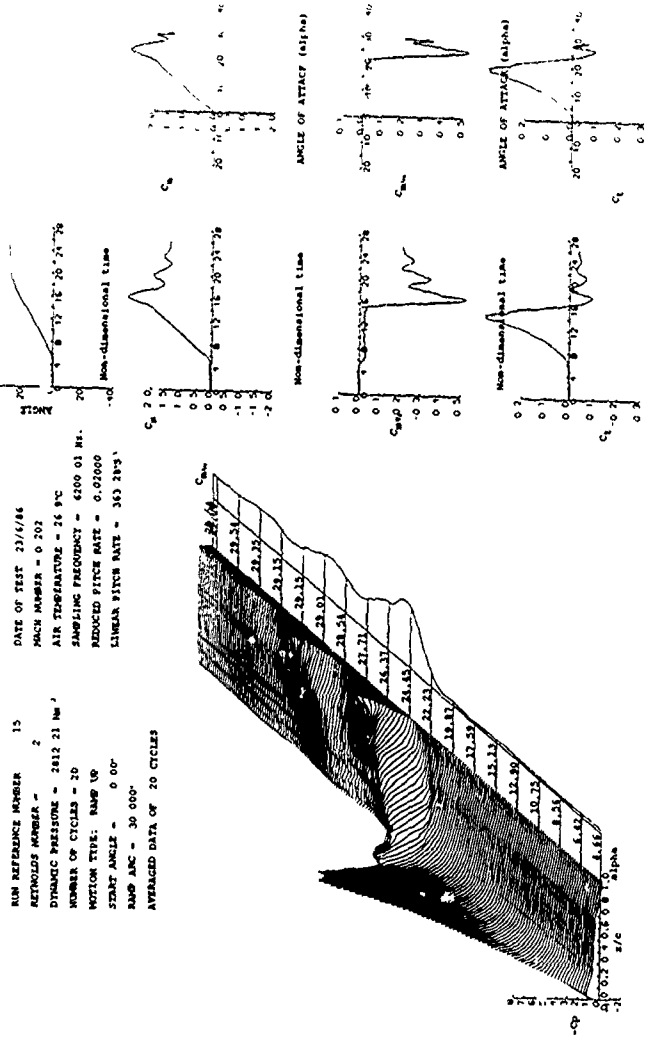
Figure 43b. Standard plot for Lorber & Carta's data. r=0.02, 0:30 deg ramp up

Pressure coefficient scale

Non-dimensional time

Angle of incidence
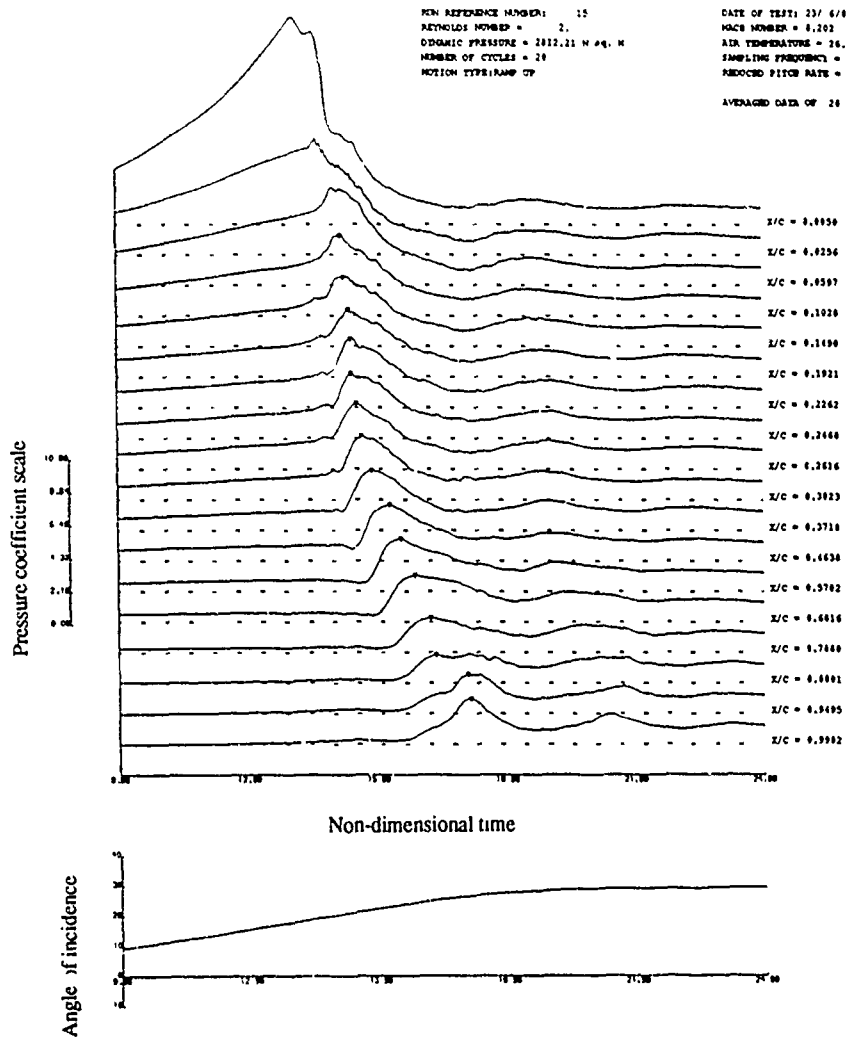
Figure 44.   Individual pressure transducer traces for figure
              43b. The trailing edge isat the bottom of the
              figure and the leading edge is at the top. The path
              of the stall vortex is indicated by the symbols.

UNSTEADY AERODYNAMIC DATA - LOMMER 6 CARTS

RUN REFERENCE NUMBER: 15   DATE OF TEST: 23/ 4/86
REYNOLDS NUMBER =   2.   MACH NUMBER = 0.202
DYNAMIC PRESSURE = 2612.21 N/sq M   AIR TEMPERATURE = 16 9
NUMBER OF CYCLES = 20   SAMPLING FREQUENCY = 4200 01 Hz
MOTION TYPE:RAMP UP   REDUCED PITCH RATE =   0 02000

AVERAGED DATA OF 20 CYCLES

STRAIGHT LINE FIT:

Y = 0.32934X + -4.86092
CORR = 0.991883
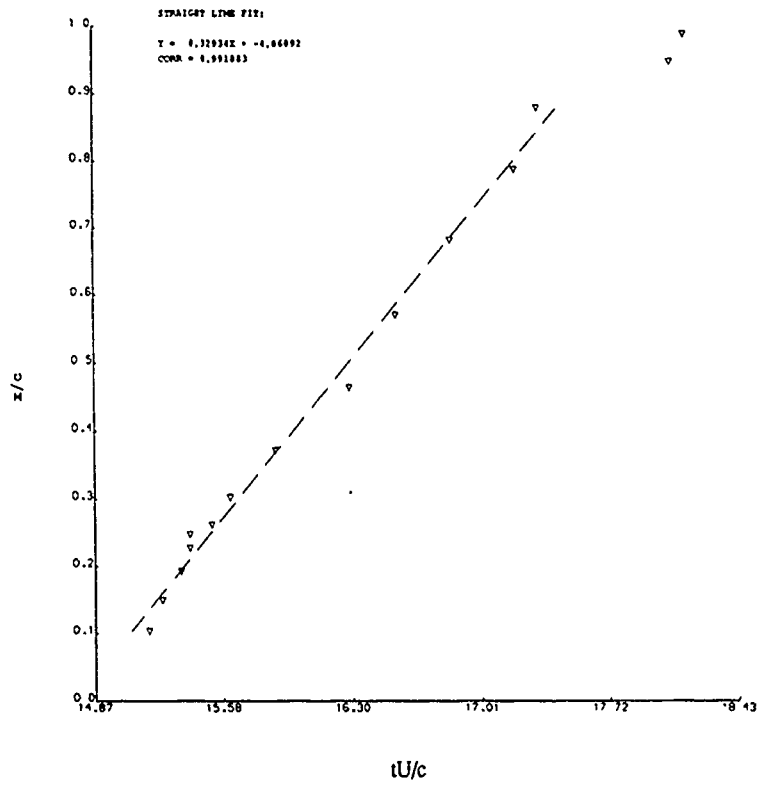
Figure 45.   Stall vortex position versus time from figure 44.

REYNOLDS NUMBER = 2000000
MACH NUMBER = 0.200
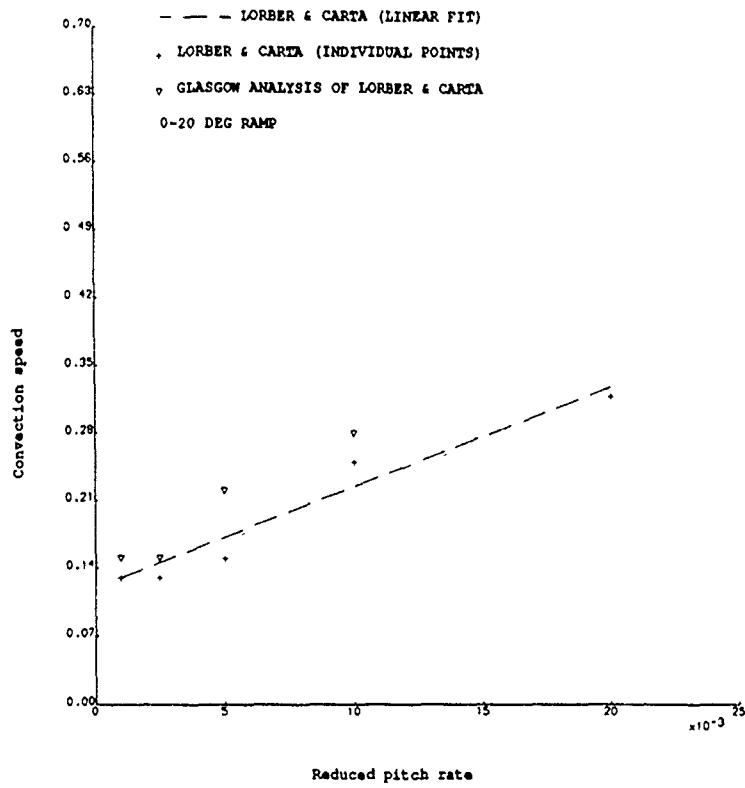
Figure 46a.   University of Glasgow measurements of the convection speed from Lorber & Carta's 0-20 deg ramp-up data. Also shown are Lorber & Carta's original assessments of their 0-30 deg ramp-up data.

Convection speed

- — — — LORBER & CARTA (LINEAR FIT)
- . LORBER & CARTA (INDIVIDUAL POINTS)
- ▽ GLASGOW ANALYSIS OF LORBER & CARTA
- 0-30 DEG RAMP

Reduced pitch rate
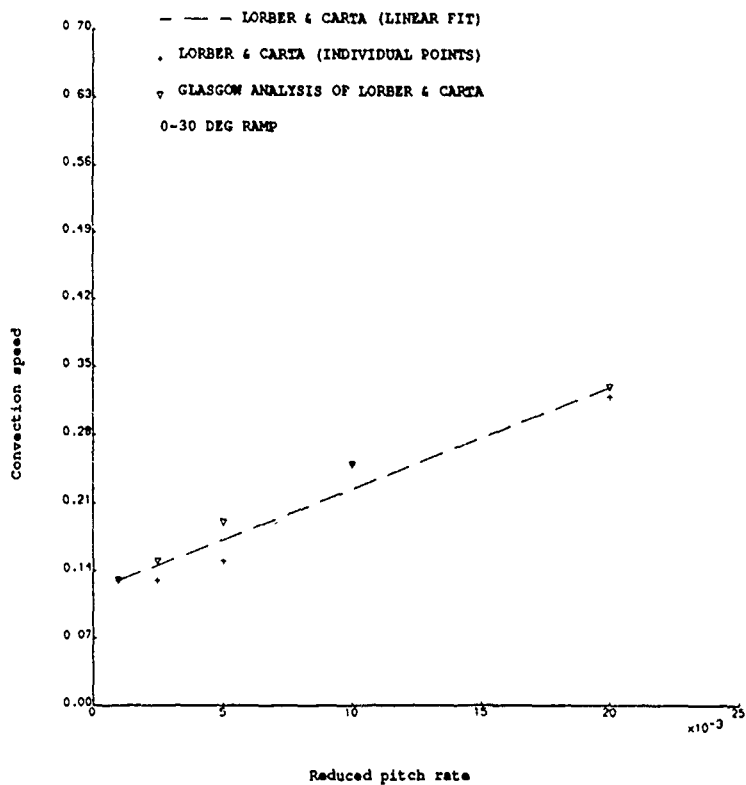
Figure 46b.   University of Glasgow measurements of the
convection speed from Lorber & Carta's 0-30
deg ramp-up data. Also shown are Lorber &
Carta's original assessments of their 0-30 deg
ramp-up data

UNSTEADY AERODYNAMIC DATA - LORBER & CARTA

RUN REFERENCE NUMBER   0   DATE OF TEST: 10/ 6/86
REYNOLDS NUMBER =   2   MACH NUMBER = 0 206
DYNAMIC PRESSURE = 2927 35 N/sq M   AIR TEMPERATURE = 20.0
NUMBER OF CYCLES = 20   SAMPLING FREQUENCY = 470 00 Hz
MOTION TYPE:RAMP UP   REDUCED PITCH RATE =   0 00100

                                        AVERAGED DATA OF 20 CYCLES

Pressure coefficient scale

X/C = 0.0050
X/C = 0 0256
X/C = 0 0597
X/C = 0.1020
X/C = 0.1490
X/C = 0 1921
X/C = 0.2262
X/C = 0 2468
X/C = 0.2616
X/C = 0.3023
X/C = 0.3718
X/C = 0.4638
X/C = 0 5702
X/C = 0.6816
X/C = 0 7588
X/C = 0.8801
X/C = 0 9195
X/C = 0.9902

Non-dimensional time

Angle of incidence
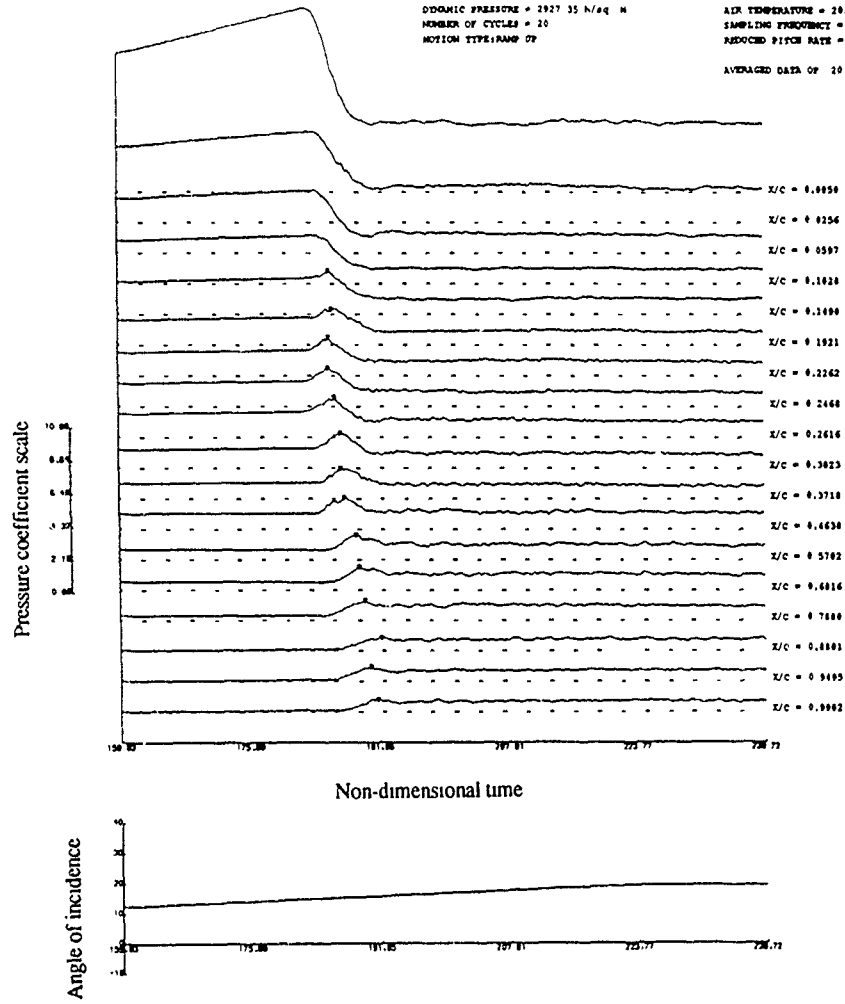
Figure 47.   Individual pressure traces from Lorber &
              Carta's data at r=0.001.
              Sampling frequency=470Hz.

RUN REFERENCE NUMBER: 20321
REYNOLDS NUMBER =1463737
DYNAMIC PRESSURE = 1001 95 N/sq M
NUMBER OF CYCLES = 5
MOTION TYPE:RAMP UP

DATE OF TEST: 17/12/90
MACH NUMBER = 0 118
AIR TEMPERATURE = 26.6
SAMPLING FREQUENCY = 54 18 Hz
REDUCED PITCH RATE = 0.00144

AVERAGED DATA OF 5 CYCLES

CH 15 X/C = 0.0003
CH 14 X/C = 0.0025
CH 13 X/C = 0.0100
CH 12 X/C = 0.0250
CH 11 X/C = 0.0500
CH 10 X/C = 0.1000
CH 9 X/C = 0.1700
CH 8 X/C = 0.2600
CH 7 X/C = 0.3700
CH 6 X/C = 0.5000
CH 5 X/C = 0.5900
CH 4 X/C = 0.7000
CH 3 X/C = 0.8300
CH 2 X/C = 0.9500
CH 1 X/C = 0.9800

PRESSURE COEFFICIENT SCALE

9.00
6.75
4.50
2.25
0.00

4 13   20.10   36.07   52.05   68 02   83 99

Non-dimensional time

ANGLE OF INCIDENCE

40
30
20
10
0
-10

4 13   20.10   36.07   52.05   68 02   85.99
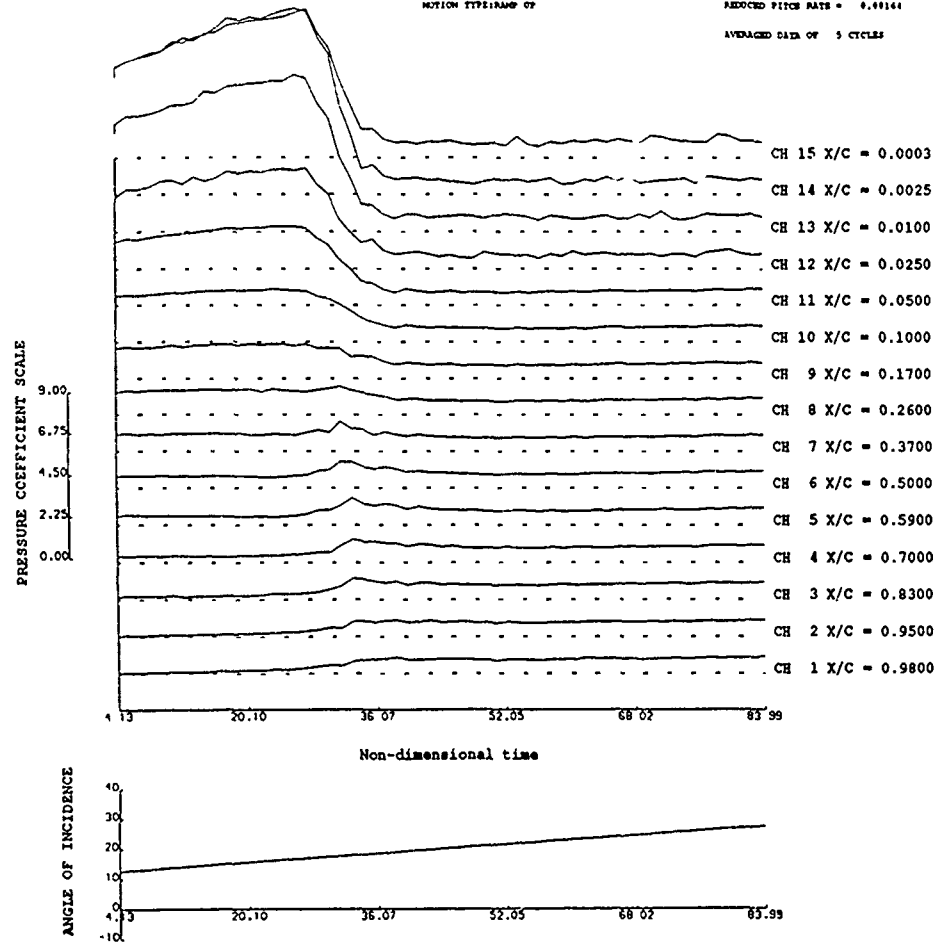
Figure 48.   Individual pressure traces from the NACA
0012 at r=0.0016.
Sampling frequency=54Hz.

RUN REFERENCE NUMBER: 2C292
REYNOLDS NUMBER =1476326.
DYNAMIC PRESSURE = 1000.26 N/sq. M
NUMBER OF CYCLES = 5
MOTION TYPE:RAMP UP

DATE OF TEST: 17/ 1/91
MACH NUMBER = 0.110
AIR TEMPERATURE = 25.4
SAMPLING FREQUENCY = 186.99 Hz.
REDUCED PITCH RATE = 0.00670

AVERAGED DATA OF 5 CYCLES

CH 15 X/C = 0.0003
CH 14 X/C = 0.0025
CH 13 X/C = 0.0100
CH 12 X/C = 0.0250
CH 11 X/C = 0.0500
CH 10 X/C = 0.1000
CH 9 X/C = 0.1700
CH 8 X/C = 0.2600
CH 7 X/C = 0.3700
CH 6 X/C = 0.5000
CH 5 X/C = 0.5900
CH 4 X/C = 0.7000
CH 3 X/C = 0.8300
CH 2 X/C = 0.9500
CH 1 X/C = 0.9800

PRESSURE COEFFICIENT SCALE

Non-dimensional time

ANGLE OF INCIDENCE
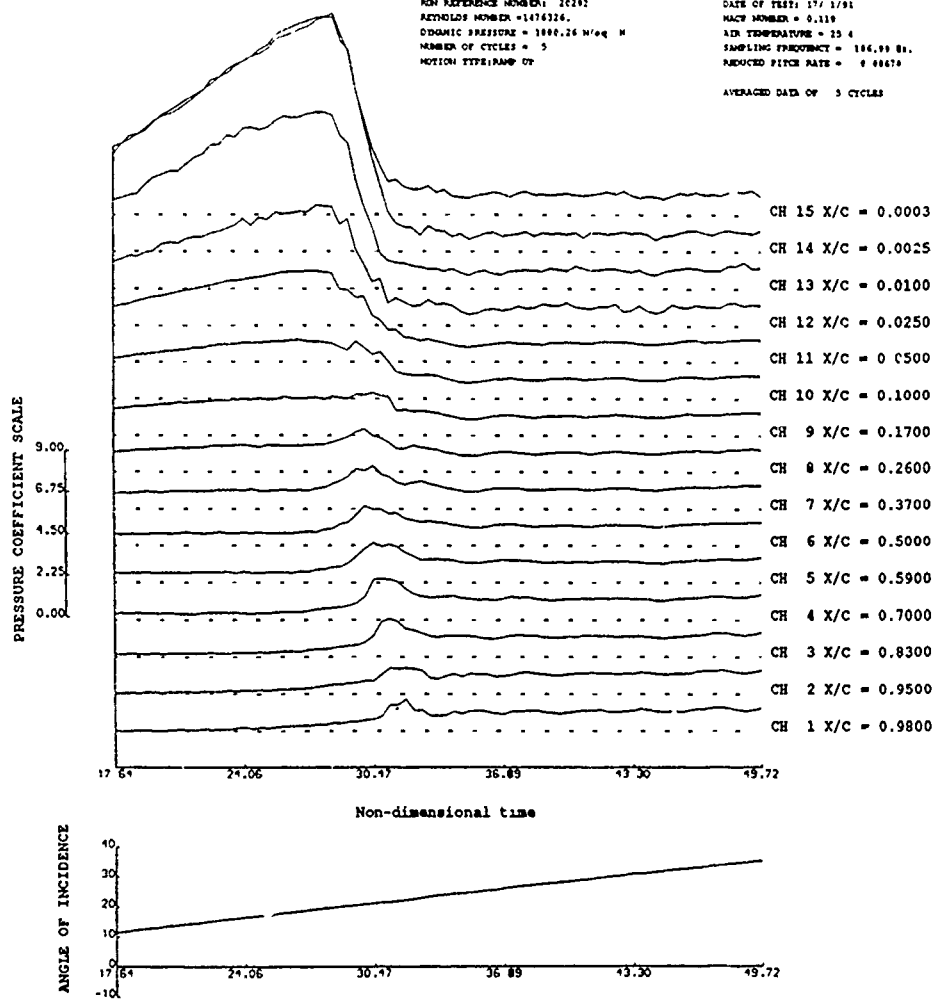
Figure 49a. Individual pressure traces from the NACA 0012 at r=0.0068. Sampling frequency=187Hz.

UNSTEADY AERODYNAMIC DATA - NACA 0012

RUN REFERENCE NUMBER: 24311   DATE OF TEST: */ 3 91
REYNOLDS NUMBER =1349918.   MACH NUMBER = 0 115
DYNAMIC PRESSURE = 987.51 N/sq M   AIR TEMPERATURE = 25.5
NUMBER OF CYCLES = 4   SAMPLING FREQUENCY = 550 05 Hz
MOTION TYPE:RAMP UP   REDUCED PITCH RATE = 0.00623

                                               AVERAGED DATA OF 5 CYCLES
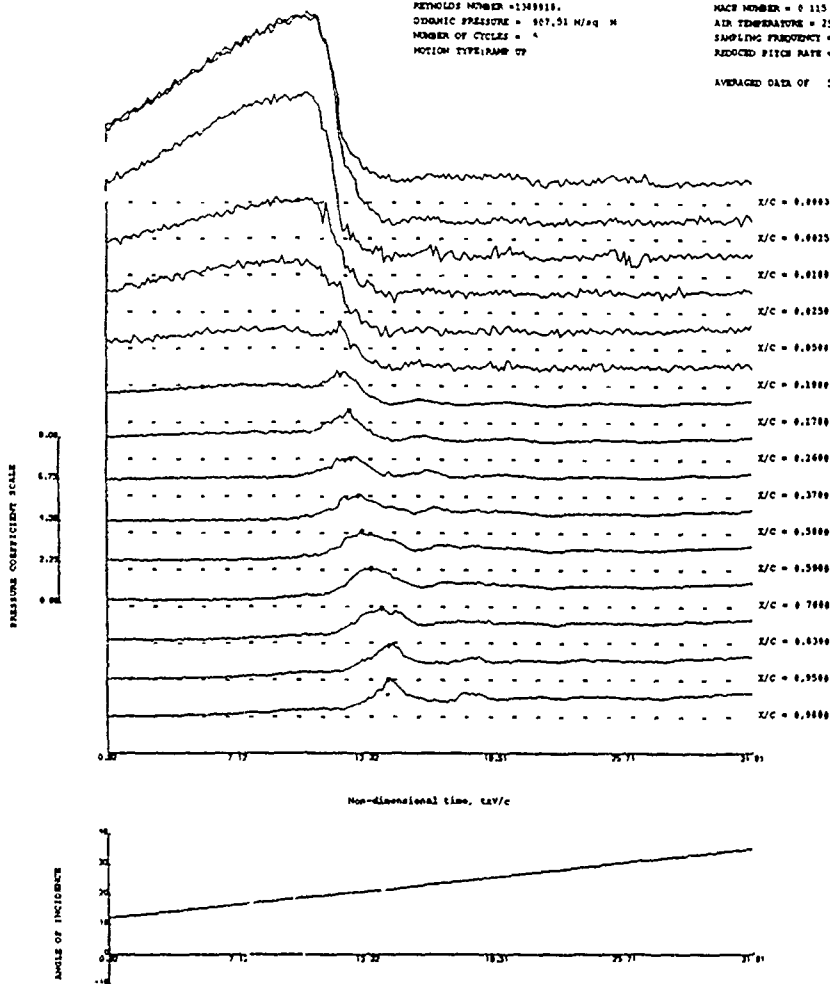
Figure 49b.   Individual pressure traces from the NACA
               0012 at r=0.0062.
               Sampling frequency=550Hz. The stall vortex
               suction peaks are indicated by the symbols.
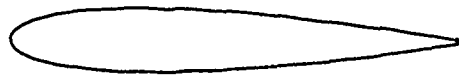
NACA 0015 PROFILE

Chordwise positions of
pressure transducers.

UPPER SURFACE			LOWER SURFACE	
channel	x/c		channel	x/c
1	0.98		16	0.0003
2	0.95		17	0.0025
3	0.83		18	0.01
4	0.70		19	0.025
5	0.59		20	0.05
6	0.50		21	0.10
7	0.37		22	0.17
8	0.26		23	0.26
9	0.17		24	0.37
10	0.10		25	0.50
11	0.05		26	0.59
12	0.025		27	0.70
13	0.01		28	0.83
14	0.0025		29	0.95
15	0.0003		30	0.98

Figure 50. Aerofoil profile and transducer positions for the high aspect
ratio NACA 0015
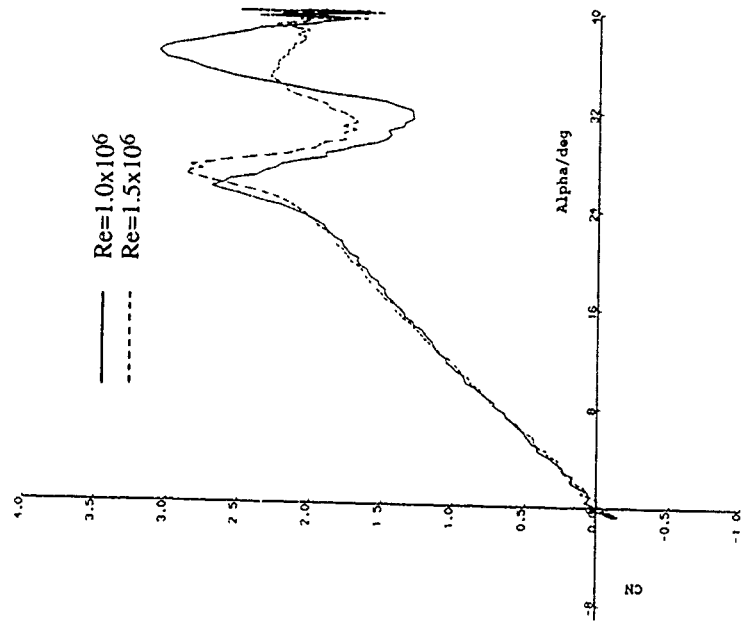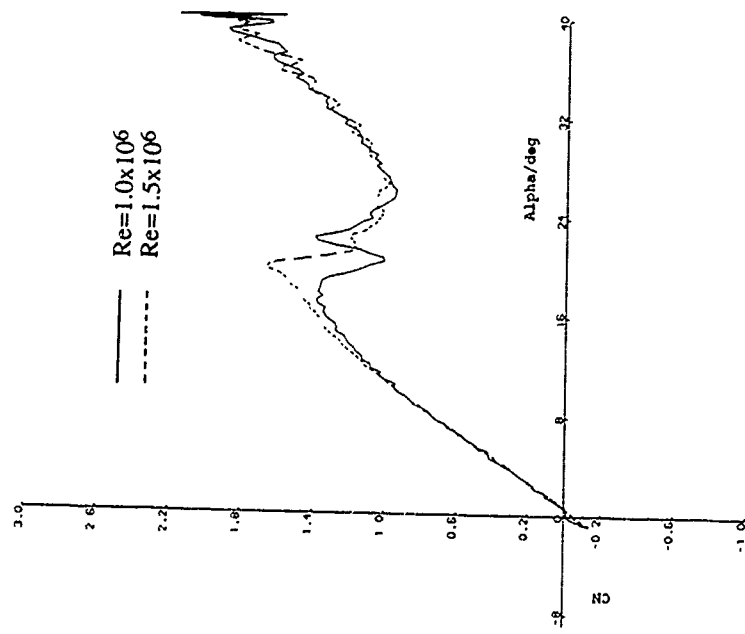
Figure 51b. Cn vs α for the standard sized NACA 0015 for Re=1.5x10⁶ and Re=1.0x10⁶. Ramp-up test at r=0.017.

Figure 51a. Cn vs α for the standard sized NACA 0015 for Re=1.5x10⁶ and Re=1.0x10⁶. Ramp-up test at r=0.005.

High AR model
Standard model

CN

Alpha/deg
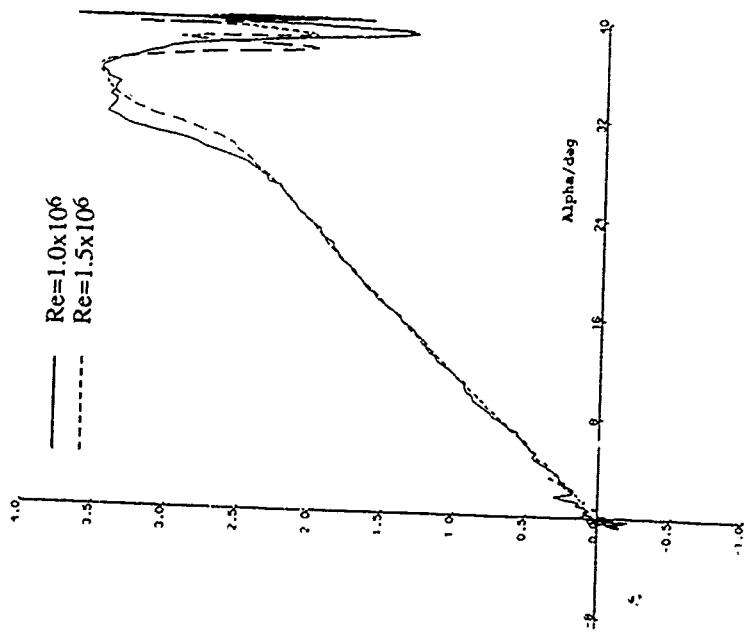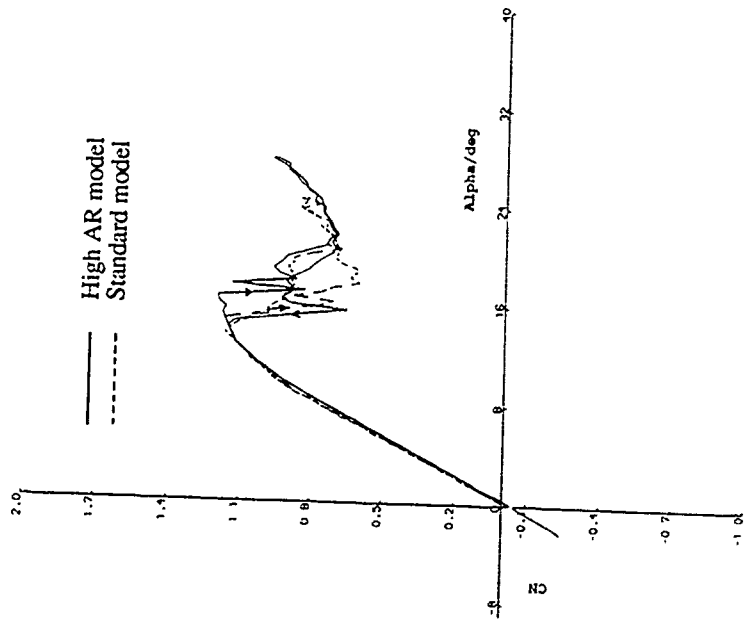
Figure 52. Comparison of Cn vs α for static tests between the standard and high aspect ratio NACA 0015 n⋯⋯ls.

Re=1.0x10⁶
Re=1.5x10⁶

Alpha/deg

Figure 51c. Cn vs α for the standard sized NACA 0015 for Re=1.5x10⁶ and Re=1.0x10⁶. Ramp-up test at r=⋯⋯.
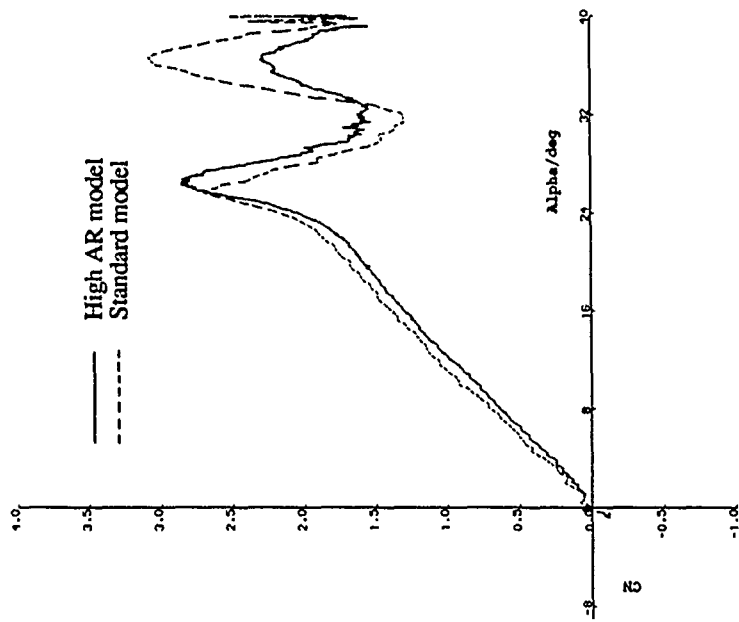
Figure 53b. Comparison of Cn vs α plots between ramp-up tests on the standard and high AR models. r=0.017. Standard model at Re=1.1x10⁶, high AR model at Re=0.8x10⁶.
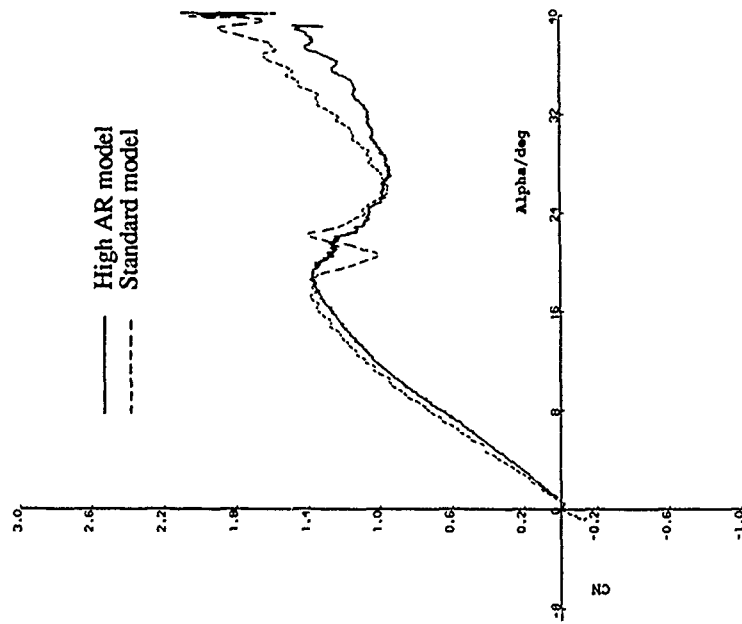
Figure 53a. Comparison of Cn vs α plots between ramp-up tests on the standard and high AR models. r=0.005. Standard model at Re=1.0x10⁶, high AR model at Re=0.8x10⁶.

High AR model
Standard model

Alpha/deg

Cn

Figure 53d. Comparison of Cn vs α plots between ramp-up tests on the standard and high AR models. r=0.017. Standard model at Re=1.5x10^6 , high AR model at Re=1.0x10^6 .

High AR model
Standard model

Alpha/deg

Cn
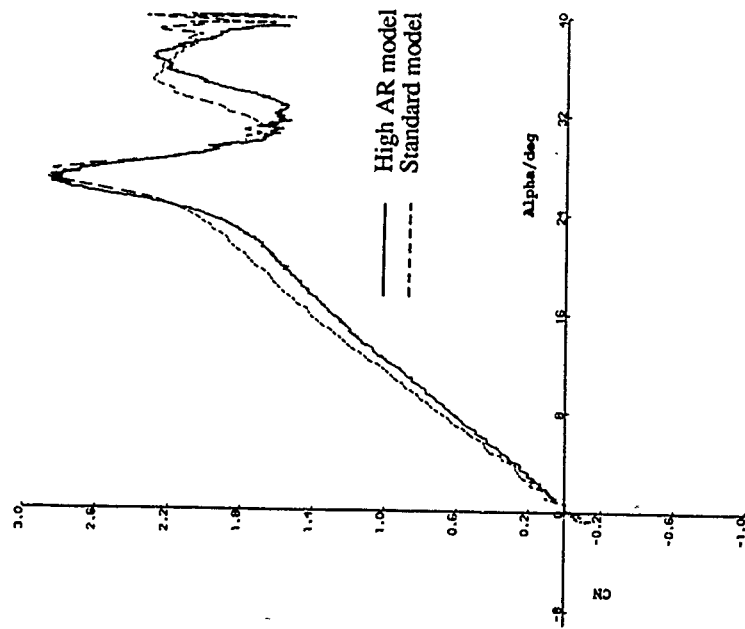
Figure 53c. Comparison of Cn vs α plots between ramp-up tests on the standard and high AR models. r=0.017. Standard model at Re=1.5x10^6 , high AR model at Re=0.8x10^6 .

MAXIMUM CN FOR NACA 0015

REYNOLDS NUMBER = 1500000.
MACH NUMBER = 0.112
MOTION TYPE: RAMP-UP

STRAIGHT LINE FIT:
Y = 62.4968X + 1.3497
CORR = 0.942757

Reduced pitch rate
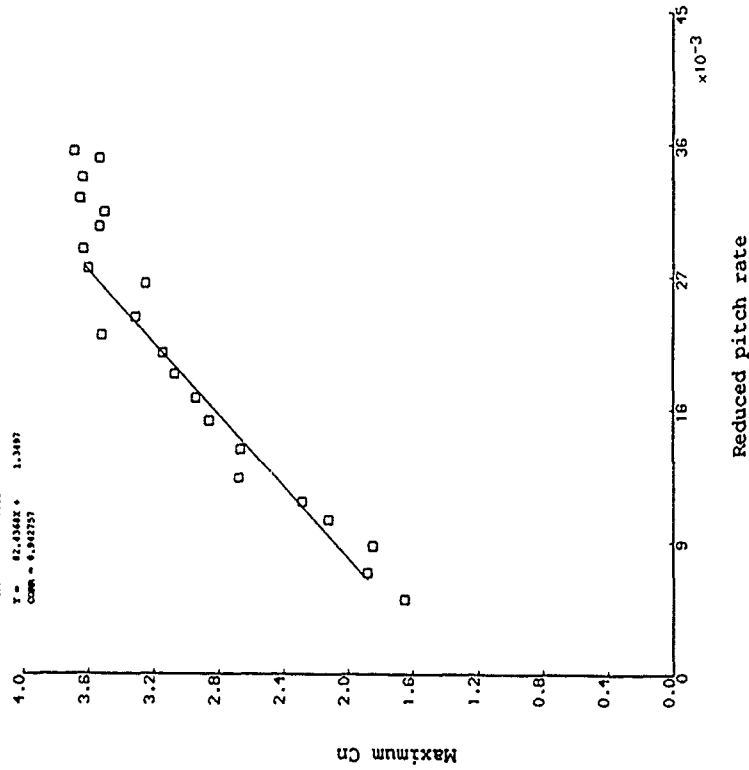
Maximum Cn

Figure 54a. Cn_{max} vs r for the standard model at Re=1.5x10^6.

High AR model
Standard model

Alpha/deg

CN
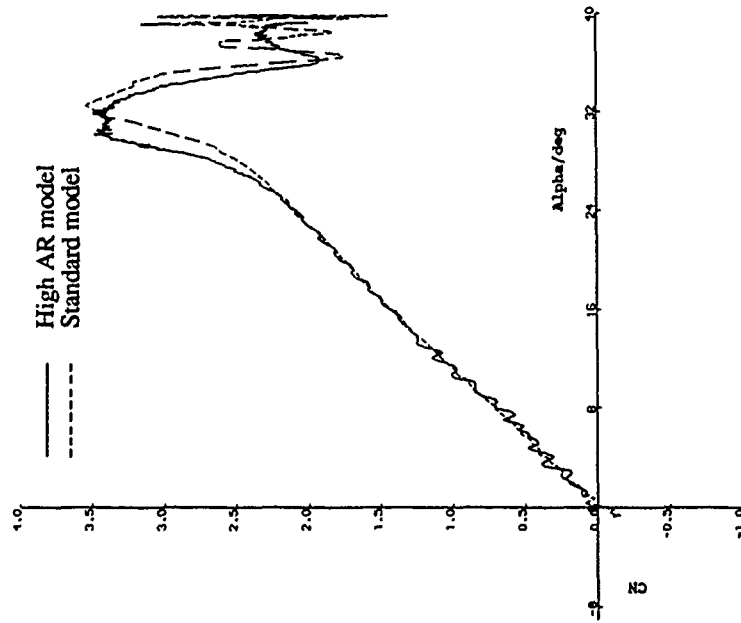
Figure 53e. Comparison of Cn vs α plots between ramp-up tests on the standard and high AR models. r=0.03. Standard model at Re=1.0x10^6, high AR model at Re=0.8x10^6.

MAXIMUM CN FOR NACA 0015 (HIGH AR)

MAXIMUM CN FOR NACA 0015 (HIGH AR)

Figure 54c. Cn_{max} vs r for the high AR model at $Re=1.0 \times 10^6$.
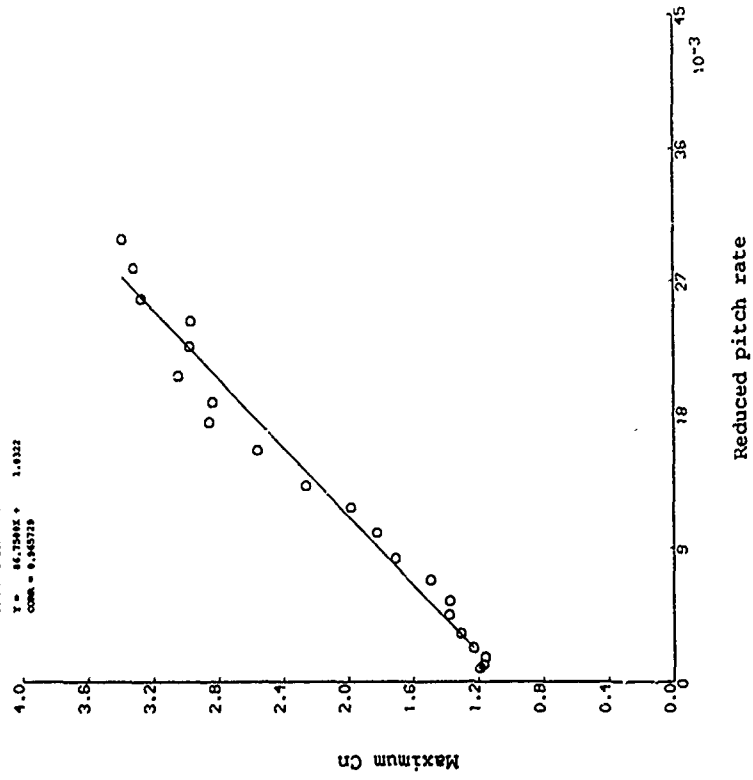
Figure 54b. Cn_{max} vs r for the high AR model at $Re=0.8 \times 10^6$.

ALPHA AT MAX CN FOR NACA 0015 (HIGH AR)

Figure 55b.   α at Cn_{max} vs r for the high AR model at Re=0.8x10⁶.

ALPHA AT MAX CN FOR NACA 0015

Figure 55a.   α at Cn_{max} vs r for the standard model at Re=1.5x10⁶.

ALPHA AT CN RISE FOR NACA 0015

REYNOLDS NUMBER = 1500000,
MACH NUMBER = 0.112
MOTION TYPE: RAMP-UP

STRAIGHT LINE FIT:
Y = 391.999X + 16.4719
CORR = 0.952885

Reduced pitch rate
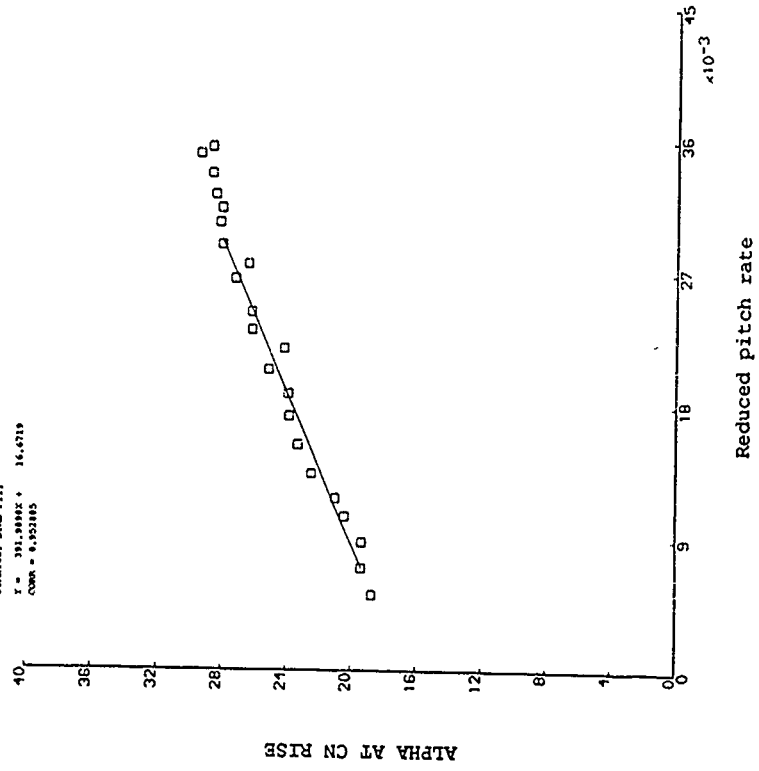
Figure 56a. α at Cn_{rise} vs r for the standard model at $Re=1.5\times10^6$.

ALPHA AT MAX CN FOR NACA 0015 (HIGH AR)

REYNOLDS NUMBER = 1000000,
MACH NUMBER = 0.170
MOTION TYPE: RAMP-UP

STRAIGHT LINE FIT:
Y = 584.282X + 17.7741
CORR = 0.940258

Reduced pitch rate

Figure 55c. α at Cn_{max} vs r for the high AR model at $Re=1.0\times10^6$.

ALPHA AT CN RISE FOR NACA 0015   (HIGH AR)

REYNOLDS NUMBER = 1000000,
MACH NUMBER = 0.170
MOTION TYPE: RAMP-UP

STRAIGHT LINE FIT:
Y = 360.210X + 16.3744
CORR = 0.907410

ALPHA AT CN RISE

Reduced pitch rate

×10⁻³

Figure 56c. α at Cn_{rise} vs r for the high AR model at Re=1.0x10⁶.

ALPHA AT CN RISE FOR NACA 0015   (HIGH AR)

REYNOLDS NUMBER = 800000,
MACH NUMBER = 0.140
MOTION TYPE: RAMP-UP

STRAIGHT LINE FIT:
Y = 297.347X + 17.1113
CORR = 0.970075

ALPHA AT CN RISE

Reduced pitch rate

×10⁻³

Figure 56b. α at Cn_{rise} vs r for the high AR model at Re=0.8x10⁶.

Figure 57.   Comparison of Cn vs α plots between ramp-up
tests on the standard and high AR models at
r=0.018. Both models tested at Re=1.0×10^6 .
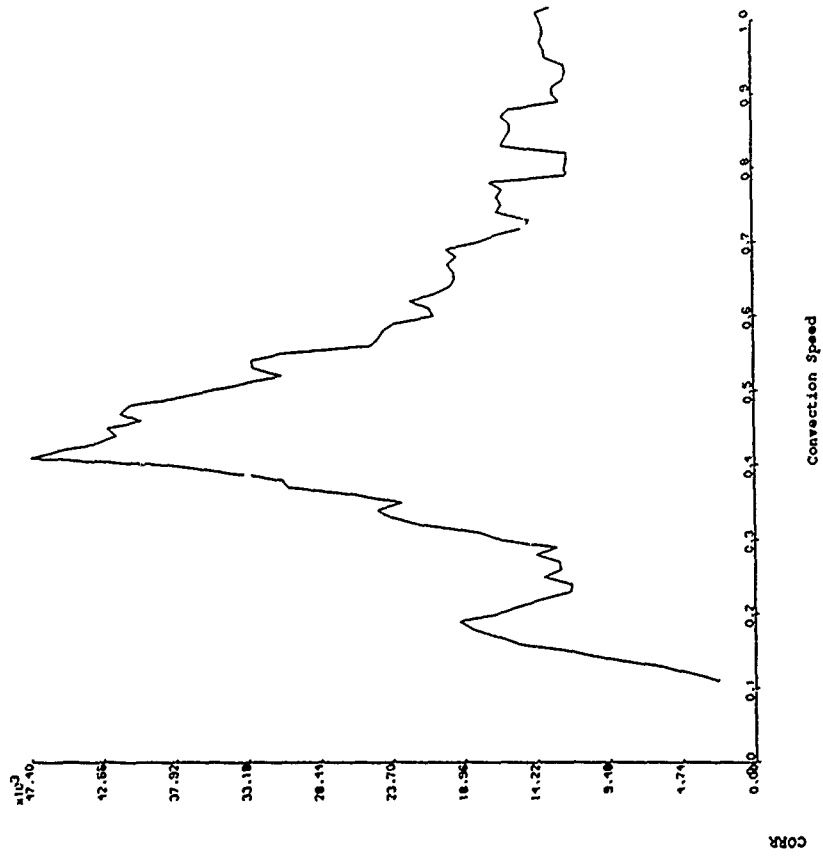
Figure 58a.   Pressure trace cross-correlation coefficient as a
function of convection speed for a strong case.
The chosen convection speed is the peak value at
u/U=0.42.
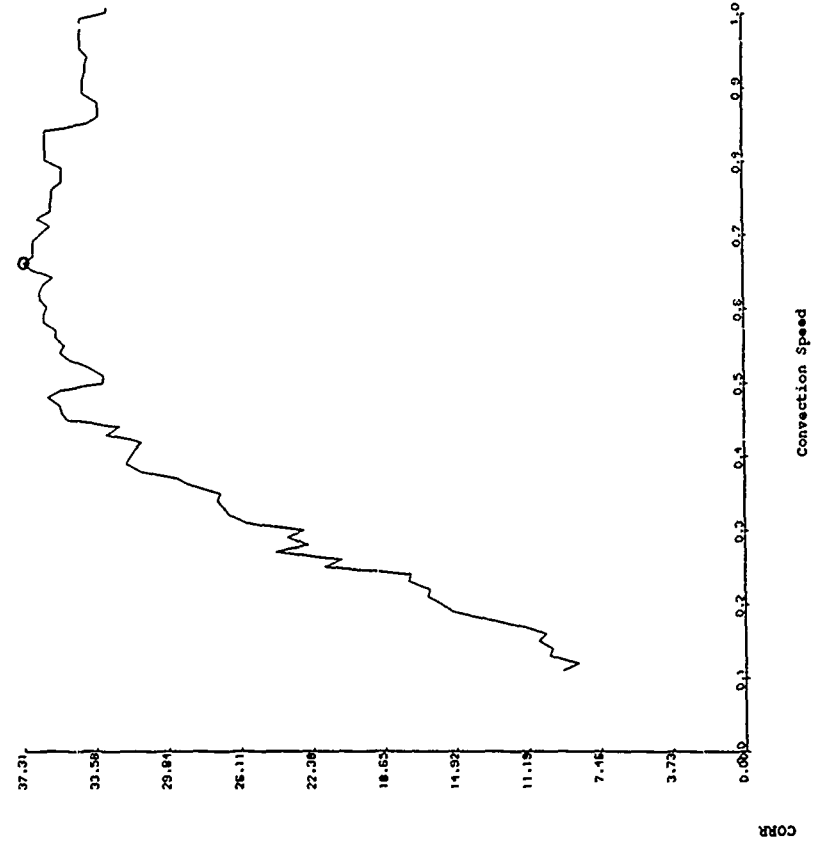
Figure 58b.   Pressure trace cross-correlation coefficient as a
function of convection speed for a weak case.
The chosen convection speed is shown at
u/U=0.66.
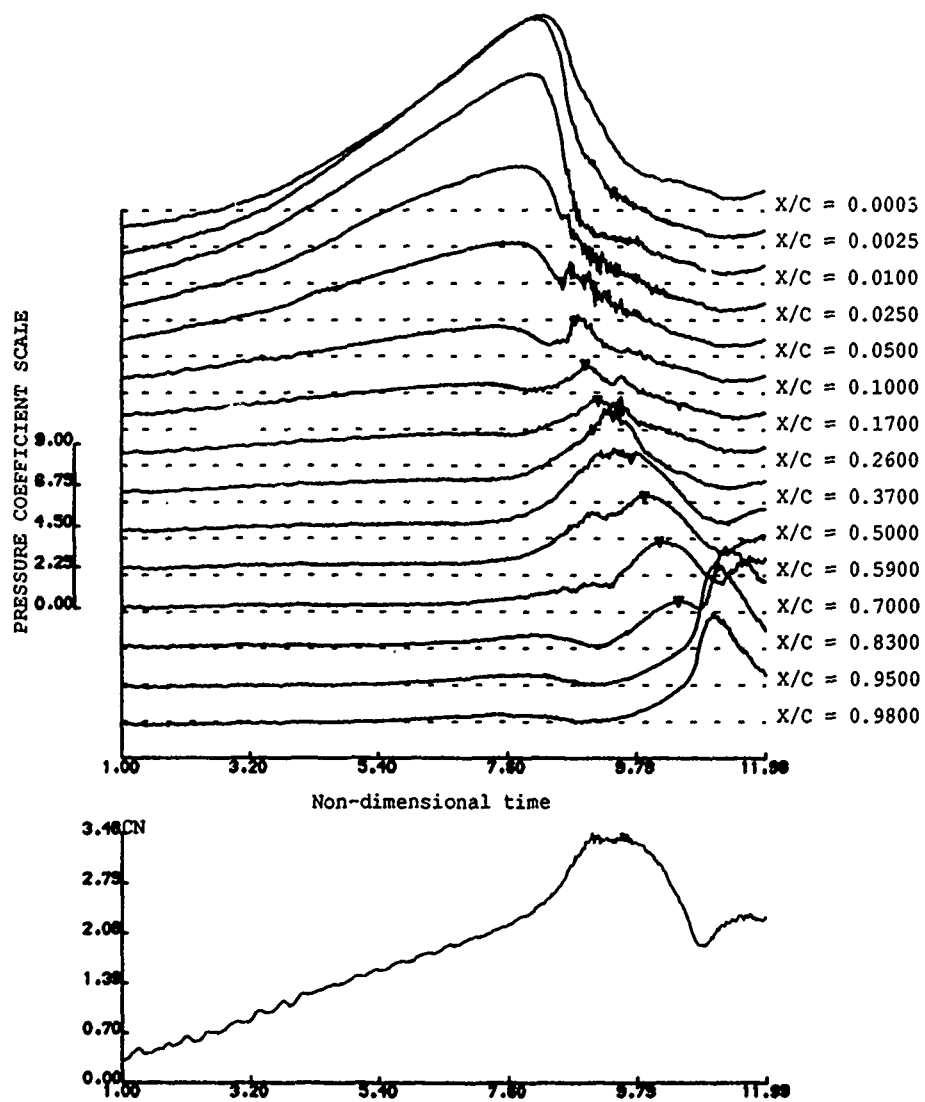
Figure 59a.   Individual pressure traces plotted as a function of
time for a ramp-up test on the high AR model at
r=0.03, Re=0.8x10^6. The symbols indicate the
timing points for the maximum (strong)
correlation coefficient shown in figure 58a.

PRESSURE COEFFICIENT SCALE

X/C = 0.0003
X/C = 0.0025
X/C = 0.0100
X/C = 0.0250
X/C = 0.0500
X/C = 0.1000
X/C = 0.1700
X/C = 0.2600
X/C = 0.3700
X/C = 0.5000
X/C = 0.5900
X/C = 0.7000
X/C = 0.8300
X/C = 0.9500
X/C = 0.9800

Non-dimensional time
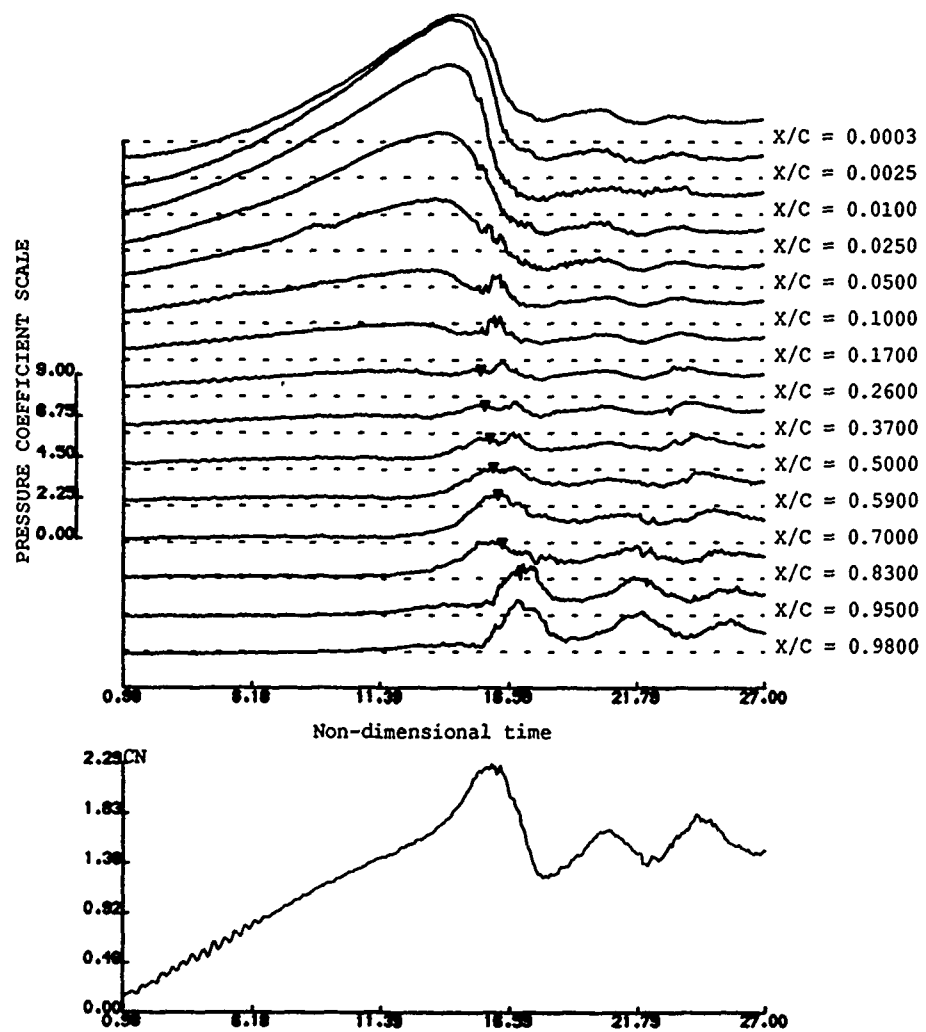
Figure 59b.   Individual pressure traces plotted as a function of
time for a ramp-up test on the high AR model at
r=0.013, Re=0.8x10^6. The symbols indicate the
timing points for the maximum (weak)
correlation coefficient shown in figure 58b.

STALL VORTEX CONVECTION SPEED

NOMINAL REYNOLDS NUMBER = 1000000.
NOMINAL MACH NUMBER = 0.170
MOTION TYPE: RAMP-UP

▲ NACA 0018

▼ NACA 0015

+ NACA 0015 (HIGH AR, Re=0.8)

× NACA 0015 (HIGH AR, Re=1.0)

CONVECTION SPEED
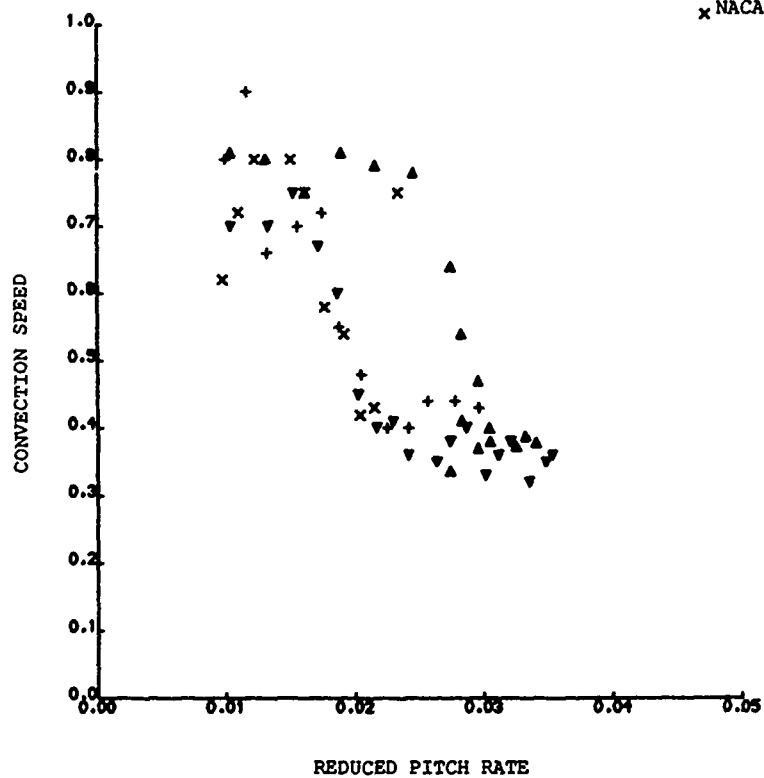
REDUCED PITCH RATE

Figure 60.   Stall vortex convection speed plotted as a
              function of reduced pitch rate for the high AR
              NACA 0015. Also shown are the results for the
              standard NACA 0015 and NACA 0018 models.
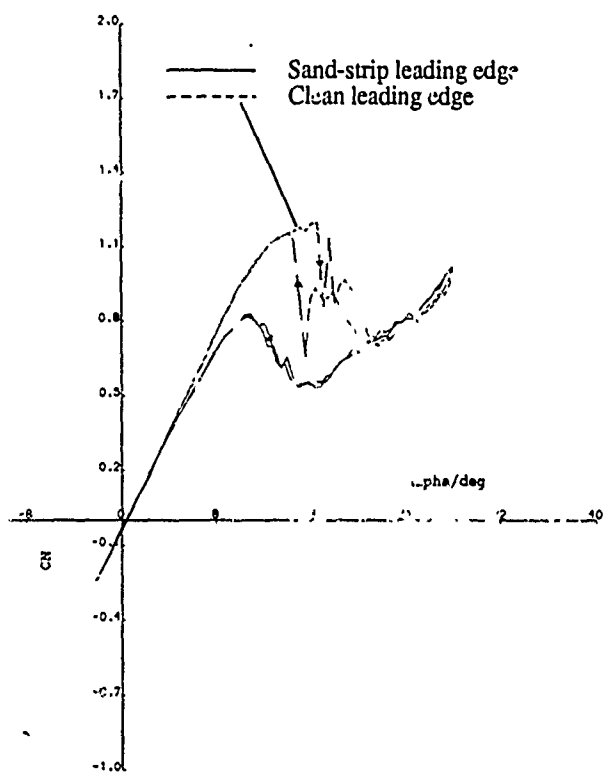
Figure 61.   Comparison of Cn vs α for static ι ω between
              the clean and sand strip leading edge high aspect
              ratio NACA 0015. Re=1.0x10^6.

Figure 62. Standard plot for the high AR model. Ramp-up test at r=0.0215, Re=1.0x10⁶. Clean leading edge. Vortex growth appears as a bulge as indicated.
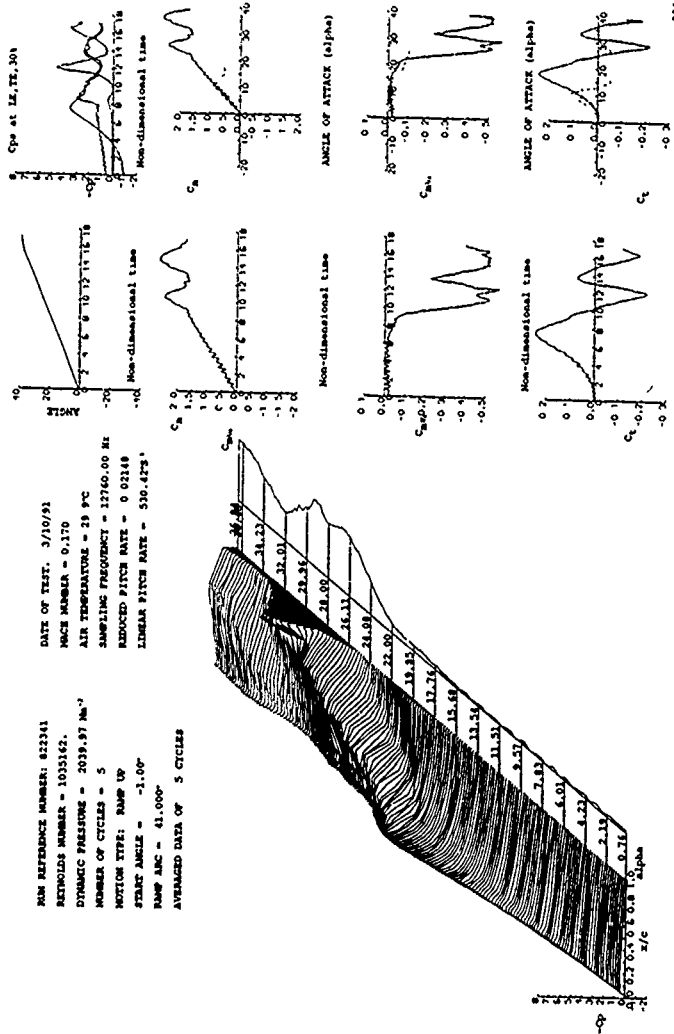
Figure 63. Standard plot for the high AR model. Ramp-up test at r=0.0215, Re=1.0x10⁶. Sand strip leading edge. Vortex convection orginates from the leading edge.

Figure 64. Standard plot for the high AR model. Ramp-up test at r=0.0074, Re=1.0x10⁶. Clean leading edge. Vortex growth appears as a bulge as indicated, although it is now very weak.
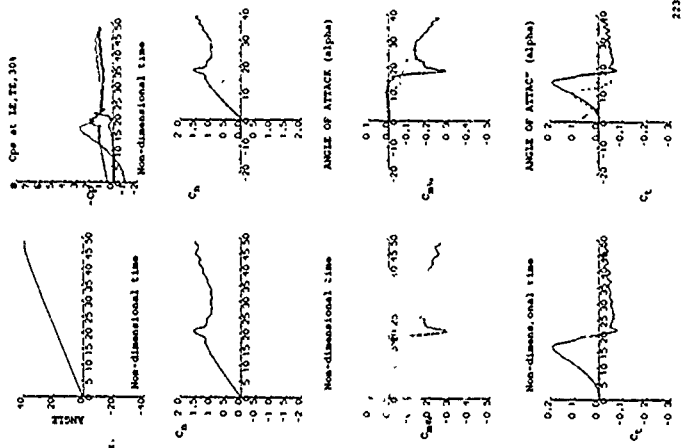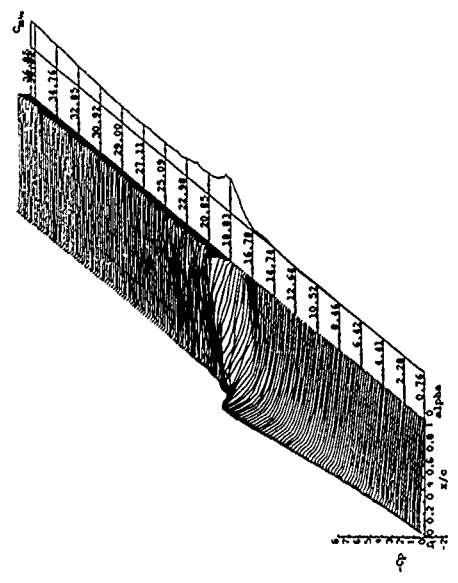
Figure 65. Standard plot for the high AR model. Ramp-up test at r=0.0074, Re=1.0x10⁶. Sand strip leading edge. Vortex convection originates from the leading edge.

223

Sand-strip leading edge
Clean leading edge

CN

Alpha/deg

Figure 67.   Comparison of Cn *vs* α plots for a ramp-up test between the clean and sand strip leading edge high AR NACA 0015. r=0.0074, Re=1.0x10⁶. The two runs correspond to figures 64 and 65.

Sand-strip leading edge
Clean leading edge

CN

Alpha/deg
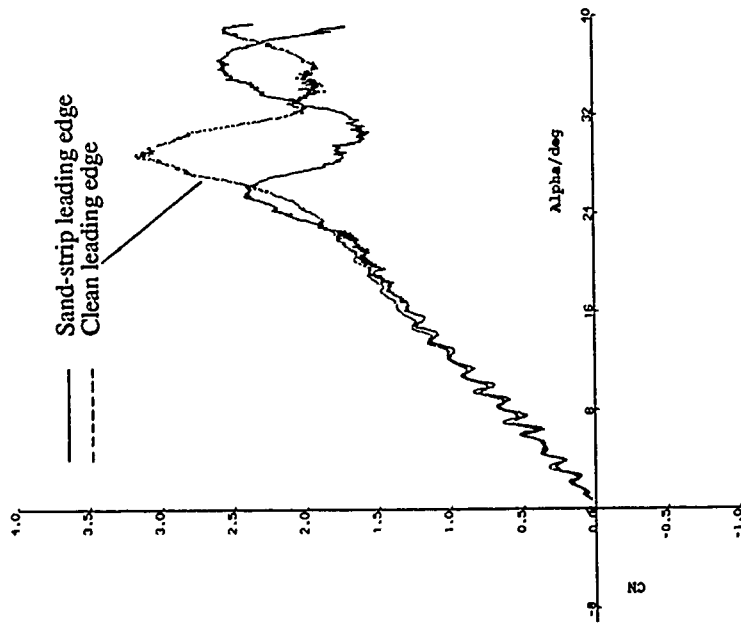
Figure 66.   Comparison of Cn *vs* α plots for a ramp-up test between the clean and sand strip leading edge high AR NACA 0015. r=0.0215, Re=1.0x10⁶. The two runs correspond to figures 62 and 63.

ALPHA AT CN RISE FOR NACA 0015 (HIGH AR)

REYNOLDS NUMBER = 1100000.
MACH NUMBER = 0.178
MOTION TYPE: RAMP-UP
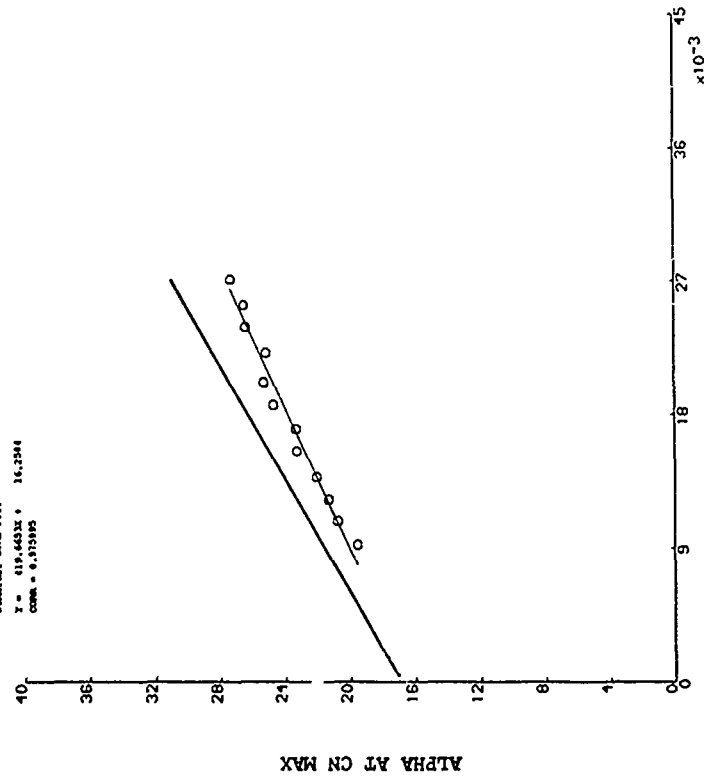
STRAIGHT LINE FIT:
Y = 356.147RX + 12.7463
CORR = 0.953747
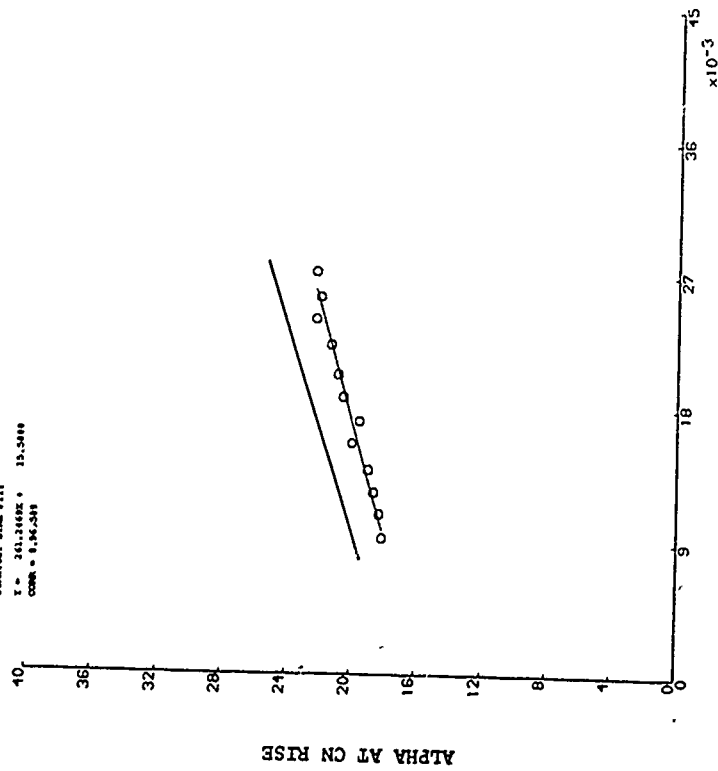
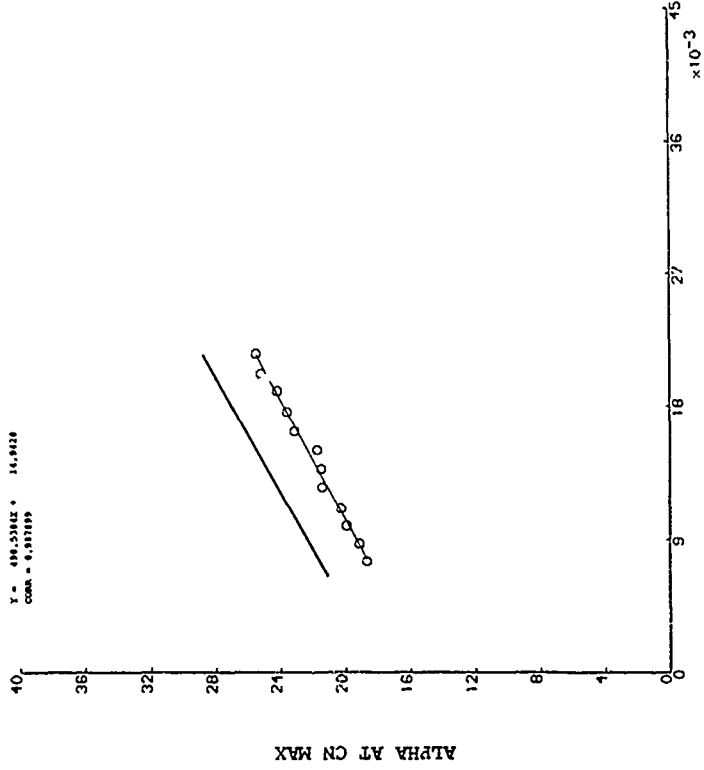Figure 68b. α at Cn_{rise} vs r for the sand strip high AR model at Re=1.0x10⁶. The straight line fit for the clean leading edge case is also shown.

ALPHA AT CN RISE FOR NACA 0015 (HIGH AR)

REYNOLDS NUMBER = 660000.
MACH NUMBER = 0.120
MOTION TYPE: RAMP-UP

STRAIGHT LINE FIT:
Y = 261.266RX + 15.5000
CORR = 0.965388

Figure 68a. α at Cn_{rise} vs r for the sand strip high AR model at Re=0.8x10⁶. The straight line fit for the clean leading edge case is also shown.

ALPHA AT MAX CN FOR NACA 0015 (HIGH AR)

REYNOLDS NUMBER = 1100000.
MACH NUMBER = 0.180
MOTION TYPE: RAMP-UP

STRAIGHT LINE FIT:
Y = 498.5380X + 14.9420
CORR = 0.937899

Reduced pitch rate

×10⁻³

ALPHA AT CN MAX

Figure 69b. α at Cn_{max} vs r for the sand strip high AR model at Re=1.0x10⁶. The straight line fit for the clean leading edge case is also shown.

ALPHA AT MAX CN FOR NACA 0015 (HIGH AR)

REYNOLDS NUMBER = 860000.
MACH NUMBER = 0.140
MOTION TYPE: RAMP-UP

STRAIGHT LINE FIT:
Y = 418.6463X + 14.2304
CORR = 0.972095

Reduced pitch rate

×10⁻³

ALPHA AT CN MAX

Figure 69a. α at Cn_{max} vs r for the sand strip high AR model at Re=0.8x10⁶. The straight line fit for the clean ...ng e... ...ase ... so s... .

MAXIMUM CN FOR NACA 0015 (HIGH AR)
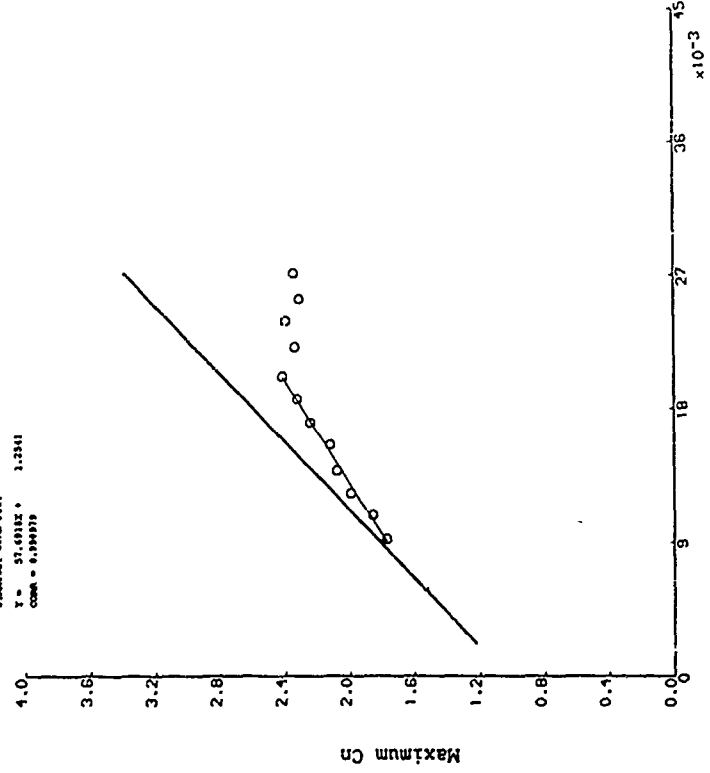
Figure 70a. Cn$_{max}$ vs r for the sand strip high AR model at Re=0.8x10^6. The straight line fit for the clean leading edge case is also shown.

MAXIMUM CN FOR NACA 0015 (HIGH AR)
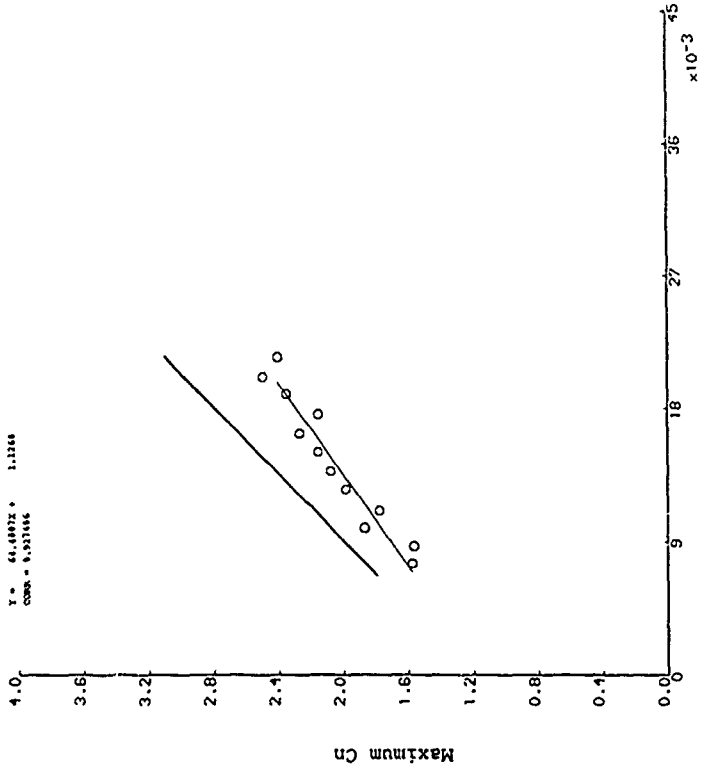
Figure 70b. Cn$_{max}$ vs r for the sand strip high AR model at Re=1.0x10^6. The straight line fit for the clean leading edge case is also shown.

STALL VORTEX CONVECTION SPEED

NOMINAL REYNOLDS NUMBER = 1100000.
NOMINAL MACH NUMBER = 0.170
MOTION TYPE: RAMP-UP

▲ NACA 0015 (HIGH AR, Re=0.8)

▼ NACA 0015 (HIGH AR, Re=1.0)

+ NACA 0015 (HIGH AR, SAND, Re=0.85)

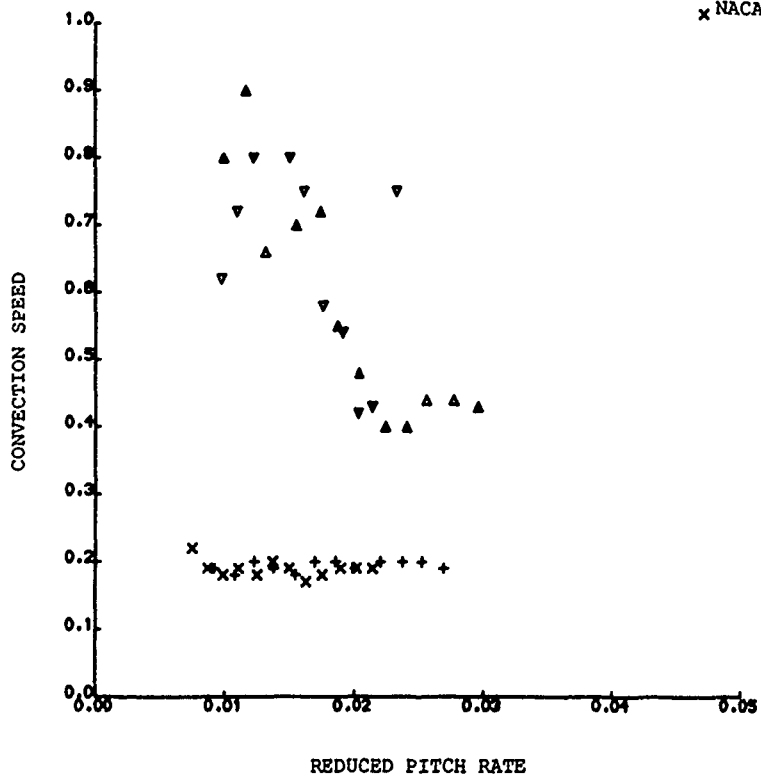× NACA 0015 (HIGH AR, SAND, Re=1.1)

Figure 71.   Convection speed as a function of reduced pitch
rate for the high AR model tests. Both the clean
and sand strip leading edges are shown.

DYNAMIC CHARACTERISTICS FOR THE NACA 0012

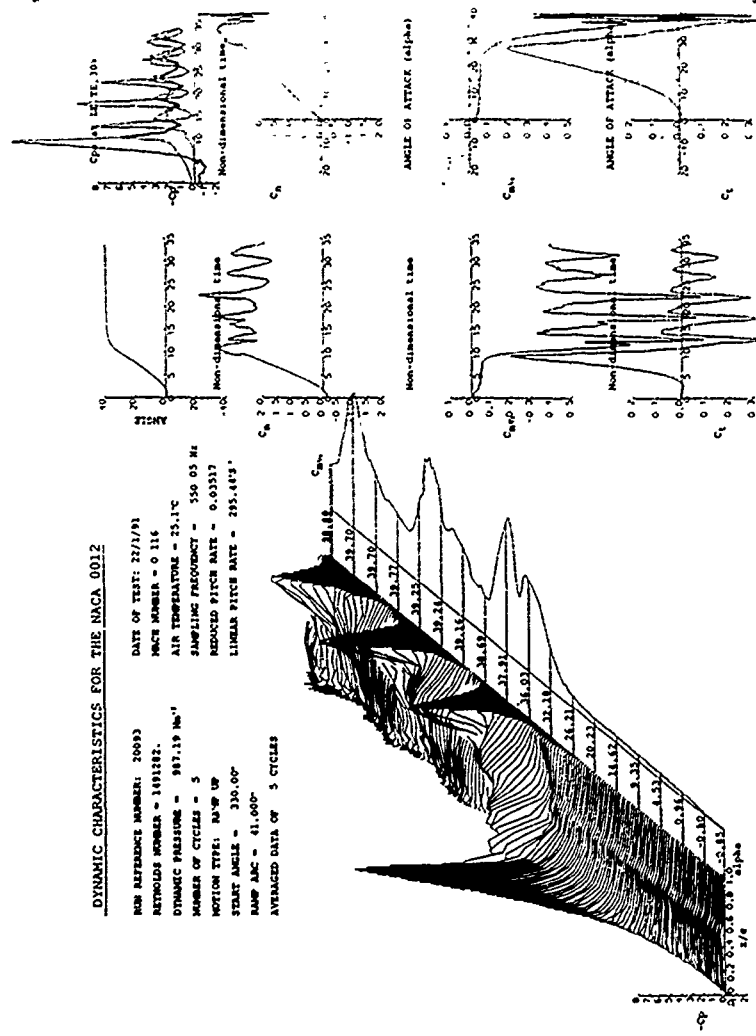|	
RUN REFERENCE NUMBER: 2009	DATE OF TEST: 22/1/91
REYNOLDS NUMBER = 1491282.	MACH NUMBER = 0.116
DYNAMIC PRESSURE = 987.19 Nm⁻¹	AIR TEMPERATURE = 25.1°C
NUMBER OF CYCLES = 5	SAMPLING FREQUENCY = 550.05 Hz
MOTION TYPE: RAMP UP	REDUCED PITCH RATE = 0.03517
START ANGLE = 330.00°	LINEAR PITCH RATE = 295.44°/s
RAMP ARC = 41.000°	
AVERAGED DATA OF 5 CYCLES	

Figure 72.   Standard plot for the NACA 0012 model,
Ramp-up test at r=0.039. Re=1.5x10⁶. The stall
vortex originates from just behind the leading
edge.
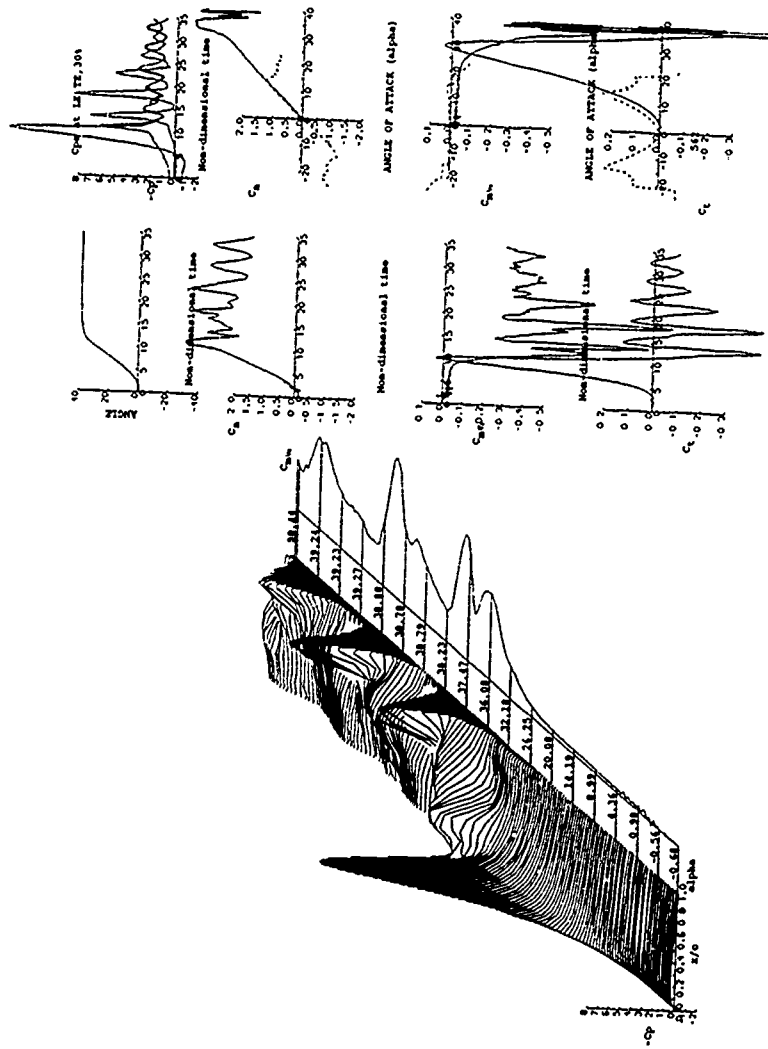
Figure 73   Standard plot for the standard chord NACA 0015
model. Ramp-up test at r=0.039. Re=1.5x10⁶.
The stall vortex first appears as the Cp bulge
around the mid-chord.

Figure 74. Stall vortex convection speed plotted as a
function of reduced pitch rate for all the
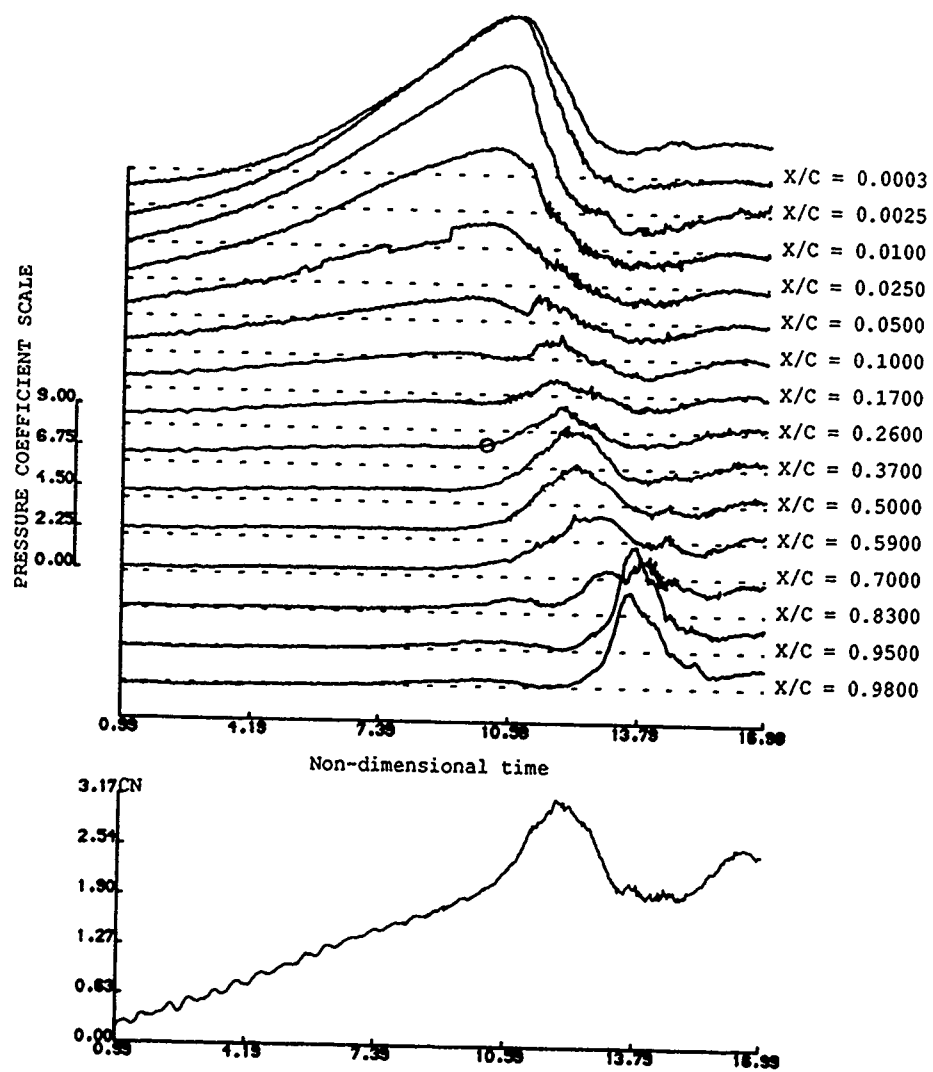symmetrical sections tested at the University of
Glasgow.

Figure 75. Individual pressure transducer traces for the clean leading edge, high AR model. Ramp-up test at r=0.0215, Re=1.0x10^6. The initial vortex growth region is indicated at the mid-chord.
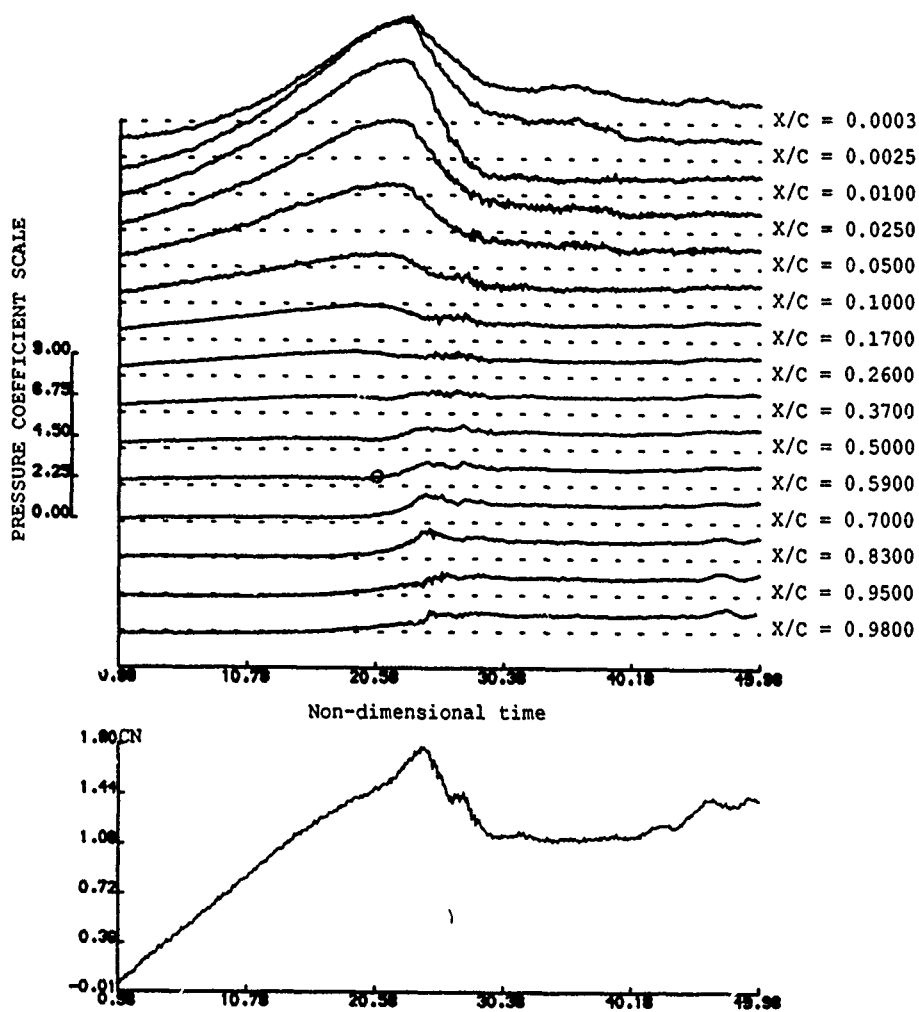
Figure 76.   Individual pressure transducer traces for the clean leading edge, high AR model. Ramp-up test at r=0.0074, Re=1.0x10⁶. The initial vortex growth region is indicated aft of the mid-chord.